

In presenting the dissertation as a partial fulfillment of the requirements for an advanced degree from the Georgia Institute of Technology, I agree that the Library of the Institute shall make it available for inspection and circulation in accordance with its regulations governing materials of this type. I agree that permission to copy from, or to publish from, this dissertation may be granted by the professor under whose direction it was written, or, in his absence, by the Dean of the Graduate Division when such copying or publication is solely for scholarly purposes and does not involve potential financial gain. It is understood that any copying from, or publication of, this dissertation which involves potential financial gain will not be allowed without written permission.

3/17/65

b

THE ABLATION OF SLIP-CAST FUSED SILICA

A THESIS

Presented to

The Faculty of the Graduate Division

by

Charles Everage Willbanks

In Partial Fulfillment

of the Requirements for the Degree

Doctor of Philosophy

In the School of Mechanical Engineering

Georgia Institute of Technology

January, 1967

THE ABLATION OF SLIP-CAST FUSED SILICA

Approved:

\_\_\_\_\_  
Chairman

\_\_\_\_\_  
\_\_\_\_\_  
Date approved by Chairman: 5/12/67

## ACKNOWLEDGMENTS

The author is very grateful to the many people who have encouraged and assisted him in his educational endeavor, especially to his parents who impressed upon him the value of higher education and to his wife for her patience and understanding throughout his graduate study.

Sincere appreciation is expressed to Dr. Charles W. Gorton, the author's thesis advisor, for his guidance and encouragement throughout the entire work. A special note of thanks is due the High Temperature and Materials Branch of the Georgia Institute of Technology for the use of the rocket test facility, and especially to branch members Messrs. C. A. Murphy and A. T. Sales for their assistance in obtaining the experimental data. Appreciation is also extended to Dr. Henderson C. Ward and Dr. James E. Sunderland for their helpful comments in reviewing the work.

The financial support of the National Aeronautics and Space Administration is gratefully acknowledged.

## TABLE OF CONTENTS

	Page
ACKNOWLEDGMENTS . . . . .	ii
LIST OF TABLES . . . . .	v
LIST OF ILLUSTRATIONS . . . . .	vi
SUMMARY . . . . .	ix
NOMENCLATURE . . . . .	xii
Chapter	
I. INTRODUCTION . . . . .	1
II. LITERATURE SURVEY . . . . .	4
III. PHENOMENOLOGICAL MODELS . . . . .	10
A Model for Flow in the Liquid Layer The Gas-Liquid Interface During Ablation	
IV. THEORETICAL ANALYSIS . . . . .	18/3
Melting Ablation The Gas Boundary Layer Summary of Theoretical Results	
V. EXPERIMENTAL INVESTIGATION . . . . .	65
Experimental Apparatus Test Specimens Experimental Procedure Experimental Results Experimental Error	
VI. THEORETICAL PERFORMANCE OF SLIP-CAST FUSED SILICA . . . . .	84
Theoretical Behavior of Slip-Cast Fused Silica in the Rocket Exhaust Performance of Slip-Cast Fused-Silica Along Illustrative Trajectories	

	Page
VII. COMPARISON OF EXPERIMENTAL AND THEORETICAL RESULTS. . . . .	109
Discussion of the Comparison of Theoretical and Experimental Results	
VIII. CONCLUSIONS AND RECOMMENDATIONS . . . . .	113
APPENDIX	
A. ROCKET TEST FACILITY. . . . .	117
B. CONVERGENCE AND STABILITY OF THE DIFFERENCE EQUATIONS . . . .	139
C. HYPOTHETICAL ABLATION PROBLEM . . . . .	144
D. JUSTIFICATION FOR NEGLECTING Si AND SiH <sub>4</sub> VAPOR. . . . .	150
E. DYNAMICS OF ATMOSPHERIC RE-ENTRY. . . . .	154
F. THERMODYNAMIC AND TRANSPORT PROPERTY DATA . . . . .	156
G. COMPUTER PROGRAM. . . . .	163
H. NEWTON'S METHOD . . . . .	174
REFERENCES . . . . .	176
VITA . . . . .	182

LIST OF TABLES

Table		Page
1.	Summary of Operating Conditions of H <sub>2</sub> -O <sub>2</sub> Rocket Motor . . .	65
2.	Estimated Errors in the Experimental Ablation Rate . . . . .	83
3.	Stability Criteria for the Numerical Solution . . . . .	143
4.	Free Energy Data . . . . .	157
5.	Some Parameters for Predicting Transport Properties . . . .	159
6.	Specific Heats and Enthalpies of Individual Species . . . .	161

## LIST OF ILLUSTRATIONS

Figure	Page
1. Coordinate System for Melt Layer and Gas Boundary Layer. . . . .	20
2. Sketch of Cross Section of Typical Specimen After Testing. . . . .	58
3. Photograph of H <sub>2</sub> -O <sub>2</sub> Rocket Motor. . . . .	66
4. Sketch of Transient Calorimeter . . . . .	68
5. Sketch of Stagnation Pressure Probe . . . . .	69
6. Correction Factor for Finite Thermal Conductivity of Calorimeter Slug. . . . .	73
7. Heat Flux versus Distance from Exit of Rocket Motor. . . . .	75
8. Stagnation Pressure versus Distance from Exit of Rocket Motor . . . . .	77
9. Ablation Velocity versus Position in Rocket Exhaust . . . . .	79
10. Heat of Ablation of Slip-Cast Fused Silica in Rocket Exhaust. . . . .	80
11. Backside Temperature versus Time. . . . .	81
12. Theoretical Steady-State Vaporization Fraction, Surface Temperature and Ablation Velocity versus Distance from Exit of Rocket Motor . . . . .	86
13. The Effect of Accommodation Coefficient on Surface Temperature, Ablation Velocity and Vaporization Fraction at Six Inches from the Exit of the Rocket Motor. . . . .	88
14. Stagnation Pressure, Flight Velocity and Altitude versus Time from Re-entry at 300,000 ft: ICBM. . . . .	93
15. Stagnation Pressure, Flight Velocity and Altitude versus Time from Re-entry at 300,000 ft: IRBM. . . . .	94

Figure	Page
16. Stagnation Pressure, Flight Velocity and Altitude versus Time from Re-entry at 300,000 ft: Trailblazer II Vehicle. . . . .	95
17. Stagnation Point Heat Flux versus Time from Re-entry at 300,000 ft: ICBM . . . . .	96
18. Stagnation Point Heat Flux versus Time from Re-entry at 300,000 ft: IRBM . . . . .	97
19. Stagnation Point Heat Flux versus Time from Re-entry at 300,000 ft: Trailblazer II Vehicle. . . . .	98
20. Ablation Velocity and Surface Temperature versus Time from Re-entry at 300,000 ft: ICBM . . . . .	99
21. Vaporization Fraction versus Time from Re-entry at 300,000 ft: ICBM. . . . .	100
22. Ablation Velocity and Surface Temperature versus Time from Re-entry at 300,000 ft: IRBM . . . . .	102
23. Vaporization Fraction versus Time from Re-entry at 300,000 ft: IRBM . . . . .	103
24. Ablation Velocity and Surface Temperature versus Time from Re-entry at 300,000 ft: Trailblazer II Vehicle. . . . .	104
25. Vaporization Fraction versus Time from Re-entry at 300,000 ft: Trailblazer II Vehicle . . . . .	105
26. Effect of Lewis Number on Heat Transfer . . . . .	108
27. Sketch of Flow Regimes in Rocket Exhaust. . . . .	123
28. Mass Fractions of Species versus Nondimensional Centerline Velocity in Rocket Exhaust for Frozen Mixing. . . . .	127
29. Mach Number and Temperature Distribution Along Centerline of Rocket Exhaust versus Nondimensional Centerline Velocity. . . . .	128
30. Stagnation Temperature and Molecular Weight versus Nondimensional Centerline Velocity Immediately Ahead of Shock. . . . .	134

Figure		Page
31.	Stagnation Pressure versus Nondimensional Centerline Velocity. . . . .	135
32.	Nondimensional Centerline Velocity versus Distance from Exit of Rocket Motor. . . . .	136
33.	Stagnation Point Heat Flux Parameter versus Nondimensional Centerline Velocity in Rocket Exhaust. . . . .	138
34.	Surface Temperature versus Time for Hypothetical Ablation Problem . . . . .	148
35.	Ablation Velocity versus Time for Hypothetical Ablation Problem . . . . .	149

## SUMMARY

The primary objective of the reported research was to investigate experimentally and theoretically the ablation of slip-cast fused silica in the exhaust of an oxy-hydrogen rocket motor. In addition, the theoretical behavior of slip-cast fused silica as an ablative heat shield material for re-entry vehicles was determined for three illustrative re-entry trajectories.

A theory was developed for the ablation of slip-cast fused silica in air and in the exhaust of an oxy-hydrogen rocket motor. The analysis was restricted to the stagnation point of an axially symmetric body at zero angle of attack. The density, specific heat and thermal conductivity of slip-cast fused silica were assumed to be constant while the viscosity of the melt layer was assumed to obey an Arrhenius-type equation. That is, the viscosity was assumed to vary exponentially with the reciprocal of the absolute temperature. Thermal radiation from the ablating surface was treated in an approximate manner by using an apparent emissivity. Nonequilibrium vaporization at the gas-liquid interface was considered through the use of a modified form of the Hertz-Knudsen-Langmuir relation for nonequilibrium vaporization of a pure element.

Analyses were made for the gas boundary layer, the gas-liquid interface, flow in the melt layer and unsteady heat conduction in the ablating body. The equations for the gas boundary layer were solved

by analogy to existing solutions for boundary layer flows. Compatibility equations that relate the element mass fractions at the wall to the element mass fractions at the outer edge of the gas boundary layer were derived. The equations governing heat transfer and melt flow in the ablating body were solved by a combination of an approximate closed form solution and a numerical integration. The continuity and momentum equations in the liquid layer were integrated approximately by using an assumed temperature distribution in the liquid layer. The energy equation for the ablating body was solved numerically through the use of finite difference equations.

In order to give proper consideration to the interaction of slip-cast fused silica with the environment of the oxy-hydrogen rocket motor, an analysis of the oxy-hydrogen rocket motor test facility was made. Separate analyses for flow in the rocket motor itself, mixing of the rocket exhaust with the atmosphere and flow through the shock that stands ahead of a body placed in the exhaust were made. The combined analyses made possible the determination of the variables which characterize the environment of the rocket exhaust from only the experimentally determined stagnation pressure distribution along the centerline of the rocket exhaust.

Flat plates of slip-cast fused silica placed normal to the flow were tested at four, five, six and seven inches from the exit of an oxy-hydrogen rocket motor. The average ablation rate at the stagnation point for the samples was calculated by measuring the depth of ablation and dividing the depth by the duration of exposure to the rocket exhaust. Several samples were fitted with thermocouples on the backside in an

attempt to measure the backside temperature response during ablation.

Numerical results for the ablation of slip-cast fused silica under the environmental conditions expected in the exhaust of the oxy-hydrogen rocket motor were obtained from the theory developed. A comparison was made between the theoretical and experimental ablation rates and the agreement was found to be good. A comparison was also made between the experimentally and theoretically determined backside temperature response; however, in this case, the agreement was not very good. It was found that theoretical ablation rates for equilibrium and nonequilibrium vaporization at the surface were virtually identical; however, the fraction of material vaporized under the condition of equilibrium vaporization was considerably larger than the fraction vaporized under the condition of nonequilibrium vaporization.

The theoretical performance of slip-cast fused silica as an ablative heat shield material was determined for an illustrative ICBM and IRBM and also for a test vehicle--Trailblazer II.

It was recommended that slip-cast fused silica be investigated experimentally over a wider range of conditions with particular attention being paid to the design of ablation experiments that could be compared more directly with theory. It was also recommended that the theory developed for the ablation of slip-cast fused silica in the oxy-hydrogen rocket motor be extended to other ablative materials.

## NOMENCLATURE

## Symbol

Arabic Letters

$\bar{a}$	constant in Equation (C-3), page 145
$a_c$	accommodation coefficient
$A$	cross sectional area in rocket nozzle, ft <sup>2</sup>
$A_D$	drag reference area for re-entry vehicle, ft <sup>2</sup>
$A_i$	constant in collision integral correlation Equation (F-6), page 158
$B_i$	constant in collision integral correlation Equation (F-6), page 158
$c_i$	mass fraction of species $i$
$\bar{c}_i$	element mass fraction of element $i$
$c_c$	specific heat of calorimeter slug, Btu/lbm-°R
$c_{P_i}$	constant pressure specific heat of species $i$ , Btu/lbm-°R
$c_P$	constant pressure specific heat, Btu/lbm-°R
$C$	viscosity—density parameter defined by Equation (4-34c), page 38
$C_H$	Stanton number
$C_{H_0}$	zero mass transfer Stanton number
$C_1$	constant in viscosity Equation (3-1), page 11
$C_2$	constant in viscosity Equation (3-1), page 11
$C_1'$	constant in Equation (C-4), page 145
$C_2'$	constant in Equation (C-4), page 145
$C_3$	constant in Equation (C-4), page 145

$C_4'$	constant in Equation (C-4), page 145
$C_D$	drag coefficient for re-entry vehicle
$\bar{C}_p$	specific heat, Btu/mole-°R
$d$	exit diameter of rocket nozzle, ft
$D_{12}$	binary diffusion coefficient, ft <sup>2</sup> /sec
$E_i$	Eucken correction factor for species $i$
$f(n)$	transformation variable defined by Equation (4-34d), page 38
$\bar{F}(x)$	function of $x$ used in discussion in Appendix H, page 174
$F_v$	vaporization fraction
$\Delta F_f^\circ$	free energy function in Equation (F-2), page 122
$g(n)$	nondimensional enthalpy function defined by Equation (4-42a), page 42
$g_T(n)$	nondimensional enthalpy function defined by Equation (4-34g), page 38
$G(n; f(0); A)$	function defined by Equation (4-39), page 41
$G_{ik}$	term defined by Equation (F-4), page 158
$h$	chemical enthalpy of gas mixture, Btu/lbm
$h(L)$	chemical enthalpy of liquid silica, Btu/lbm
$h_i$	chemical enthalpy of species $i$ , Btu/lbm
$h_T$	sensible enthalpy of gas mixture, Btu/lbm
$\bar{h}$	sensible enthalpy plus kinetic enthalpy in rocket motor exhaust defined by Equation (A-21), page 125, Btu/lbm
$h_i^\circ$	enthalpy of formation of species $i$ , Btu/lbm
$\bar{H}$	nondimensional enthalpy, defined by Equation (A-14b), page 122
$\tilde{H}$	chemical enthalpy, Btu/mole

I	total enthalpy of gas mixture, kinetic energy plus chemical enthalpy $h$ , Btu/lbm
$k_s$	thermal conductivity of slip-cast fused silica, Btu-ft/ft <sup>2</sup> -sec-°R
$\bar{K}_i$	nondimensional mass fraction variable, defined by Equation (A-14c), page 122
$K_{P_j}$	equilibrium constant for reaction $j$ defined by Equation (F-2), page 156
$L(t)$	instantaneous thickness defined by Equation (4-7), page 24, ft
$L_c$	length of calorimeter slug, ft
$Le$	Lewis number
$L_o$	initial thickness of slip-cast fused silica body at the stagnation point, ft
$L_v$	latent heat of vaporization, Btu/lbm
$\dot{m}_v$	rate of vaporization, lbm/ft <sup>2</sup> -sec
$M$	Mach number
$\bar{M}_i$	molecular weight of species $i$ , lbm/lbmole
$\bar{M}_v$	molecular weight ratio
$n$	mass flux, lbm/ft <sup>2</sup> -sec
$n_i$	mass flux of species $i$ , lbm/ft <sup>2</sup> -sec
$n'$	viscosity index defined by Equation (4-10a), page 26
$\bar{n}$	element mass flux, lbm/ft <sup>2</sup> -sec
$\bar{n}_i$	element mass flux of element $i$ , lbm/ft <sup>2</sup> -sec
$p$	absolute pressure, lbf/ft <sup>2</sup>
$P_i$	absolute partial pressure of species $i$ , lbf/ft <sup>2</sup>
$Pr$	Prandtl number

$\dot{q}$	heat flux, Btu/ft <sup>2</sup> -sec
$Q^*$	heat of ablation, Btu/lbm
$r$	position coordinate defined in Figure 27, page 123, ft
$\bar{r}$	radius of cross section taken normal to centerline of axially symmetric slip-cast fused silica body, ft
$R$	radius of curvature at stagnation point of axially symmetric slip-cast fused silica body, ft
$\bar{R}_u$	universal gas constant, Btu/lbmole-°R
$s$	position coordinate defined in Figure 1, page 20, ft
$\bar{s}$	transformation variable defined by Equation (4-34b), page 38
$Sc$	Schmidt number
$t$	time, sec
$\Delta t$	finite time increment, sec
$T$	absolute temperature °R
$T_I$	initial temperature of slip-cast fused silica body, °R
$T_o$	initial surface temperature in hypothetical ablation problem of Appendix C, page 144, °R
$T_{bs}$	backside temperature, °R
$T'_o$	reference temperature used in Equation (4-10), page 26, °R
$T_w$	surface temperature at gas-liquid interface, °R
$u$	velocity component in gas boundary layer and also in the liquid layer defined in Figure 1, page 20, ft/sec
$U$	velocity component in rocket motor and rocket motor exhaust defined in Figure 27, page 123, ft/sec
$\bar{U}$	nondimensional velocity component, defined by Equation (A-14a), page 122

$v$	velocity component in gas boundary layer and also in the liquid layer defined in Figure 11, page 20, ft/sec
$v_o$	constant in Equation (C-3), page 145
$V$	velocity component in rocket motor exhaust defined in Figure 27, page 123, ft/sec
$V_F$	vehicle flight velocity, ft/sec
$W$	vehicle mass, lbm
$x$	variable used in discussion in Appendix H, page 174
$X_i$	mole fraction of species $i$
$\bar{X}$	simplification variable defined by Equation (4-77c), page 62
$y$	position coordinate defined in Figure 11, page 20, ft
$\Delta y$	finite difference increment in position coordinate $y$ , ft
$\bar{Y}$	simplification variable defined by Equation (4-77d), page 63
$Y_a$	altitude, ft
$z$	position coordinate defined in Figure 27, page 123
$Z_i$	nondimensional mass fraction variable defined by Equation (4-34h), page 39
$\bar{Z}_i$	nondimensional element mass fraction variable defined by Equation (4-42b), page 42

#### Greek Letters

$\alpha$	parameter defined by Equation (4-77e), page 63
$\alpha_c$	thermal diffusivity of calorimeter slug, ft <sup>2</sup> /sec
$\alpha_s$	thermal diffusivity of slip-cast fused silica, ft <sup>2</sup> /sec
$\beta$	parameter defined by Equation (4-77f), page 63
$\gamma$	ratio of specific heats or isentropic exponent
$\delta$	small change in $x$

$\delta_c$	constant in Equation (C-2), page 144
$\delta T$	small change in T
$\delta_T$	thermal thickness defined by Equation (4-13), page 277
$\epsilon_R$	emissivity
$\bar{\epsilon}$	criterion for acceptable accuracy
$\eta$	transformation variable defined by Equation (4-34a), page 38
$\eta'$	dummy variable of integration
$\eta''$	dummy variable of integration
$\theta$	re-entry angle
$\lambda_i$	thermal conductivity of gas species i, Btu-ft/ft <sup>2</sup> -sec-°R
$\lambda$	thermal conductivity of gas mixture, Btu-ft/ft <sup>2</sup> -sec-°R
$\Lambda$	denotes Pr or Sc
$\mu_i$	viscosity of gas species i, lbm/ft-sec
$\mu$	viscosity of gas mixture, lbm/ft-sec
$\mu_s$	viscosity of slip-cast fused silica melt, lbm/ft-sec
$\nu$	integer
$\rho$	density of gas mixture, lbm/ft <sup>3</sup>
$\rho_s$	density of slip-cast fused silica, lbm/ft <sup>3</sup>
$\sigma$	Stefan Boltzmann constant, Btu/ft <sup>2</sup> -sec-°R <sup>4</sup>
$\sigma_i$	molecular diameter species i, Å
$\tau$	shear stress, lbf/ft <sup>2</sup>
$\phi_i$	variable defined by Equations (4-27a) - (4-27c), page 34
$\psi(\Lambda)$	function defined by Equation (4-59d), page 51
$\bar{\psi}$	transformation variable defined by Equations (4-34e) and (4-34f), page 38

$\dot{\omega}_i$  rate of production of species  $i$ ,  $\text{lbm/ft}^3\text{-sec}$

$\Omega_{\mu_i}$  collision integral of species  $i$

Subscripts Unless defined otherwise above, the subscripts used have the meanings as indicated below

air refers to the composition of air

bs refers to the backside of the calorimeter slug

c refers to the rocket motor combustion chamber

cw refers to a cold surface

e refers to the outer edge of the gas boundary layer

E refers to the exit of the rocket motor nozzle

f refers to the rocket motor combustion chamber composition

i refers to species  $i$

-L refers to the position  $y = -L(t)$

o refers to zero mass transfer conditions

r refers to reference temperature  $77^\circ\text{F}$

R refers to radiation

s refers to slip-cast fused silica

sp refers to the stagnation point

t refers to throat in rocket nozzle

x refers to conditions immediately upstream of the normal shock

y refers to the position  $y = y$  in the finite difference equations, except in Appendix A where it refers to conditions immediately downstream of the normal shock

w refers to gas-liquid interface

$\infty$  refers to conditions far from rocket exhaust

Superscripts

- t refers to time  $t = t$  in finite difference equations
- + refers to gas side of gas-liquid interface
- refers to liquid side of gas-liquid interface
- ' differentiation unless otherwise defined in nomenclature

## CHAPTER I

## INTRODUCTION

During the last decade, considerable research effort has been expended in the investigation of ablative thermal protection systems. In many applications, ablative thermal protection systems are far superior to protection systems utilizing a heat sink or injection cooling. Perhaps the greatest attribute of an ablative thermal protection system is its simplicity. Foremost among ablative phenomena are surface melting with flow, vaporization, chemical reaction of the products of vaporization with the external environment, thermal radiation and heat conduction and convection.

Hundreds of different kinds of materials have been investigated to determine their feasibility as ablators. Clearly the specific application is an important consideration in the selection of a material for use in an ablative thermal protection system. In the selection of a material many thermal and physical properties of the material as well as the external environment must be considered.

Considerable attention has been devoted to investigating the use of various ceramic materials for use in ablative thermal protection systems. Quartz and Pyrex glass have been investigated extensively. Recently, there has been an interest in the use of slip-cast fused silica for this purpose. Slip-cast fused silica possessed many desirable properties which make it a likely candidate for future use in ablative

thermal protection systems or as electromagnetic windows. A few of its desirable properties are listed below:

1. High viscosity of melt
2. Vaporizes rather readily with approximately 5000 Btu of heat absorbed for every pound vaporized
3. Opaque; therefore some cooling due to thermal radiation from the surface is obtained
4. Very low thermal conductivity
5. Relatively large heat capacity
6. Excellent resistance to thermal shock
7. Inexpensive
8. Easily fabricated
9. Relatively high tensile strength
10. Essentially transparent to electromagnetic waves

The evaluation of the merits of a material for use in an ablative thermal protection system is best carried out by means of a combined experimental and analytical effort. For convenience or of necessity, the performance of materials for particular applications is often determined theoretically. For example, at present there are no ground facilities available for complete simulation of conditions expected on a vehicle re-entering the atmosphere along a ballistic trajectory; therefore, the performance of a material as an ablative heat shield on a vehicle for a particular re-entry trajectory must also be evaluated theoretically. In order to gain some degree of confidence in the theory used, it is often compared to experimental ablation studies conducted in ground test facilities. It should be pointed out that agreement

between theory and experiment at one set of conditions does not guarantee agreement between theory and actual behavior along a flight path. For this reason, experimental tests should be designed to reflect as many of the important effects as possible. It may be necessary to consider more than one set of test conditions in order for all effects to be demonstrated experimentally.

The investigation of the ablation of slip-cast fused silica in this study is conducted in three major phases. The availability facility for testing was an oxy-hydrogen rocket motor; thus a theory is developed for the ablation of slip-cast fused silica in this environment. The results of tests conducted in the exhaust of the rocket motor are reported and compared with the theory. The performance of slip-cast fused silica is then predicted for illustrative ICBM and IRBM trajectories and also for a test vehicle--Trailblazer II.

## CHAPTER II

## LITERATURE SURVEY

The first analytical approach to the ablation of a material whose viscosity varies greatly with temperature appears to be that of Sutton (1)\*. Sutton used a Mangler transformation to convert the differential equations governing steady-state ablation to ordinary differential equations. Numerical results were presented for the stagnation point ablation of Pyrex glass with no vaporization for a particular altitude and Mach number. Sutton was the first investigator to point out the important role played by the viscosity of the molten material in determining the amount of material ablated.

Bethe and Adams (2) obtained an approximate solution to the problem of ablation of a highly viscous, glassy material having a strongly temperature dependent viscosity. Their solution is for steady-state ablation in the absence of thermal radiation. Although the solution is for the stagnation point, Bethe and Adams outlined a technique whereby it could be extended around the body. In addition to melting, vaporization was also included in the analysis.

Lees (3) made an analysis of the two-phase boundary layer produced by surface melting. Both melting and vaporization are discussed and both laminar and turbulent flow in the gas boundary layer are

---

\*Numbers in parentheses refer to the references on page 176.

considered. In this paper Lees was concerned primarily with "scaling laws" and similarity parameters for melting.

Adams, Powers and Georgiev (4) reported the results of an experimental and theoretical study of quartz ablation at the stagnation point. The theory was essentially the same as reported in (2) but was extended to include the effects of radiation in depth in an approximate manner. The experimental data were obtained from a plasma arc wind tunnel.

Georgiev (5) extended the work of Bethe and Adams to the transient ablation process for nonradiating glassy materials at the stagnation point. His results indicate that transient effects do not appreciably affect the amount of material ablated along a trajectory; however, for trajectories where there may be time for temperature equilibration after ablation ceases, transient effects may significantly affect the amount of material required to keep the backside temperature below a prescribed value.

Hidalgo (6), following the suggestion of Bethe and Adams extended their theory of stagnation point ablation to predict ablation away from the stagnation point on a body of revolution. Laminar and turbulent flow in the gas boundary layer adjacent to the ablating body were considered.

Scala and Sutton (7) outlined an exact solution for hypersonic ablation and presented numerical results for the stagnation point ablation of Pyrex glass at a Mach number of 20 and an altitude of  $10^5$  feet. Vaporization was included by assuming that only  $B_2O_3$  vaporizes from the glass. The dissociation of  $B_2O_3$  vapor to  $BO$  was also considered.

Roberts (8,9,10) made a theoretical study of the shielding mechanism near the stagnation point when melting and vaporization occur simultaneously. He made use of the von Kármán integral technique in his analysis and presented results for the rate of mass loss at the body surface and thickness of the liquid layer at the surface in terms of the rate of heat transfer to the unshielded body.

Scala and Vidale (11) and Scala (12) reported studies of the vaporization of a material into the gas boundary layer during hypersonic flight. Nonequilibrium vaporization effects were considered in their analyses.

Fledderman and Hurwicz (13) made an exact analysis of transient heat and mass transfer in an ablating three-phase system. They outlined a technique for accounting for radiation in depth when the ablating material is semi-transparent to thermal radiation. An approximate method based on effective heat of ablation and constant surface temperature was developed.

Zlotnick and Nordquist (14) formulated the transient ablation problem of a material which melts and vaporizes on the basis that the physical properties of the ablating material and the conditions at the outer edge of the gas boundary layer are known. Numerical results for a typical satellite trajectory are presented. Although a finite slab thickness was considered, the boundary conditions at the backside of the slab were not stated for the example given.

Koh and Hartnett (15,16) investigated the multiphase hypersonic boundary layer on a flat plate of ablating material. In Part I (15) the boundary layer equations describing the multiphase boundary layer

on a flat plate were developed and a method for solving these equations was outlined. An illustrative calculation was carried out for the ablation of Pyrex glass at Mach 20 at an altitude of 65,000 feet. In Part II (16) a simplified approach to the solution of the multiphase hypersonic boundary layer was developed.

Adams (17) made an investigation of melting glassy heat shields in the absence of vaporization. The performance of 36 different finitely thick glass shields with assumed combinations of material properties was investigated for a typical IRBM trajectory. Slip-cast fused silica was not considered in the investigation.

McFarland and Harmon (18) made a two-dimensional steady-state analysis of the melt layer on a homogeneous wall exposed to a hot external flow. A power law melt layer velocity profile was assumed and variation in viscosity with temperature was accounted for in their analysis. Vaporization was not considered.

Adams (19) presented an analysis of the transient performance of quartz and teflon ablative heat shields for a particular re-entry mission of a vehicle returning from an extra terrestrial mission to the earth. Representative values for the weight, ballistic factor, re-entry speed and deceleration force were assumed. Melt flow was assumed to be an insignificant portion of the ablation process and was neglected in the analysis.

Steg and Lew (20) presented the results of a rather comprehensive experimental study in hypersonic ablation. Three distinct classes of materials were investigated--glasses being one of them. The experimental studies were conducted in a plasma arc wind tunnel, and the results cover

a considerable portion of the spectrum for actual flight conditions encountered by manned satellites and vehicles and ballistic missiles on re-entry.

Chen and Allen (21) and Chen (22) reported the results of a similarity analysis for transient melting and vaporizing ablation. To obtain a similarity solution the authors assumed that the external flow velocity varied in a hyperbolic manner with time. Although they indicate that their analysis applies to finite as well as semi-infinite slabs, their results are presented only for semi-infinite slabs.

Hidalgo and Kadanoff (23) compared the theory developed in (6) to a full scale flight test of a quartz ICBM nose cone. Due to the classified nature of the data, the quantitative comparison between theory and experiment was limited to indicating the relative magnitudes of the actual and predicted ablated thicknesses.

Schick (24) reported the results of an analysis of some of the physical and chemical properties of silica which are important in ablation behavior. The author brings together the results of many investigations on the properties of silica. Chemical reactions of importance for silica reacting with air and other environments are discussed and enthalpy and free energy correlations for the reactions are given along with an estimate of their accuracy.

Pierson (25) reported the results of a study of the behavior of slip-cast fused silica in some plasma environments. Due to the nature of the tests, it is not possible to make a direct comparison of the experimentally determined ablation rates and heats of ablation with theory. The influence of several additives on the properties of slip-

cast fused silica was discussed.

Slip-cast fused silica has been investigated extensively by the High Temperature Materials Branch of the Engineering Experiment Station of the Georgia Institute of Technology. Only a small portion of this work has been concerned with ablation in a quantitative manner, however. References (26-30) describe in some detail the results of many of the investigations performed. These reports describe the casting processes, applications, electrical, mechanical, physical, chemical and thermal properties and many other aspects of interest to a potential user or investigator of slip-cast fused silica. As a compendium of the properties of fused silica, the "Fused Silica Manual" by Fleming, et al., (30) is quite useful.

## CHAPTER III

## PHENOMENOLOGICAL MODELS

A theoretical study of the ablation of slip-cast fused silica requires the construction of a number of phenomenological models in order to describe the behavior of the material. Therefore, it is appropriate to discuss some of the properties and characteristics of slip-cast fused silica that pertain to its application as an ablative material.

Slip-cast fused silica is formed by sintering a casting formed in a plaster mold from an aqueous suspension of vitrified silica. The vitrified silica is usually made from sand and is nearly pure silicon dioxide which has the chemical formula  $\text{SiO}_2$ . Since vitreous silica does not have a well-defined structure and the casting process results in the entrapment of vast numbers of minute air pockets, it follows that slip-cast fused silica has an extremely complex structure on the microscopic level. The density of S.C.F.S.\* is approximately 15 per cent lower than the density of pure quartz.

Like quartz, S.C.F.S. does not have a latent heat of melting and exhibits no distinct change in phase in its transition from the solid to liquid state.

---

\*Since the term "slip-cast fused silica" appears so many times throughout this work, it is convenient to abbreviate the term as simply S.C.F.S.

Below the softening temperature of silica, which is approximately 3200 °F, S.C.F.S. is virtually opaque to thermal radiation. The entrapped air pockets provide numerous internal reflecting surfaces which limit the transmittance of thermal radiation to a small fraction of the energy transferred by conduction.

#### A Model for Flow in the Liquid Layer

Intense surface heating of a S.C.F.S. body results in the formation of a thin film of molten silica on the surface of the body. Usually convective heating is accompanied by shear and pressure forces which cause the liquid to flow. The nature of this type of flow has been discussed by a number of authors (1,3) and it has been amply demonstrated that the motion is very slow and can be properly classified as a Stokes' flow.

The viscosity of liquid silica is very high in comparison to the viscosities of other ceramic materials. The viscosity increases rapidly with decreasing temperature, and experimental viscosity data fit an Arrhenius-type of equation with reasonable accuracy. Thus

$$\mu_s = C_2 \exp(C_1/T) \quad (3-1)$$

The following numerical values for the constants in Equation (3-1) were given in reference 31 for silica:

$$C_1 = 109,500 \text{ } ^\circ\text{R}$$

$$C_2 = \exp(-16.7) \text{lbm/ft-sec}$$

These values were obtained by a curve fit of the Corning data (32).

Analysis of the melt layer on S.C.F.S. under ablating conditions is complicated by the presence of air bubbles which come from the entrapped air pockets. It appears that the order of magnitude of the diameter of a typical bubble is of the same order of magnitude as the thickness of the liquid layer itself. Thus, existing theories for the effect of the bubbles on the viscosities of liquids are inapplicable to this situation. However, it is reasonable to assume the viscosity of the melt on S.C.F.S. under ablating conditions is the same as the viscosity of liquid silica and obeys Equation (3-1) with the numerical constants  $C_1$  and  $C_2$  as given above.

Although it cannot be rigorously defended, it is also reasonable to treat the liquid melt as being a homogeneous incompressible liquid having a density equal to the density of solid S.C.F.S.

It follows that the equations of motion for flow in the liquid layer are the equations of motion for a homogeneous incompressible liquid with a temperature dependent viscosity. The nature of the viscosity variation with temperature and the absence of a latent heat of melting make it unnecessary to consider a distinct liquid layer, and for purposes of analysis an ablating body of S.C.F.S. can be treated as being entirely liquid--the transition from liquid to solid being characterized by a continuous increase in viscosity.

### The Gas-Liquid Interface During Ablation

When silica vaporizes into air the  $\text{SiO}_2$  vapor dissociates to the extent that the partial pressure of  $\text{SiO}$  is considerably larger than the partial pressure of  $\text{SiO}_2$  at the surface. The details of the surface chemistry are not well known for this type of surface-gas phase reaction and a rigorous treatment of the vaporization process would require more than a superficial knowledge of the chemical kinetics of the several chemical reactions which are possible at the surface. In studies of surface-gas phase reactions, several authors (33,34) have assumed that the surface is in chemical equilibrium with the gas phase. The assumption of chemical equilibrium at the surface will be made here except when nonequilibrium vaporization is considered. In the case of nonequilibrium vaporization, it will be assumed that the gas phase is in chemical equilibrium within one mean free path of the surface, but not necessarily in equilibrium with the surface itself. It might first appear that the assumption of chemical equilibrium in the gas phase near the surface would be paradoxical in the case of nonequilibrium vaporization; however, such is not the case since the kinetics of the vaporization process and the kinetics of chemical reactions in the gas phase are two separate phenomena and are not necessarily related.

The following result can be derived from kinetic theory (11) and is applicable to the nonequilibrium vaporization of an element or compound in the absence of chemical reactions:

$$P_{sv} - P_v = \frac{1}{a_c} \sqrt{2\pi R_u T/M} \dot{m}_v \quad (3-2)$$

where

$T$  = absolute temperature of surface

$\bar{M}$  = molecular weight of vaporizing component

$\dot{m}_v$  = net rate of mass transfer from surface

$\bar{R}_u$  = universal gas constant

$p_v$  = partial pressure of vaporizing component

$p_{sv}$  = saturation pressure of vaporizing component corresponding to the temperature  $T$

$a_c$  = evaporation or accommodation coefficient

Normally the accommodation coefficient  $a_c$  is experimentally determined and it can be shown that it is bounded in the manner

$$0 < a_c \leq 1$$

Note that  $p_v$  is always less than  $p_{sv}$  if there is a net mass transfer from the surface. This result is frequently referred to as the Hertz-Knudsen-Langmuir relation for nonequilibrium vaporization. Since silica dissociates to a large degree upon vaporization, this relation cannot be applied directly without modification.

Polezhaev (35) treated nonequilibrium vaporization by modifying the Hertz-Knudsen-Langmuir relation in the following manner. He assumed that during the heating and vaporization process there are no chemical transformations. That is, insofar as vaporization is concerned, the material behaves as a pure element. Thermodynamic equilibrium in the gas phase within one mean free path of the surface is also assumed. It follows that Equation (3-2) is applicable to this situation if  $p_v$  is

taken to be the partial pressure of  $\text{SiO}_2$  vapor alone and  $p_{sv}$  is taken to be the saturation pressure of  $\text{SiO}_2$  at the temperature  $T$ . Polezhaev indicates that the molecular weight  $\bar{M}$  in the Hertz-Knudsen-Langmuir relation should be the molecular weight of the evaporating vapor. That is

$$\bar{M}_{ec} = \bar{M}_{\text{SiO}_2} \frac{P_{\text{SiO}} + P_{\text{SiO}_2}}{P_{\text{SiO}_2s}} \quad (3-3)$$

where

- $\bar{M}_{ec}$  = mol wt of evaporating vapor
- $P_{\text{SiO}}$  = partial pressure of  $\text{SiO}$  vapor
- $P_{\text{SiO}_2}$  = partial pressure of  $\text{SiO}_2$  vapor
- $P_{\text{SiO}_2s}$  = saturation pressure of  $\text{SiO}_2$  vapor at the surface temperature

However, it is believed that within the framework of the assumptions made, the correct molecular weight to be used in Equation (3-2) for vaporizing silica is the molecular weight of  $\text{SiO}_2$ .

The molecular weight of  $\text{SiO}_2$  will be used in Equation (3-2) for the nonequilibrium calculations made in this investigation.

The model of nonequilibrium vaporization of silica proposed by Polezhaev has not been experimentally verified; however, it does provide a means for theoretical analysis of the nonequilibrium vaporization process and will be used here in the portion of the analysis that considers nonequilibrium vaporization. The accommodation coefficient  $a_c$  will be taken to be unity in most of the numerical calculations since there are no data available for vaporizing silica. It should be pointed

out that this choice of  $a_c$  gives an upper bound on the rate of vaporization, and if nonequilibrium vaporization is significant for  $a_c = 1$ , then it will be even more important for lower values of  $a_c$ . Some results of calculations for a range of values for  $a_c$  will also be given in order to illustrate the effect of  $a_c$  on nonequilibrium vaporization and ablation.

#### Thermal Radiation

Although S.C.F.S. is opaque to thermal radiation below its softening temperature, it behaves as a semi-transparent material at temperatures higher than its softening temperature. That is, thermal radiation is emitted, scattered and absorbed within the material; thus, under ablating conditions, S.C.F.S. radiates in depth.

Studies of the optical and total radiation temperatures of S.C.F.S. under ablating conditions (27,28,29) indicate that the net radiation from the ablating body can be estimated from the formula

$$\dot{q}_R = \sigma \epsilon_R T^4 \quad (3-4)$$

where

$\sigma$  = Stefan Boltzmann constant

$T$  = surface temperature

$\epsilon_R$  = emissivity

The apparent emissivity of S.C.F.S. as a function of temperature is given in reference 27. Below the softening temperature the emissivity of S.C.F.S. is between 0.6 and 0.7 and above the softening temperature the emissivity is between 0.3 and 0.4. For the cases considered in this

study, radiation will not be important when the surface temperature is below the softening temperature; therefore, the emissivity will be assumed to be constant and equal to 0.3 for all calculations involving thermal radiation.

Although no solution for the problem is offered, it should be pointed out that even though Equation (3-4) gives a reasonably reliable way of estimating the net radiation from the ablating body, the thermal radiation has other effects which cannot be accounted for by using this equation. The most important effect would appear to be the influence of radiation in depth on the temperature distribution, and therefore, the influence on the ablation rate.

## CHAPTER IV

## THEORETICAL ANALYSIS

In this chapter a theory is developed for the ablation of S.C.F.S. in air and in an oxy-hydrogen rocket motor exhaust. The analysis presented here is restricted to the stagnation point of an axially symmetric body at zero angle of attack. Behavior at a stagnation point is of interest for a number of reasons. Since the flow in the neighborhood of a stagnation point is laminar, it lends itself readily to analytical treatment. Only one geometric parameter of the body needs to be specified for a stagnation point analysis, namely the radius of curvature at the stagnation point; whereas, analysis of points away from the stagnation point requires complete specification of the body shape. The measured ablated depth at the stagnation point may be readily compared to the theoretical predictions. Experimental and analytical results for stagnation point ablation provide an insight into the mechanism of ablation and provide information necessary for predicting the ablation at any point on a given body.

The analysis of the ablation of S.C.F.S. to follow is made within the framework of the assumptions set forth in Chapter III. The first portion of the analysis is concerned with the melt-flow problem, and the second portion is concerned with the gas boundary layer adjacent to the vaporizing silica.

### Melting Ablation

Since silica does not have a latent heat of melting and its viscosity increases rapidly with decreasing temperature, it is not essential to consider separately the liquid and solid regions in an analysis of the ablation of S.C.F.S. Examination of the equations of motion governing the problem at hand shows that each term in the momentum and continuity equations of the melt layer approaches zero continuously as the solid region is approached. Furthermore, the energy equation is essentially the same for both regions. Thus, for purposes of analysis both the liquid and solid regions can be treated as one liquid region--the transition from liquid to solid being characterized by an increase in viscosity.

### Equations

Since the flow is restricted to a thin region near the gas-liquid interface, the flow is of the boundary layer type and the equations are the momentum, energy and continuity boundary layer equations for a homogeneous incompressible fluid having a temperature-dependent viscosity. The density, thermal conductivity and specific heat are taken to be constant in this analysis. Since the motion is very slow, viscous dissipation is negligible. A derivation of the equations of motion is given by Adams (36), and with reference to the coordinate system illustrated in Figure 1 on page 20, the equations are as follows:

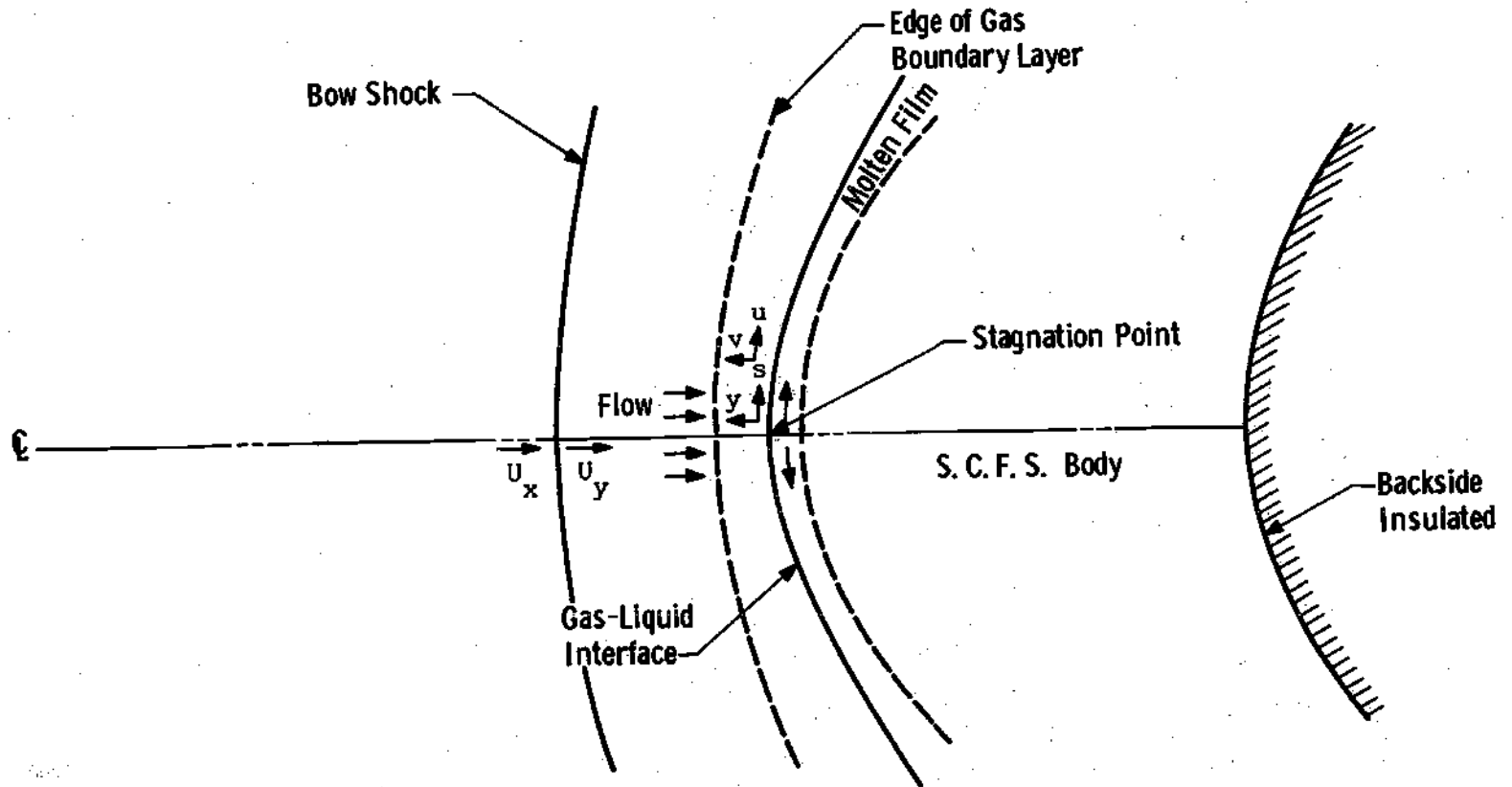


Figure 1. Coordinate System for Melt Layer and Gas Boundary Layer

Continuity

$$\frac{\partial(su)}{\partial s} + \frac{\partial(sv)}{\partial y} = 0 \quad (4-1)$$

Momentum

$$\frac{\partial u}{\partial t} + u \frac{\partial u}{\partial s} + v \frac{\partial u}{\partial y} = - \frac{1}{\rho_s} \frac{dp}{ds} + \frac{1}{\rho_s} \frac{\partial}{\partial y} \left( \mu_s \frac{\partial u}{\partial y} \right) \quad (4-2)$$

Energy

$$\frac{\partial T}{\partial t} + u \frac{\partial T}{\partial s} + v \frac{\partial T}{\partial y} = \alpha_s \frac{\partial^2 T}{\partial y^2} \quad (4-3)$$

The continuity Equation (4-1) is valid only near a stagnation point since the approximation  $\bar{r} \approx s$  has been introduced and valid only if the liquid layer is thin. The body force term due to acceleration of the body in the  $s$  direction has not been retained in Equation (4-2) since there is no acceleration of a body in the rocket exhaust, and for a blunt, axially symmetric body in flight at zero angle of attack, there is

no component of acceleration in the  $s$  direction at the stagnation point. For very slow motion the viscous forces predominate over the inertial forces and Equation (4-2) can be written

$$\frac{dp}{ds} = \frac{\partial}{\partial y} \left( \mu_s \frac{\partial u}{\partial y} \right) \quad (4-2a)$$

Near the axis of the body the temperature gradient in the axial direction is much greater than the temperature gradient in the radial direction. Considering that the axial velocity is of the same order of magnitude as the radial velocity, it follows that Equation (4-3) can be simplified to give

$$\frac{\partial T}{\partial t} + v \frac{\partial T}{\partial y} = \alpha_s \frac{\partial^2 T}{\partial y^2} \quad (4-3a)$$

Thus, Equations (4-1), (4-2a), and (4-3a) are the equations to be solved in this approach to the solution of melting ablation. These equations are virtually identical to the equations given by Fledderman and Hurwicz (16).

#### Boundary Conditions

The following boundary conditions are applicable to Equations (4-1), (4-2a) and (4-3a):

At  $y=0$

$$\frac{\partial u}{\partial y} = - \tau_w / \mu_s \quad (4-4a)$$

$$\frac{\partial T}{\partial y} = [-\dot{q}_w - \epsilon_R \sigma T_w^4 - (\rho_s v_w^-)(h_w - h(L))]/k_s \quad (4-4b)$$

$$T = T_w \quad (4-4c)$$

at  $y = -L(t)$

$$u = 0 \quad (4-5a)$$

$$\frac{\partial u}{\partial y} = 0 \quad (4-5b)$$

$$\frac{\partial u}{\partial s} = 0 \quad (4-5c)$$

$$\frac{\partial T}{\partial y} = 0 \quad (4-5d)$$

The boundary conditions (4-4a) and (4-4b) arise from the continuity of shear stress and energy at the gas-liquid interface, respectively.

Boundary conditions (4-5a) — (4-5c) are the result of assuming that the backside of the ablating body remains solid during ablation. It may be observed that the boundary condition (4-5d) on the temperature distribution corresponds to an insulated backside. During the initial phases of the present investigation it was thought that the choice of backside temperature condition might have considerable influence on the ablation rate for thin S.C.F.S. bodies. However, it was found that the influence of the backside temperature condition is small for bodies thick enough.

to be structurally practical; thus, the insulated backside condition is imposed here since it gives an upper bound on the rise in backside temperature with time for any practical choice of this condition.

#### Initial Conditions

Since Equations (4-1), (4-2a) and (4-3a) are time dependent, it is necessary to specify initial conditions on the equations. It is assumed that the body is initially at a uniform temperature low enough for the body to be solid. Thus, the initial conditions are as follows:

At  $t=0$

$$u = 0 \quad (4-6a)$$

$$v = 0 \quad (4-6b)$$

$$T = T_I \quad (4-6c)$$

The instantaneous thickness  $L(t)$  is given by the quadrature

$$L(t) = L_0 - \int_0^t v_{-L}(t') dt' \quad (4-7)$$

#### Method of Solution

Equations (4-1), (4-2a) and (4-3a) together with the prescribed boundary and initial conditions constitute a nonlinear two point boundary value problem. No general closed form solution is known for this boundary value problem. Attempts to find a general closed form solution are hampered by the complexity of the boundary conditions and the floating

boundary caused by the ever decreasing thickness. The most straightforward approach to the solution of this problem is a numerical integration of the partial differential equations on a high speed digital computer. However, the approach taken here is a combination of an approximate closed form solution and a numerical integration. It was found that the computing time necessary for numerical integration of Equations (4-1), (4-2a) and (4-3a) altogether is an order of magnitude greater than the computing time necessary to integrate the equations using this approach and with little increase in accuracy. It was felt that the slightly greater accuracy of the numerical integration altogether could not be justified for the present study.

Following the approach used by Bethe and Adams (2), Equation (4-2a) can be integrated twice to give the quadrature

$$u = -\tau_w \int_{-L(t)}^y \frac{dn'}{\mu_s} + \frac{dp}{ds} \int_{-L(t)}^y \frac{n'}{\mu_s} dn' \quad (4-8)$$

Using Equation (4-8) the continuity Equation (4-1) can be integrated to give

$$v = v_w - 2 \frac{d\tau_w}{ds} \int_0^y \int_{-L(t)}^{n'} \frac{1}{\mu_s} dn'' dn' + 2 \frac{d^2 p}{ds^2} \int_0^y \int_{-L(t)}^{n'} \frac{n''}{\mu_s} dn'' dn' \quad (4-9)$$

Over a limited temperature range, the Arrhenius-type viscosity temperature equation of silica can be approximated by (2)

$$\mu_s = \mu_s(T'_0) \left( \frac{T'}{T'_0} \right)^{n'} \quad (4-10)$$

where

$$n' = \frac{C_1}{T'_0} \quad (4-10a)$$

This approximation is acceptable for use here since the flow is confined to a thin layer in which the temperature changes by less than 10 per cent if  $T'_0$  is taken to be the surface temperature. In terms of Equation (4-10), Equation (4-9) is

$$v = v_w^- - \left\{ 2 \frac{d\tau_w}{ds} \int_0^y \int_{-L(t)}^{n'} \left( \frac{T}{T_w} \right)^{n'} d\eta'' d\eta' \right. \quad (4-11)$$

$$\left. - 2 \frac{d^2 p}{ds^2} \int_0^y \int_{-L(t)}^{n'} \left( \frac{T}{T_w} \right)^{n'} \eta'' d\eta'' d\eta' \right\}$$

Equation (4-11) depends only on the instantaneous temperature distribution and boundary conditions. For large viscosity index  $n'$ , the integrals in Equation (4-11) depend primarily on the temperature distribution near the surface. In order to demonstrate this point, the integrals in Equation (4-11) will be evaluated for two widely different temperature distributions and it will be observed that there is relatively little difference in the velocity  $v_{-L}(t)$  given by the different distributions. It is assumed that the temperature distribution near the surface of

the ablating body is linear then

$$T = T_w (1 + y/\delta_T) \quad (4-12)$$

where

$$\delta_T = \frac{k_s T_w}{\dot{q}_w + \epsilon_R \sigma T_w^4 + (\rho_s \bar{v}_w)(h_w - h(L))} \quad (4-13)$$

For depths greater than  $\delta_T$  the temperature is assumed to be zero.

Equation (4-11) can be formally integrated using Equation (4-12) to give

$$v_{-L} = \bar{v}_w + \frac{2\delta_T^2}{\mu_s(T_w)(n'+1)(n'+2)} \left\{ \frac{d\tau_w}{ds} + \frac{2\delta_T}{n'+3} \frac{d^2p}{ds^2} \right\} \quad (4-14)$$

For the exponential temperature distribution

$$T = T_w e^{y/\delta_T} \quad (4-15)$$

where  $\delta_T$  is given by Equation (4-13), Equation (4-11) becomes

$$v = \bar{v}_w + \frac{2\delta_T^2}{\mu_s(T_w)n'^2} \left\{ (1 - e^{-\frac{n'y}{\delta_T}}) \frac{d\tau_w}{ds} + \frac{\delta_T}{n'} (2(1 - e^{-\frac{n'y}{\delta_T}}) + \frac{n'y}{\delta_T} e^{-\frac{n'y}{\delta_T}}) \frac{d^2p}{ds^2} \right\} \quad (4-16)$$

It follows that

$$v_{-L} = v_w^- + \frac{2\delta_T^2}{\mu_s(T_w)n'^2} \left\{ \frac{dT_w}{ds} + \frac{2\delta_T}{n'} \frac{d^2p}{ds^2} \right\} \quad (4-16a)$$

For a large viscosity index  $n'$  Equations (4-14) and (4-16a) are essentially equivalent. For a surface temperature less than 5000 °R, the viscosity index of silica is greater than 20; thus, the difference in velocity computed from Equations (4-14) and (4-16a) is less than 20 per cent for the same surface temperature. Applied to a specific ablation problem, the difference will actually be much lower than this because of an adjustment in the surface temperature (37). Bethe and Adams (2) have shown that the temperature distribution at steady state is approximately exponential. Therefore, Equation (4-16) will be used as the solution to Equations (4-1) and (4-2a) in solving the energy Equation (4-3a).

Equation (4-3a) was solved numerically on a digital computer. If the partial derivatives are replaced by finite difference quotients in the same manner as given by Adams in reference 36, Equation (4-3a) becomes

$$\frac{T_y^{t+\Delta t} - T_y^t}{\Delta t} + v_y^t \frac{T_{y+\Delta y}^t - T_{y-\Delta y}^t}{2\Delta y} = \alpha_s \frac{T_{y+\Delta y}^t - 2T_y^t + T_{y-\Delta y}^t}{\Delta y^2} \quad (4-17)$$

The boundary condition at the gas-liquid interface for Equation (4-17) is obtained by writing Equation (4-4b) in finite difference form and is

$$\frac{T_{\Delta y}^{t+\Delta t} - T_o^{t+\Delta t}}{\Delta y} = \left[ - \dot{q}_w - \epsilon_R \sigma T_w^4 - (\rho_s v_w^-)(h_w - h(L)) \right] / k_s \quad (4-18)$$

The convergence and stability of the numerical solution to Equation (4-17) is discussed in Appendix B. In order to obtain an estimate of the accuracy of the overall computer program, an exact closed form solution to a hypothetical ablation problem was constructed and compared to the computer solution of the same problem. The solution to this hypothetical ablation problem is given in Appendix C along with the results of the comparison.

#### The Gas Boundary Layer

The solution to the laminar boundary layer equations for a chemically reacting surface has been investigated by a number of authors. Lees (33) considered the combustion of a pure element by surface reaction at the interface between a solid element and air. Bowen and Gorton (38) modified the approach used by Lees and derived a result which is applicable to both compound and pure element surfaces undergoing surface reactions in air. Scala (12) studied the vaporization of a class of refractory oxides into an air boundary layer.

The following analysis treats the surface reaction of a silica surface with an air boundary layer and also an oxy-hydrogen boundary

layer.\* The analysis assumes in either of the cases considered that the boundary layer is either frozen, that is, no chemical reactions occur in the boundary layer, or that the Lewis number is unity. All species are assumed to be perfect gases having temperature dependent specific heats. In order to make the treatment of ordinary diffusion tractable, an effective binary mixture is assumed (33), that is, all binary diffusivities are assumed equal. This assumption is not very good for mixtures containing relatively large amounts of species having widely different molecular weights. All species considered in this analysis have approximately the same molecular weights with the exception of  $\text{SiO}_2$  and  $\text{H}_2$ , and the concentrations of these species are small for all cases considered.

#### Boundary Layer Equations and Boundary Conditions

The derivation of the boundary layer equations from the more general equations of motion for a viscous compressible chemically reacting fluid and their validity has been discussed in detail in references 33 and 39. Therefore, it is appropriate here to omit the derivation of the equations and start with the general laminar boundary layer equations as given in (39). The equations for axially symmetric flow are given below. The coordinate system used is illustrated in

---

\*As mentioned in Chapter I, the available test facility for the experimental studies was a small oxy-hydrogen rocket motor. Due to the mixing of the exhaust with air, nitrogen is introduced into the exhaust stream; however, for convenience the environment in the rocket exhaust will simply be referred to as the oxy-hydrogen environment and the gas boundary layer that exists adjacent to a body in the exhaust as the oxy-hydrogen boundary layer although nitrogen is also present and will be considered.

Figure 1 on page 20.

Mass Continuity

$$\frac{\partial(\bar{r}\rho u)}{\partial s} + \frac{\partial(\bar{r}\rho v)}{\partial y} = 0 \quad (4-19)$$

Momentum

$$\rho u \frac{\partial u}{\partial s} + \rho v \frac{\partial u}{\partial y} = \frac{\partial}{\partial y} \left( \mu \frac{\partial u}{\partial y} \right) - \frac{\partial p}{\partial s} \quad (4-20)$$

Energy

$$\rho u \frac{\partial I}{\partial s} + \rho v \frac{\partial I}{\partial y} = \frac{\partial}{\partial y} \left[ \frac{\mu}{Pr} \frac{\partial I}{\partial y} + \mu \left( 1 - \frac{1}{Pr} \right) \frac{1}{2} \frac{\partial u^2}{\partial y} \right] \quad (4-21)$$

$$- \frac{\partial}{\partial y} \left[ \left( \frac{1}{Le} - 1 \right) \rho D_{12} \left[ h_i \frac{\partial c_i}{\partial y} \right] \right]$$

Species Continuity

$$\rho u \frac{\partial c_i}{\partial s} + \rho v \frac{\partial c_i}{\partial y} = \frac{\partial}{\partial y} \left( \rho D_{12} \frac{\partial c_i}{\partial y} \right) + \dot{\omega}_i \quad (4-22)$$

The applicable boundary conditions are as follows

at  $y = 0$

$$u = 0^*$$

---

\* Although  $u$  is not identically zero when there is melt flow, Lees (3) has shown that the low velocity at the gas-liquid interface has negligible influence on the gas boundary and for purposes of analysis  $u$  can be taken to be zero.

$$v = v_w^+ \quad (4-23b)$$

$$I = h_w \quad (4-23c)$$

$$c_i = c_{i_w} \quad (4-23d)$$

as  $y \rightarrow \infty$

$$u = u_e \quad (4-24a)$$

$$I = I_e \quad (4-24b)$$

$$c_i = c_{i_e} \quad (4-24c)$$

#### Compatibility Relations for Surface Species

If a closed vessel contains a number of gaseous species which may interact chemically and if the gases in the vessel are in chemical equilibrium at a given temperature and pressure, the mole fractions of each species can be calculated in principle, providing the total mass of each element is known. A similar situation exists in regard to calculating the mass fractions of the species present near the surface when silica vaporizes into a gas boundary layer. Additional equations to the equations of chemical equilibrium are needed to completely determine the species' mass fractions. These equations are compatibility equations and are obtained by considering the diffusion and convection in the boundary layer itself. The technique followed is similar to the

technique used by Bowen and Gorton (38) in their study of the combustion of boron nitride.

Silica Vaporizing into Air. Schick (24) compiled the results of a number of studies of the interaction of silica with air at elevated temperatures. The results of the studies indicate that the principal species present are  $\text{SiO}_2$ ,  $\text{SiO}$ ,  $\text{N}_2$ ,  $\text{O}_2$ , and  $\text{O}$ . The analysis here will consider only these species. The elemental mass fractions may be calculated in the following manner:

$$\bar{c}_{\text{Si}} = \frac{\bar{M}_{\text{Si}}}{\bar{M}_{\text{SiO}_2}} c_{\text{SiO}_2} + \frac{\bar{M}_{\text{Si}}}{\bar{M}_{\text{SiO}_2}} c_{\text{SiO}_2} \quad (4-25a)$$

$$\bar{c}_{\text{O}} = c_{\text{O}} + c_{\text{O}_2} + \frac{\bar{M}_{\text{O}_2}}{\bar{M}_{\text{SiO}_2}} c_{\text{SiO}_2} + \frac{\bar{M}_{\text{O}}}{\bar{M}_{\text{SiO}}} c_{\text{SiO}} \quad (4-25b)$$

$$\bar{c}_{\text{N}} = c_{\text{N}_2} \quad (4-25c)$$

In terms of elemental mass fractions the diffusion equations can be written as below. There is no production term since elements must be conserved in chemical reactions.

$$\rho u \frac{\partial \bar{c}_{\text{Si}}}{\partial s} + \rho v \frac{\partial \bar{c}_{\text{Si}}}{\partial y} = \frac{\partial}{\partial y} \left( \rho D_{12} \frac{\partial \bar{c}_{\text{Si}}}{\partial y} \right) \quad (4-26a)$$

$$\rho u \frac{\partial \bar{c}_{\text{O}}}{\partial s} + \rho v \frac{\partial \bar{c}_{\text{O}}}{\partial y} = \frac{\partial}{\partial y} \left( \rho D_{12} \frac{\partial \bar{c}_{\text{O}}}{\partial y} \right) \quad (4-26b)$$

$$\rho u \frac{\partial \bar{c}_N}{\partial s} + \rho v \frac{\partial \bar{c}_N}{\partial y} = \frac{\partial}{\partial y} \left( \rho D_{12} \frac{\partial \bar{c}_N}{\partial y} \right) \quad (4-26c)$$

For convenience the following new variables are defined:

$$\phi_{Si} = \frac{\bar{c}_{Si} - \bar{c}_{Si_w}}{\bar{c}_{Si_e} - \bar{c}_{Si_w}} \quad (4-27a)$$

$$\phi_0 = \frac{\bar{c}_0 - \bar{c}_{0_w}}{\bar{c}_{0_e} - \bar{c}_{0_w}} \quad (4-27b)$$

$$\phi_N = \frac{\bar{c}_N - \bar{c}_{N_w}}{\bar{c}_{N_e} - \bar{c}_{N_w}} \quad (4-27c)$$

The boundary conditions on these new variables are identical, namely

at  $y=0$

$$\phi_{Si} = \phi_0 = \phi_N = 0 \quad (4-28a)$$

as  $y \rightarrow \infty$

$$\phi_{Si} = \phi_0 = \phi_N = 1 \quad (4-28b)$$

If the diffusion Equations (4-26a), (4-26b) and (4-26c) are written in terms of the new variables, it becomes obvious that all of the new variables must satisfy the same differential equation, and since they

satisfy the same boundary conditions also, they must be equal. That is,

$$\phi_{\text{Si}} = \phi_0 = \phi_{\text{N}} \quad 0 \leq y < \infty \quad (4-29)$$

It follows that

$$\frac{\left. \frac{\partial \bar{c}_{\text{Si}}}{\partial y} \right|_w}{\bar{c}_{\text{Si}_e} - \bar{c}_{\text{Si}_w}} = \frac{\left. \frac{\partial \bar{c}_0}{\partial y} \right|_w}{\bar{c}_{0_e} - \bar{c}_{0_w}} = \frac{\left. \frac{\partial \bar{c}_{\text{N}}}{\partial y} \right|_w}{\bar{c}_{\text{N}_e} - \bar{c}_{\text{N}_w}} \quad (4-29a)$$

The diffusion equation for an effective binary mixture written in terms of the element mass fractions yields

$$\bar{n}_{\text{Si}_w} = -\rho D_{12} \left. \frac{\partial \bar{c}_{\text{Si}}}{\partial y} \right|_w + (\bar{c}_{\text{Si}} \bar{n})_w \quad (4-30a)$$

and

$$\bar{n}_{0_w} = -\rho D_{12} \left. \frac{\partial \bar{c}_0}{\partial y} \right|_w + (\bar{c}_0 \bar{n})_w \quad (4-30b)$$

But

$$\bar{n}_{\text{Si}} = \frac{\bar{M}_{\text{Si}}}{\bar{M}_{\text{SiO}_2}} \bar{n}_w \quad (4-31a)$$

and

$$\bar{n}_O = \frac{\bar{M}_{O_2}}{\bar{M}_{SiO_2}} \bar{n}_w \quad (4-31b)$$

Combining Equations (4-29a) — (4-31b) leads to the result

$$\frac{\bar{c}_{N_e}}{\bar{c}_{O_e}} = \frac{1 - \bar{c}_{Si_w} - \bar{c}_{O_w}}{\bar{c}_{O_w} - \bar{M}_{O_2} \bar{c}_{Si_w} / \bar{M}_{SiO_2}} \quad (4-32a)$$

If the element mass fractions are written in terms of partial pressures, this result takes the form

$$\frac{\bar{c}_{N_e} \bar{M}_{O_2}}{\bar{c}_{O_e} \bar{M}_{N_2}} = \frac{P_{N_2_w}}{(P_{O_2} + \frac{1}{2} P_O - \frac{1}{2} P_{SiO})_w} \quad (4-32b)$$

It is interesting to note that Equation (4-32b) is equivalent to the equation derived by Hidalgo (6) in his study of the ablation of quartz without consideration of convection and diffusion in the boundary layer. This equation together with the equations of chemical equilibrium completely determines the concentrations of species at the surface for any given temperature and pressure if the gas phase is in chemical equilibrium with the surface. If the vaporization process is one of the nonequilibrium that is described by the model given in Chapter III, then Equations (3-1) and (4-32b) together with the equations of chemical equilibrium determine the species concentrations near the surface of the

vaporizing silica for any given temperature and pressure.

Silica Vaporizing into an Oxy-Hydrogen Environment. In their study of equilibrium between hydrogen gas and silica to 1926 °K, Tombs and Welch (40) observed only the gases  $\text{SiO}_2$ ,  $\text{H}_2\text{O}$ ,  $\text{H}_2$  and  $\text{SiO}$  to be present. This observation is supported in part by calculations made in Appendix D on page 150. The analysis given here assumes the following species to be present:  $\text{H}_2$ ,  $\text{H}$ ,  $\text{O}_2$ ,  $\text{O}$ ,  $\text{SiO}$ ,  $\text{SiO}_2$ ,  $\text{OH}$ , and  $\text{N}_2$ . Nitrogen must be considered since it is introduced into the test environment by the turbulent mixing of the rocket exhaust with the atmosphere (see Appendix A on page 117). Following the same approach as used above for silica vaporizing into air, the following compatibility equations can be derived for silica vaporizing into an oxy-hydrogen environment.

$$\frac{\bar{c}_{\text{O}_e}}{\bar{c}_{\text{N}_e}} = \frac{\bar{M}_{\text{O}_2} (p_{\text{O}_2} + \frac{1}{2} p_{\text{O}} + \frac{1}{2} p_{\text{OH}} + \frac{1}{2} p_{\text{H}_2\text{O}} - \frac{1}{2} p_{\text{SiO}})_w}{\bar{M}_{\text{N}_2} (p_{\text{N}_2})_w} \quad (4-33a)$$

$$\frac{\bar{c}_{\text{H}_e}}{\bar{c}_{\text{N}_e}} = \frac{\bar{M}_{\text{H}_2} (p_{\text{H}_2} + \frac{1}{2} p_{\text{H}} + \frac{1}{2} p_{\text{OH}} + p_{\text{H}_2\text{O}})_w}{\bar{M}_{\text{N}_2} (p_{\text{N}_2})_w} \quad (4-33b)$$

#### Transformation of the Boundary Layer Equations

It is convenient at this time to transform the boundary layer equations into a system of ordinary differential equations. The transformation of the boundary layer equations for the gas boundary layer is essentially the same as given by Dorrance (39) and is included here.

for the sake of completeness. Two cases will be considered, namely frozen flow and Lewis number equal to unity. For the latter case, it is not necessary to make any assumptions regarding reactions in the gas phase (33).

Frozen Flow. The Lees-Dorodnitsyn transformation variables and other convenient variables are defined as follows:

$$\eta = \frac{\rho_e u_e}{\sqrt{2\xi}} \int_0^y \frac{\rho}{\rho_e} dy \quad (4-34a)$$

$$\bar{s} = \int_0^s \rho_e \mu_e u_e \bar{r}^2 ds \quad (4-34b)$$

$$C = \rho \mu / \rho_e \mu_e \quad (4-34c)$$

$$f(\eta) = \bar{\psi}(s, y) / \sqrt{2\xi} \quad (4-34d)$$

where

$$\frac{\partial \bar{\psi}}{\partial y} = \rho u \bar{r} \quad (4-34e)$$

and

$$\frac{\partial \bar{\psi}}{\partial s} = -\rho v \bar{r} \quad (4-34f)$$

$$g_T(\eta) = \frac{h_T}{h_{T_e}} \quad (4-34g)$$

$$Z_i(\eta) = \frac{c_i}{c_{i_e}} \quad (4-34h)$$

The conditions under which the boundary layer equations possess similar solutions, that is, transform to ordinary differential equations have been discussed by Dorrance (39). For isoenergetic and frozen flow at the edge of the boundary layer, it can be shown that similarity does exist in the neighborhood of a stagnation point on a blunt body in axially symmetric flow. Therefore, the transformed equations for the frozen boundary layer at a stagnation point are (39).

Momentum

$$(Cf'')' + ff'' + 2[\rho_e/\rho - (f')^2] = 0 \quad (4-35a)$$

Energy

$$\left( \frac{C}{Pr} g_T' \right)' + f g_T' = 0 \quad (4-35b)$$

Diffusion

$$\left( \frac{C}{Sc} Z_i' \right)' + f Z_i' = 0 \quad (4-35c)$$

---

\* Primes refer to differentiation with respect to  $\eta$ .

The above equations contain the additional assumptions that the mass specific heats of all species are equal and that  $C$ ,  $Pr$  and  $Sc$  vary with  $\eta$  alone.

The transformed boundary conditions on the equations are

at  $\eta = 0$

$$f' = 0 \quad (4-36a)$$

$$f = f(0) \quad (4-36b)$$

$$Z_i = Z_i(0) \quad (4-36c)$$

$$g_T = g_T(0) \quad (4-36d)$$

as  $\eta \rightarrow \infty$

$$f' = 1 \quad (4-37a)$$

$$Z_i = 1 \quad (4-37b)$$

$$g_T = 1 \quad (4-37c)$$

Since Equation (4-35a) is coupled to Equations (4-35b) and (4-35c) through the dependence of  $C$  and  $\rho_e$  on  $g_T$ , it must be solved simultaneously with them. However, the solution to Equations (4-35b) and (4-35a) is by

quadrature

$$g_T = [1 - g_T(0)] \frac{G(n; f(0); Pr)}{G(\infty; f(0); Pr)} - g_T(0) \quad (4-38a)$$

and

$$Z_i = [1 - Z_i(0)] \frac{G(n; f(0); Sc)}{G(\infty; f(0); Sc)} - Z_i(0) \quad (4-38b)$$

where

$$G(n; f(0); \Lambda) = \int_0^n \frac{\Lambda}{C} \exp\left(-\int_0^{n'} \frac{\Lambda}{C} f dn''\right) dn' \quad (4-39)$$

The function  $G(n; f(0); \Lambda)$  is the same as the function  $G(n; f(0); Z)$  given by Dorrance (39). It follows that

$$g_T'(0) = \left(\frac{Pr}{C}\right)_w \frac{1 - g_T(0)}{G(\infty; f(0); Pr)} \quad (4-40a)$$

and

$$Z_i'(0) = \left(\frac{Sc}{C}\right)_w \frac{1 - Z_i(0)}{G(\infty; f(0); Sc)} \quad (4-40b)$$

Unity Lewis Number. Following the same approach as was used for the frozen boundary layer, it can be shown that

$$g'(0) = \left(\frac{Pr}{C}\right)_w \frac{1 - g(0)}{G(\infty; f(0); Pr)} \quad (4-41a)$$

and

$$\bar{Z}'_i(0) = \left(\frac{Sc}{C}\right)_w \frac{1 - \bar{Z}_i(0)}{G(\infty; f(0); Sc)} \quad (4-41b)$$

where

$$g(\eta) = \frac{I}{I_e} \quad (4-42a)$$

and

$$\bar{Z}_i(\eta) = \frac{c_i}{c_{i_e}} \quad (4-42b)$$

### Surface Heat Transfer

The net energy transfer to the surface by conduction and mass transfer is

$$-\dot{q}_w = \lambda \left(\frac{\partial T}{\partial y}\right)_w - \sum_i (n_i h_i)_{i_w} \quad (4-43a)$$

or

$$-\dot{q}_w = \left(\frac{C}{Pr}\right)_w \frac{\rho_e u_e u_e \bar{r}}{\sqrt{2S}} [h_{T_e} g'_T(0) + Le \sum_i h_{i_w} c_{i_e} Z'_i(0)] \quad (4-43b)$$

The Stanton number with mass transfer is defined as

$$C_H = \frac{\mu_e \bar{r}}{\sqrt{2\bar{s}} G(\infty; f(0); Pr)} \quad (4-44a)$$

and without mass transfer as

$$C_{H_0} = \frac{\mu_e \bar{r}}{\sqrt{2\bar{s}} G(\infty; 0; Pr)} \quad (4-44b)$$

Since  $\bar{s}$  is zero at the stagnation point, the Stanton number is not defined, in the mathematical sense, there. However, as will be seen below, the Stanton number always appears in a product with  $u_e$ , which is zero at the stagnation point, and the product of the Stanton number with  $u_e$  is defined and finite at the stagnation point. For the frozen boundary layer, the following result can be derived by combining Equations (4-40a), (4-43b) and (4-44a):

$$-\dot{q}_w = C_H \rho_e u_e (I_e - h_w) \left[ 1 + \frac{G(\infty; f(0); Pr)}{G(\infty; f(0); Sc)} \frac{\sum (c_{i_e} - c_{i_w}) h_{i_e}^0}{I_e - h_w} \right] \quad (4-45a)$$

In a like manner, for a Lewis number equal unity, the surface heat transfer can be written as

$$-\dot{q}_w = C_H \rho_e u_e (I_e - h_w) \quad (4-45b)$$

It should be again remarked that no assumptions regarding chemical reactions in the gas phase had to be made in order to arrive at Equation

(4-45b).

Surface Mass Transfer

The net mass loss of surface material by vaporization must be the sum of the mass loss of elements Si and O. By writing the diffusion equation in terms of element mass fractions, the following can be derived:

$$\bar{n}_w = -\rho D_{12} \left( \frac{\partial \bar{c}_{Si}}{\partial y} + \frac{\partial \bar{c}_O}{\partial y} \right) + (\bar{c}_{Si} + \bar{c}_O) \bar{n}_w \quad (4-46)$$

From Equation (4-40b) it follows that the mass transfer into the frozen boundary layer is given by the expression

$$(\rho v)_w^+ = \frac{(\bar{c}_{Si} + \bar{c}_O)_e - (\bar{c}_{Si} + \bar{c}_O)_w}{1 - (\bar{c}_{Si} + \bar{c}_O)_w} \frac{\rho_e u_e \bar{r}}{\sqrt{2S} G(\infty; f(0); Sc)} \quad (4-47a)$$

or

$$(\rho v)_w^+ = \frac{(\bar{c}_N)_e - (\bar{c}_N)_w}{(\bar{c}_N)_w} \rho_e u_e C_H \frac{G(\infty; f(0); Pr)}{G(\infty; F(0); Sc)} \quad (4-47b)$$

For a Lewis number of unity, Equation (4-41b) can be used to show that the mass transfer is

$$(\rho v)_w^+ = \frac{(\bar{c}_{Si} + \bar{c}_O)_e - (\bar{c}_{Si} + \bar{c}_O)_w}{1 - (\bar{c}_{Si} + \bar{c}_O)_w} \frac{\rho_e u_e \bar{r}}{\sqrt{2S} G(\infty; f(0); 1)} \quad (4-48a)$$

or

$$(\rho v)_w^+ = \frac{(\bar{c}_N)_e - (\bar{c}_N)_w}{(\bar{c}_N)_w} \rho_e u_e C_H \quad (4-48b)$$

### Surface Shear Stress

The surface shear stress is given by the expression

$$\tau_w = -\mu_w \left. \frac{\partial u}{\partial y} \right|_w^+ \quad (4-49a)$$

Combining Equations (4-34a), (4-34d) and (4-34e) with Equation (4-49a) gives

$$\tau_w = -\frac{C_w \rho_e u_e^2 \mu_e \bar{r} f''(0)}{\sqrt{2\xi}} \quad (4-49b)$$

as the surface shear stress for either case of frozen flow or a unity Lewis number. In terms of the Stanton number

$$\tau_w = -C_w \rho_e u_e^2 C_H G(\infty; f(0); Pr) f''(0) \quad (4-49c)$$

Clearly the shear stress is zero at the stagnation point since  $u_e$  is zero there. However, as was shown in Equation (4-16) it is the shear stress gradient at the stagnation point that determines the rate of melt flow there rather than the shear stress itself. From Equation (4-49c) it follows that

$$\frac{d\tau_w}{ds} = -C_w \rho_e u_e C_H G(\infty; f(0); Pr) f''(0) \frac{du_e}{ds} \quad (4-49d)$$

The Approximate Solution to the Transformed Boundary

Layer Equations by Analogy to Existing Solutions

In order to calculate the heat transfer, mass transfer and shear stress at the surface, the parameters  $C_H$ ,  $G(\infty; f(0); \Lambda)$  and  $f''(0)$  must first be known. The most obvious way to calculate these parameters is to solve the transformed boundary layer equations subject to their prescribed boundary conditions. The solution to the boundary layer equations could readily be handled by numerical integration on a digital computer; however, due to the assumptions made to simplify the equations and the uncertainty in the available transport property data, it is felt that nothing would be gained by exact solution over the simplified approach which follows.

The Effect of Mass Addition on Transport Processes at the

Interface. At hypersonic flight speeds and for a cold surface, Lees (41) showed that the effect of pressure gradient is small since  $f' \approx \rho_e/\rho$ . The effect of pressure gradient will be assumed to be negligibly small even at low supersonic Mach numbers such as expected in the oxy-hydrogen rocket motor test facility. This is justified to some extent by the relatively high temperatures in the rocket exhaust. Equation (4-35a) can then be written approximately

$$(Cf'')' + ff'' = 0 \quad (4-50a)$$

and by quadrature

$$f'(\eta) = \left(\frac{1}{C}\right)_w \frac{G(\eta; f(0); 1)}{G(\infty; f(0); 1)} \quad (4-50b)$$

It follows that

$$f''(0) = \left(\frac{1}{C}\right)_w \frac{1}{G(\infty; f(0); 1)}$$

The Equations (4-35b), (4-35c) and (4-50a) together with the boundary conditions for them are identical to the boundary layer equations and boundary conditions for compressible laminar flow over a flat plate with mass injection. Mickley, et al. (42) reported a solution to this system of equations wherein  $C$ ,  $Pr$  and  $Sc$  are taken as constant through the boundary layer. By calculating  $C$  according to the reference temperature concept of Young and Janssen or Eckert (39) the effect of variable  $\rho\mu$  through the boundary layer can be taken into account. It is felt that the solution of Mickley, et al. can be used with reasonable accuracy to obtain the ratio  $G(\infty; f(0); \Lambda)/G(\infty; f(0); Pr)$  and to determine the effect of mass addition on  $C_H$ , that is, to relate  $C_H$  to  $C_{H_0}$ .

An approximate correlation of the solution of reference 42 for moderate mass transfer rates yields

$$\frac{1}{G(\infty; f(0); \Lambda)} = \frac{\sqrt{C^*}}{2.11\Lambda^{2/3}} \left[ 1 + \Lambda^{2/5} f(0) \sqrt{\frac{2}{C^*}} \right] \quad (4-51a)$$

where  $C^*$  is  $C$  evaluated at the reference temperature. Equation (4-51a) is valid for any gas flowing in the boundary layer if the injected gas is the same as the gas in the boundary layer. If the injected gas is not the same as the gas flowing in the boundary layer, the results of Baron (43) indicate that Equation (4-51a) should be modified to (2)

$$\frac{1}{G(\infty; f(0); \Lambda)} = \frac{\sqrt{C^*}}{2.11\Lambda^{2/3}} \left[ 1 + \Lambda^{2/5} \bar{M}_v^{-1/4} f(0) \sqrt{\frac{2}{C^*}} \right] \quad (4-51b)$$

where  $\bar{M}_v$  is the ratio of the molecular weight of the gas flowing in the boundary layer to the molecular weight of the injected gas. Baron's study was made for nonreacting gases and since silica dissociates upon vaporization, there is some question as to what molecular weight ratio should be used in Equation (4-51b). It is reasonable to assume that the effective molecular weight of the injected gas mixture lies between the molecular weights of the lightest and heaviest species of vaporization. Since the ratio enters Equation (4-51b) raised to the one-fourth power, it is clear that the choice of molecular weight is not critical. Thus it is reasonable to take a weighted mass average for  $\bar{M}_v$  assuming that every molecule of silica that vaporizes dissociates to  $\text{SiO}$  and  $\text{O}_2$ . That is,

$$\bar{M}_v = \frac{2 \bar{M}_{\text{SiO}} + \bar{M}_{\text{O}_2}}{3 \bar{M}_m} \quad (4-51c)$$

where  $\bar{M}_m$  is the average molecular weight of the gas in the boundary layer.

From Equation (4-51b) it follows that

$$\frac{G(\infty; f(0); Pr)}{G(\infty; f(0); Sc)} = Le^{2/3} \frac{1 + Sc^{2/5} \bar{M}_v^{1/4} f(0) \sqrt{\frac{2}{C^*}}}{1 + Pr^{2/5} \bar{M}_v^{1/4} f(0) \sqrt{\frac{2}{C^*}}} \quad (4-52a)$$

for the frozen boundary layer. For low mass transfer rates or a Lewis number near unity\*,

$$\frac{G(\infty; f(0); Pr)}{G(\infty; f(0); Sc)} = Le^{2/3} \quad (4-52b)$$

From Equations (4-34a), (4-34b), (4-34d) and (4-34f)

$$(\rho v)_w^+ = - \frac{\rho_e u_e \mu_e \bar{r} f(0)}{\sqrt{2\xi}} \quad (4-53)$$

Combining Equations (4-44b), (4-51b) and (4-53) yields

$$\sqrt{\frac{2}{C^*}} f(0) = - \frac{\sqrt{2}}{2.11} \frac{(\rho v)_w^+}{\rho_e u_e C_H} \quad (4-54)$$

Now using Equations (4-44a), (4-44b), (4-51b) and (4-54) it follows

---

\* Assuming  $\bar{M}_v^{1/4} f(0) \sqrt{\frac{2}{C^*}} = \frac{1}{4}$  which would correspond to quite large rates of mass addition and taking values of 1.5 and 0.5 for the Pr and Sc, respectively, which corresponds to a Le = 3, the difference in Equations (4-51a) and (4-51b) is less than 20 per cent.

that

$$C_H = C_{H_0} \left( 1 + 0.67 \text{Pr}^{-\frac{4}{15}} \bar{M}_v^{\frac{1}{4}} \frac{(\rho v)_w^+}{\rho_e u_e C_{H_0}} \right) \quad (4-55)$$

But

$$\rho_e u_e C_{H_0} = \left\{ \left[ 1 + (\text{Le}^{2/3} - 1) \frac{\sum_i h_i^0 (c_{i_e} - c_{i_w})}{I_e - h_w} \right]^{-1} \right\} \frac{-\dot{q}_{w_0}}{I_e - h_w} \quad (4-56)$$

It is convenient to introduce the following approximation from Equation (4-56)

$$\rho_e u_e C_{H_0} = \frac{-\dot{q}_{w_0}}{I_e - h_w} \quad (4-57)$$

This approximation is justified since the mass addition is a secondary rather than primary effect and the factor in the braces of Equation (4-56) is usually near unity for the vaporization of silica (see Chapter VI). Substituting Equation (4-57) into Equation (4-55) yields

$$C_H = C_{H_0} \left( 1 - 0.67 \text{Pr}^{-\frac{4}{15}} \bar{M}_v^{\frac{1}{4}} \frac{(\rho v)_w^+ (I_e - h_w)}{-\dot{q}_{w_0}} \right) \quad (4-58)$$

Thus

$$\frac{-\dot{q}_w}{I_e - h_w} = \rho_e u_e C_{H_o} \psi(\text{Pr}) \left[ 1 + (\text{Le}^{2/3} - 1) \frac{\sum_i h_i^o (c_{i_e} - c_{i_w})}{I_e - h_w} \right], \quad (4-59a)$$

$$-\frac{\frac{dr_w}{ds}}{\frac{du_e}{ds}} = \rho_e u_e C_{H_o} \text{Pr}^{-2/3} \psi(1), \quad (4-59b)$$

and

$$(\rho v)_w^+ = \frac{(\bar{c}_N)_e - (\bar{c}_N)_w}{(\bar{c}_N)_w} \rho_e u_e C_{H_o} \text{Le}^{2/3} \psi(\text{Sc}) \quad (4-59c)$$

where

$$\psi(\Lambda) = 1 - 0.67\Lambda^{-\frac{4}{15}} \frac{1}{\bar{M}_v} \frac{(\rho v)_w^+ (I_e - h_w)}{-\dot{q}_w} \quad (4-59d)$$

In a similar manner, it can be shown that the solution of Mickley, et al., yields the following relationships for a unity Lewis number:

$$\frac{-\dot{q}_w}{I_e - h_w} = \rho_e u_e C_{H_o} \psi(\text{Pr}) \quad (4-60a)$$

$$-\frac{\frac{dr_w}{ds}}{\frac{du_e}{ds}} = \rho_e u_e C_{H_2O} Pr^{-2/3} \psi(1) \quad (4-60b)$$

and

$$(\rho v)_w^+ = \rho_e u_e C_{H_2O} \frac{(\bar{c}_N)_e - (\bar{c}_N)_w}{(\bar{c}_N)_w} \psi(Sc) \quad (4-60c)$$

where  $\psi(\Lambda)$  is given by Equation (4-59d).

The Zero Mass Transfer Stanton Number. Fay and Riddell (44)

obtained a solution to the frozen boundary layer equations for air with zero mass addition by using approximate analytical expressions for  $C$  and  $\rho_e/\rho$  as functions of  $g_T$  to represent the experimental property data. Their solution corresponds to the solution to Equations (4-35a) and (4-35b) and their applicable boundary conditions with  $f(0) = 0$ . In terms of the Stanton number, the solution can be written

$$C_{H_2O} = 0.76 \left( \frac{\rho_w \mu_w}{\rho_e \mu_e} \right)^{0.1} \frac{\sqrt{\rho_e \mu_e}}{Pr^{0.6} \rho_e u_e} \sqrt{\left( \frac{du_e}{ds} \right)_{sp}} \quad (4-61)$$

Since the parameters  $C$  and  $\rho_e/\rho$  depend to a much greater degree on temperature than on concentrations of species in the boundary layer, Equation (4-61) is also valid for the unity Lewis number case. It is noted that the influence of surface conditions on the Stanton number as given by Equation (4-61) is small since the only influence is

reflected through the parameter  $\frac{\rho_w \mu_w}{\rho_e \mu_e}$  which appears raised to the 0.1 power in the equation.

Although Equation (4-61) was derived for air, it will be used here to predict the heat transfer to a calorimeter in the exhaust of the oxy-hydrogen rocket motor (see Appendix A) and in an indirect way, to calculate the stagnation point velocity gradient on a flat face body normal to the exhaust stream of the oxy-hydrogen rocket motor. The use of Equation (4-61) in the oxy-hydrogen environment is partially justified by the agreement between the Fay and Riddell solution for air and heat transfer experiments conducted in methane-air combustion products (45).

Correlations in Terms of the Cold Surface Heat Transfer. It is useful to express the surface heat transfer mass transfer and shear stress in terms of the cold surface heat transfer with no mass addition. For the frozen boundary layer, it will be assumed that

$$\frac{1 + (Le^{2/3} - 1) \sum_i h_i^o (c_{i_e} - c_{i_w}) / (I_e - h_{cw})}{1 + (Le^{2/3} - 1) \sum_i h_i^o (c_{i_e} - c_{i_w}) / (I_e - h_w)} = 1 \quad (4-62a)$$

and

$$\left( \frac{\rho_w \mu_w}{\rho_{cw} \mu_{cw}} \right)^{0.1} = 1^* \quad (4-62b)$$

---

\* To a first approximation  $\rho_w \mu_w / \rho_{cw} \mu_{cw} = \sqrt{T_{cw} / T_w}$ . For illustrative purposes assuming that  $T_w$  is greater than  $T_{cw}$  by a factor of ten, then it follows that  $(\rho_w \mu_w / \rho_{cw} \mu_{cw})^{0.1}$  differs from unity by less than 10 per cent which supports the assumption (4-62b).

There are several combinations of conditions under which the first assumption is valid.\* It follows that

$$\frac{\dot{q}_w}{I_e - h_w} = \frac{\dot{q}_{o,cw}}{I_e - h_w} \psi(\text{Pr}) \quad (4-63)$$

where

$$\psi(\text{Pr}) = 1 - 0.67 \text{Pr}^{-\frac{4}{15}} \bar{M}_v^{\frac{1}{4}} (\rho v)_w^+ \frac{I_e - h_{cw}}{-\dot{q}_{o,cw}} \quad (4-64)$$

In Chapter VI it is shown that for silica vaporizing into air,

$$\left| (Le^{2/3} - 1) \sum_i h_i^o (c_{i_e} - c_{i_w}) / (I_e - h_w) \right| \ll 1 \quad (4-65)$$

It follows that

$$\frac{\frac{dT_w}{ds}}{\frac{du_e}{ds}} \approx - \frac{-\dot{q}_{o,cw}}{I_e - h_{cw}} \text{Pr}^{-2/3} \psi(1) \quad (4-66)$$

and

---

\* In Chapter VI it is demonstrated that the factor  $\sum_i h_i^o (c_{i_e} - c_{i_w}) / (I_e - h_w)$  is virtually independent of surface temperature  $T_w$  for silica vaporizing into air over a wide range of stagnation pressures and enthalpies. This supports the use of Equation (4-61a).

$$(\rho v)_w^+ \approx - \frac{\dot{q}_{o,cw}}{I_e - h_{cw}} Le^{2/3} \frac{(\bar{c}_N)_e - (\bar{c}_N)_w}{(\bar{c}_N)_w} \psi(Sc) \quad (4-67)$$

It can be shown in a similar manner that Equations (4-63), (4-66) and (4-67) are also valid for the unity Lewis number case.

Thus, if the parameter  $\dot{q}_{o,cw} / (I_e - h_{cw})$  is known, for example from experimental measurements, it is not necessary to consider the details of the flow in the gas boundary layer in order to estimate the ablation rate of S.C.F.S. for this value of the parameter.

Comments on the Stagnation Point Velocity Gradient. For bodies having a finite radius of curvature at the stagnation point, the Newtonian approximation can be used to calculate the stagnation point velocity gradient. Thus

$$\left. \frac{du_e}{ds} \right|_{sp} = \sqrt{\frac{2(p_e - p_x)}{\rho_e}} / R \quad (4-68)$$

As is discussed in a later chapter, flat plates of S.C.F.S. run normal to the flow were used in the experimental ablation studies conducted in the exhaust of the oxy-hydrogen rocket motor test facility. In order to compare the theory developed in this chapter with the experimental results obtained, it is necessary to have an estimate of the velocity gradient at the stagnation point of an infinite flat plate normal to the exhaust stream. For bodies which do not have a finite

radius of curvature at the stagnation point, the Newtonian theory breaks down and cannot be used. It is interesting to note that the Newtonian theory predicts a velocity gradient of zero for the infinite flat plate which is obviously in error.

The physical situation in the rocket motor is the impingement of a small supersonic stream on an infinite flat plate normal to the stream. No analytical solution to this flow problem was found in the literature which could be used for this case. As an alternate solution, the following is proposed: For a unity Lewis number and the parameter  $\left(\frac{\rho_w h_w}{\rho_e \mu_e}\right)^{0.1}$  assumed to be unity, Fay and Riddell's correlation (44) is:

$$-\dot{q}_w = 0.76 \text{Pr}^{-0.6} \sqrt{\rho_e \mu_e} (I_e - h_w) \sqrt{\left(\frac{du_e}{ds}\right)_{sp}} \quad (4-69a)$$

The applicability of this equation in the environment of the rocket exhaust was discussed earlier. Equation (4-69a) can be rewritten to give

$$\left(\frac{du_e}{ds}\right)_{sp} = \left[ \frac{\dot{q}_w \text{Pr}^{0.6}}{0.76 \sqrt{\rho_e \mu_e} (I_e - h_w)} \right]^2 \quad (4-69b)$$

It follows that if the environmental conditions at the edge of the gas boundary layer, the gas enthalpy at the surface, and the stagnation point heat flux to a flat face body are known, the stagnation point velocity gradient can be calculated from Equation (4-69b).

An analysis is presented in Appendix A that allows the determination of the environmental conditions in the rocket motor exhaust from the experimentally determined stagnation pressure distribution along the centerline. Moreover, the stagnation point heat flux distribution along the centerline of the rocket exhaust to an infinite flat plate normal to the flow has been determined experimentally (46). These experimental heat flux data are discussed in detail in Chapter V. Thus, enough data are known for the determination of the stagnation point velocity gradient here from Equation (4-69b). The theoretical calculations discussed in Chapter VI make use of this technique to estimate the stagnation point velocity gradient on a flat plate normal to the exhaust stream.

It should be pointed out that the S.C.F.S. specimens did not retain their flat surfaces when exposed to the rocket exhaust. The impingement of the hot gas stream caused the flat plate to be dished out in the manner illustrated by the sketch shown in Figure 2. As is illustrated in the sketch, visual examination of a specimen after testing showed the solidified melt around the periphery of the crater. Although the specimen becomes slightly concave at the stagnation point during testing, it is not expected that this would have a pronounced influence on the stagnation point heat flux or velocity gradient. This is supported in part by the results of the experimental study wherein it was found that there is very little difference in the average ablation rates at a particular location for run durations of 15 and 30 seconds (see Chapter V). Clearly for a run duration of 15 seconds the face would be nearly flat for a greater percentage of the time of the

run than for a run of 30 seconds duration. It follows that in the calculations to follow in Chapter VI, the stagnation point heat flux and velocity gradient are assumed to remain constant during ablation in the rocket exhaust.

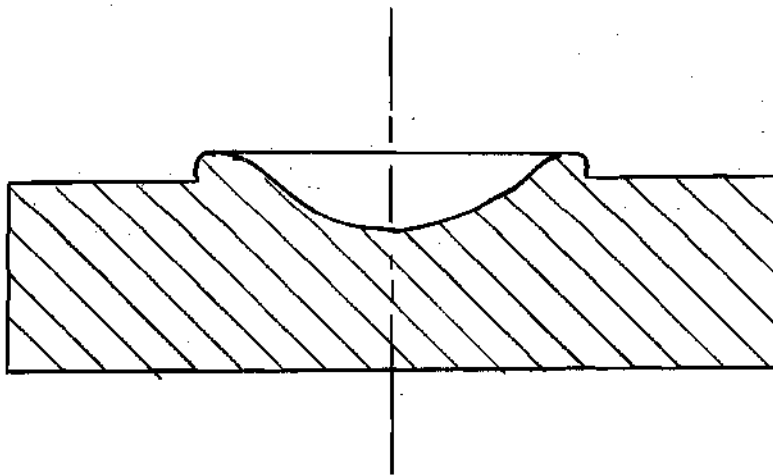
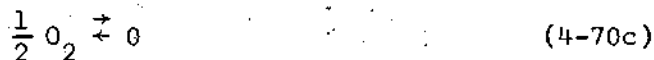
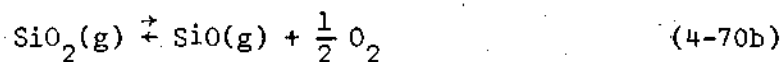


Figure 2. Sketch of Cross Section of Typical Specimen after Testing

#### Chemical Considerations at the Gas-Liquid Interface

In this section an analysis is made of the surface chemistry at the gas-liquid interface of silica vaporizing first into an air boundary layer and second into the gas boundary layer that exists on a silica body as it ablates in the exhaust of an oxy-hydrogen rocket motor.

The Air Boundary Layer. As in the derivation of the compatibility Equation (4-32b), the following species are assumed to be present at the surface:  $\text{SiO}$ ,  $\text{SiO}_2$ ,  $\text{O}_2$ ,  $\text{O}$  and  $\text{N}_2$ . Thus, the following independent reaction equations can be written:



If a mixture of perfect gases is in chemical equilibrium, the following equations can be written:

$$P_{\text{SiO}_2} = K_{P_1} \quad (4-71\text{a})$$

$$\frac{P_{\text{SiO}} \sqrt{P_{\text{O}_2}}}{P_{\text{SiO}_2}} = K_{P_2} \quad (4-71\text{b})$$

and

$$\frac{P_{\text{O}}}{\sqrt{P_{\text{O}_2}}} = K_{P_3} \quad (4-71\text{c})$$

where  $K_{P_1}$ ,  $K_{P_2}$  and  $K_{P_3}$  are the equilibrium constants in terms of partial pressures for the reactions (4-70a), (4-70b) and (4-70c), respectively (see Appendix F for a definition of  $K_P$  in terms of the free energy).

---

\*The letter L or g in parentheses refers to the liquid or gaseous state, respectively. The absence of parentheses refers to the gaseous state also.

function). Thus, Equations (4-32b), (4-70a), and (4-70b) and (4-70c) together with Dalton's law of partial pressures forms a system of five equations in five unknowns which can be solved for a given temperature and pressure. It can be shown that the unknowns can be eliminated from the equations to give the following cubic equation in the square root of the partial pressure of  $O_2$ :

$$4.77(\sqrt{p_{O_2}})^3 + 2.88K_{P_3}(\sqrt{p_{O_2}})^2 - (p_e - K_{P_1})\sqrt{p_{O_2}} + 0.88K_{P_2} = 0 \quad (4-72)$$

This equation is most conveniently solved by Newton's method and once  $p_{O_2}$  is known, it is a simple matter to use the equilibrium constant equations to calculate the partial pressures of all species. A discussion of Newton's method is given in Appendix H.

If it is assumed that the vaporization process is a nonequilibrium one which is described by the model outlined in Chapter III, then it can be shown that the square root of the partial pressure of  $O_2$  is a zero of the cubic equation

$$4.77(\sqrt{p_{O_2}})^3 + 2.88K_{P_3}(\sqrt{p_{O_2}})^2 - (p_e - P_{SiO_2})\sqrt{p_{O_2}} + 0.88K_{P_2} = 0 \quad (4-73)$$

where

$$P_{SiO_2} = K_{P_1} - \frac{1}{a_c} \sqrt{2\pi \bar{R}_u T_w / \bar{M}_{SiO_2}} (\rho v)_w^+ \quad (4-74)$$

It should be pointed out that the partial pressure of  $O_2$  is now dependent upon the rate of vaporization as well as the temperature and pressure.

The Oxy-Hydrogen Boundary Layer. Thermodynamic and chemical equilibrium is again assumed, and as in the derivation of the compatibility equations for silica vaporizing into this environment, the following species will be considered:  $SiO$ ,  $SiO_2$ ,  $O_2$ ,  $O$ ,  $H_2$ ,  $H$ ,  $OH$ ,  $H_2O$  and  $N_2$ . In addition to the reaction equations for the air boundary layer, the following reaction equations must be considered:



It follows that

$$\frac{P_H}{\sqrt{P_{H_2}}} = K_{P4} \quad (4-76a)$$

$$\frac{P_{OH}}{\sqrt{P_{O_2}} \sqrt{P_{H_2}}} = K_{P5} \quad (4-76b)$$

and

$$\frac{P_{H_2O}}{P_{H_2} \sqrt{P_{O_2}}} = K_{P_6} \quad (4-76c)$$

where  $K_{P_4}$ ,  $K_{P_5}$  and  $K_{P_6}$  are the equilibrium constants in terms of partial pressures of the reactions (4-75a), (4-75b) and (4-75c), respectively. Equations (4-33a), (4-33b), (4-71a), (4-71b), (4-71c), (4-76a), (4-76b), and (4-76c) together with Dalton's law of partial pressures constitute a system of nine equations in nine unknowns which can be solved for a given temperature and pressure. It can be shown that the system of equations can be reduced to the following two polynomials in the square roots of the partial pressures of  $O_2$  and  $H_2$ :

$$\alpha \bar{X} \bar{Y}^2 + K_{P_4} \frac{\alpha}{2} \bar{X} \bar{Y} + K_{P_5} \frac{\alpha - 1}{2} \bar{X}^2 \bar{Y} + \quad (4-77a)$$

$$K_{P_6} \frac{2\alpha - 1}{2} \bar{X}^2 \bar{Y}^2 - \bar{X}^3 - \frac{1}{2} K_{P_3} \bar{X}^2 + \frac{1}{2} K_{P_1} K_{P_2} = 0$$

$$(1 + \beta) \bar{X} \bar{Y}^2 + \left(\frac{\beta}{2} + 1\right) K_{P_4} \bar{X} \bar{Y} + \bar{X}^3 + K_{P_3} \bar{X}^2 + \quad (4-77b)$$

$$K_{P_5} \left(\frac{\beta}{2} + 1\right) \bar{X}^2 \bar{Y} + K_{P_6} (\beta + 1) \bar{X}^2 \bar{Y}^2 + K_{P_1} K_{P_2} + (K_{P_1} - p_e) \bar{X} = 0$$

where for simplicity

$$\bar{X} = \sqrt{P_{O_2}} \quad (4-77c)$$

and

$$\bar{Y} = \sqrt{p_{H_2}} \quad (4-77d)$$

In the above equations

$$\alpha = \frac{(\bar{c}_O)_e \bar{M}_{H_2}}{(\bar{c}_H)_e \bar{M}_{O_2}} \quad (4-77e)$$

and

$$\beta = \frac{(\bar{c}_N)_e \bar{M}_{H_2}}{(\bar{c}_H)_e \bar{M}_{N_2}} \quad (4-77f)$$

The solution to Equations (4-77a) and (4-77b) gives the partial pressures of  $H_2$  and  $O_2$  from which the partial pressures of all species present can be calculated.

If it is assumed that the vaporization process is a nonequilibrium one which is represented by the model given in Chapter III, then equations (4-77a) and (4-77b) are applicable if  $K_{P_1}$  in Equation (4-77b) is replaced by  $p_{SiO_2}$  where  $p_{SiO_2}$  is related to  $K_{P_1}$  and the rate of surface mass transfer by Equation (4-74).

#### Summary of Theoretical Analysis

In this chapter analyses have been presented for the ablation of S.C.F.S. in air and in the environment which exists in the exhaust of an oxy-hydrogen rocket motor. Separate analyses were made for the gas boundary layer, the chemistry at the vaporizing surface and the ablating body itself. However, these three regions are strongly

coupled and conservation of energy, mass and momentum, as well as continuity in temperature and velocity, must be preserved at the gas-liquid interface.

In order to illustrate the matching of the conditions at the interface, ablation of S.C.F.S. in air with a frozen boundary layer will be considered. The variables which characterize the environmental conditions at the edge of the gas boundary layer are presumed known functions of time. From Equation (4-72) it is evident that the partial pressure of oxygen, and therefore the mole fractions of all species and the surface enthalpy, at any given time is only a function of the surface temperature. From Equations (4-59a) — (4-59d) it becomes apparent that the aerodynamic heating, the shear stress gradient and the rate of mass loss by vaporization also depend only on the surface temperature for the given time.

For a known present temperature distribution, Equation (4-17) can be used to obtain the future temperature distribution in the ablating body excluding the surface temperature. This includes  $T_{\Delta y}^{t+\Delta t}$ . Since  $\dot{q}_w$ ,  $h_w$ ,  $h(L)_w$ , and  $(\rho v)_w^+$  are functions of only  $T_o^{t+\Delta t}$ , Equation (4-18) implicitly defines  $T_o^{t+\Delta t}$ , and clearly, the value of  $T_o^{t+\Delta t}$  that satisfies Equation (4-18) is the correct surface temperature. A method for solving Equation (4-18) for  $T_o^{t+\Delta t}$  is discussed in Appendix H.

Obviously similar discussions for the ablation of S.C.F.S. in the oxy-hydrogen environment and for the unity Lewis number case can be made.

## CHAPTER V

## EXPERIMENTAL INVESTIGATION

Experimental ApparatusRocket Motor

A photograph of the oxy-hydrogen rocket motor used in the experimental ablation study here is shown in Figure 3 on page 66.\*

The geometry, operating conditions and other related characteristics of the motor are summarized in the table below.

Table 1. Summary of Operating Conditions  
of  $H_2-O_2$  Rocket Motor

---

Fuel--Gaseous Hydrogen
Oxidizer--Gaseous Oxygen
Molar Oxygen/Hydrogen Ratio--0.25
Equivalence Ratio--2.0
Measured Chamber Pressure--275 psia (see reference 46)
Theoretical Chamber Temperature--5925 °R**
Theoretical Exit Velocity--12,500 ft/sec**
Theoretical Exit Temperature--3360 °R**
Theoretical Exit Mach Number--2.74**
Area Ratio Exit/Throat--3.14
Exit Diameter--0.276 in.
Exit Area-- $4.16 \times 10^{-4}$ ft <sup>2</sup>

---

\*\* See Appendix A.

---

\*The rocket motor used in this study is the property of the Engineering Experiment Station of the Georgia Institute of Technology and is located in Research Area 2.

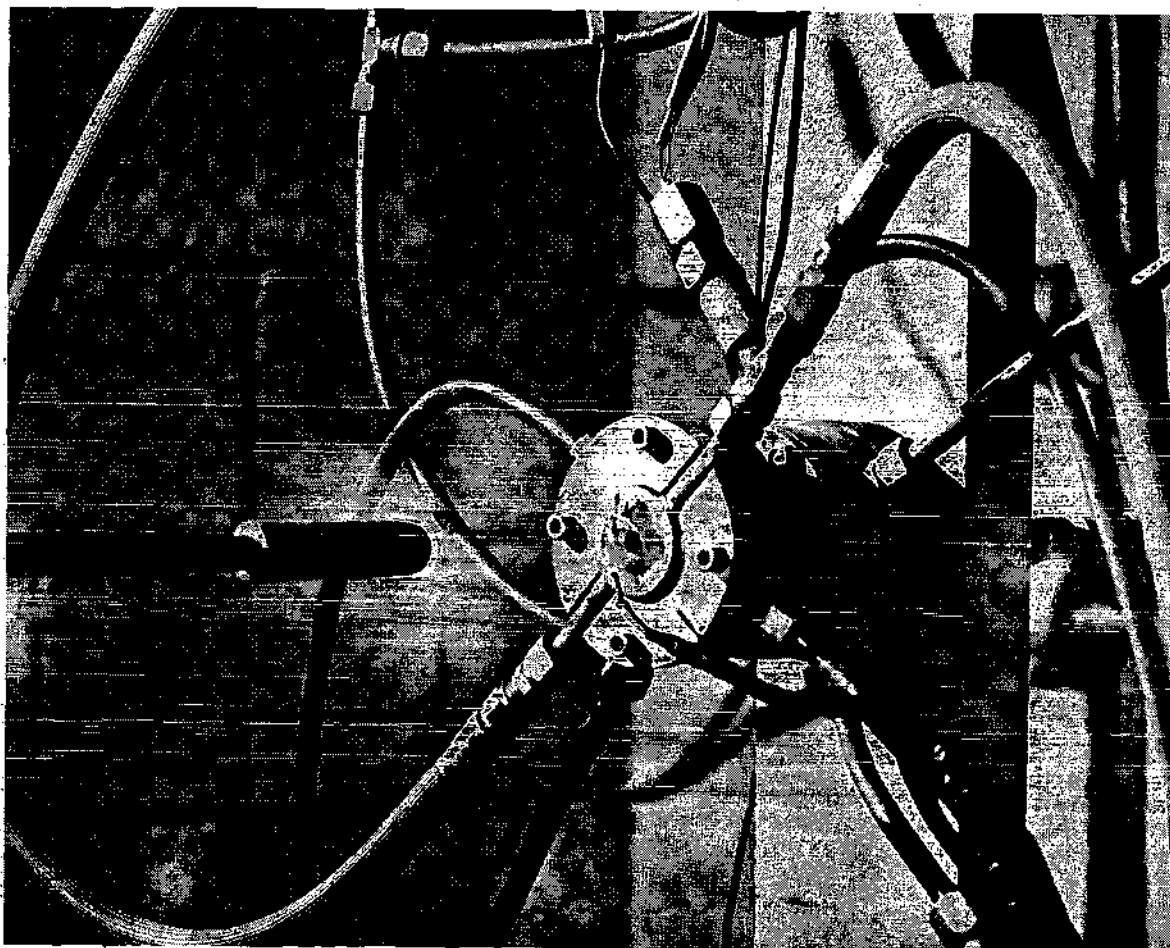


Figure 3. Photograph of  $H_2-O_2$  Rocket Motor

A detailed discussion of the construction and operating characteristics of the rocket motor may be found in reference 46.

#### Calorimeter

Figure 4 on page 68 shows a sketch of the hemispherical transient calorimeter used to measure the stagnation point heat flux along the centerline of the rocket exhaust. The response of the thermocouple affixed to the backside of the copper slug was monitored by a TEKTRONIX type 564 oscilloscope having a trace storage facility. A TEKTRONIX type 3B3 time base and type 2A63 differential amplifier were used in conjunction with the oscilloscope.

#### Stagnation Pressure Probe

Figure 5 on page 69 shows a sketch of the water-cooled probe used to measure the stagnation pressure along the centerline of the rocket exhaust. The pressure was measured with a 0-100 psi Bourdon pressure gage.

#### Test Specimens

From the standpoint of being able to compare experimental data with theory, the most desirable sample geometry is probably the cone-hemisphere. On this basis, two cone-hemisphere mandrels were machined from aluminum for the purpose of making plaster molds in which to cast the test specimens. One mandrel had a 1/2-inch nose radius and a cone half-angle of approximately seven degrees and the other mandrel had a nose radius of 1/4-inch and a cone half-angle of approximately 11 degrees. The specimens were then cast in these molds from silica

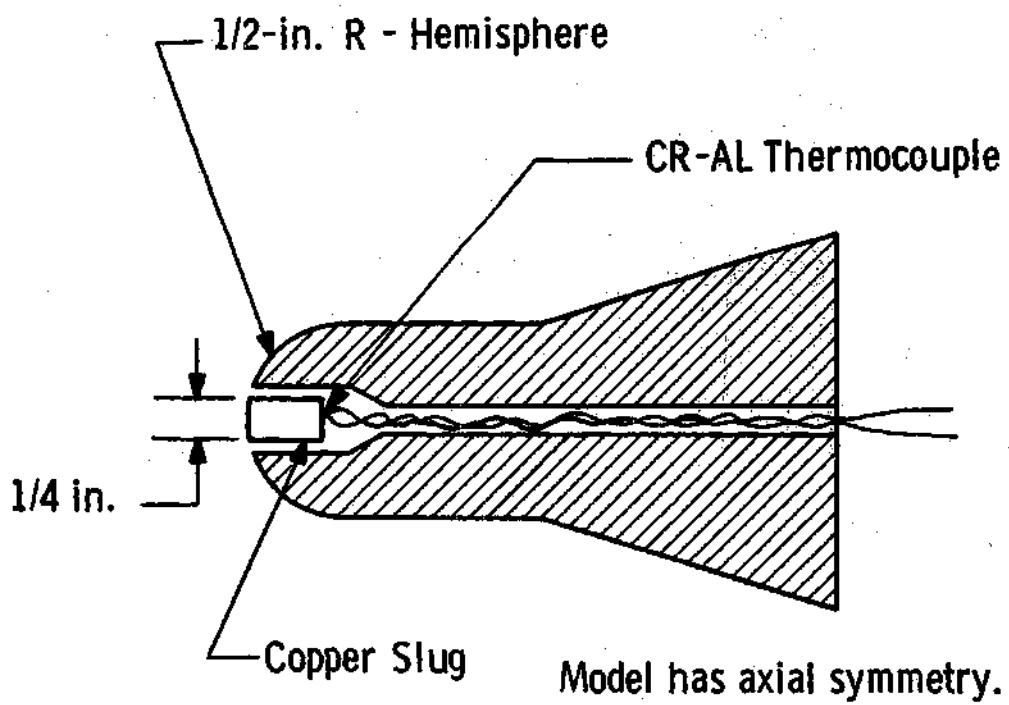


Figure 4. Sketch of Transient Calorimeter

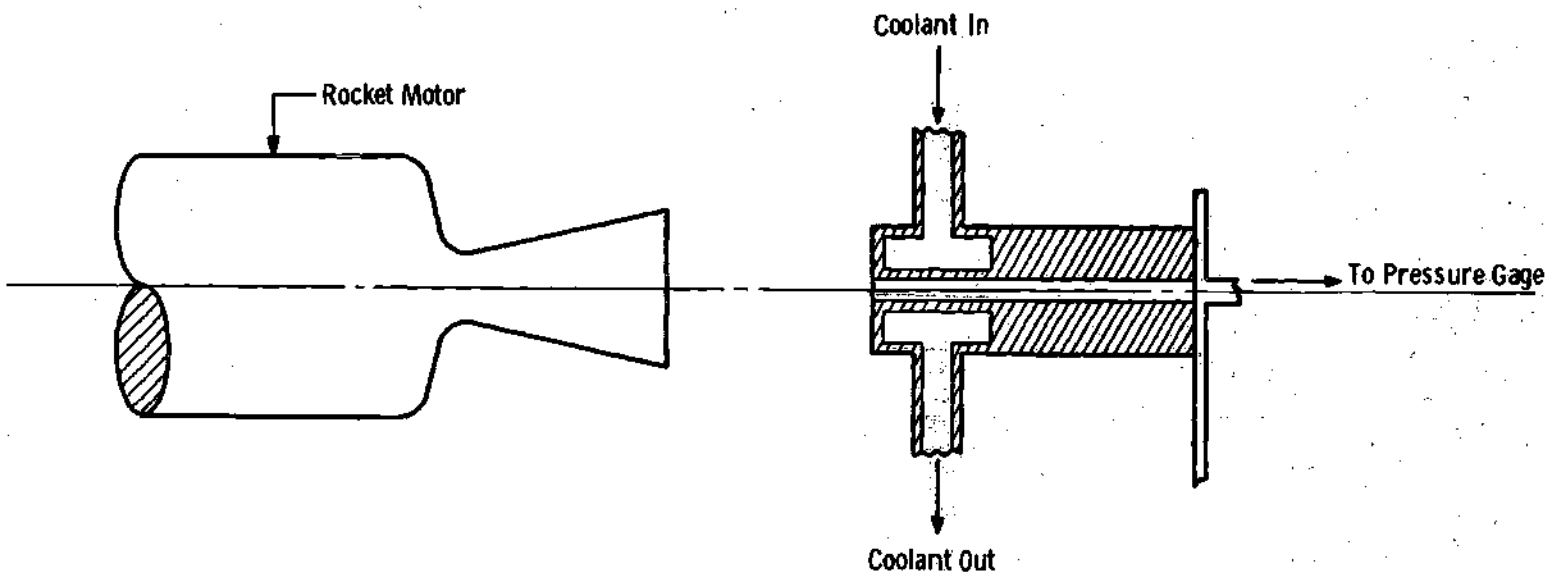


Figure 5. Sketch of Stagnation Pressure Probe

slip.\* The green specimens were fired in a kiln at approximately 2200°F for a period of four hours.

Unfortunately, these test specimens did not perform as had been expected. At a distance of 6 inches from the exit of the rocket motor, the hot gas stream ablated a cavity having a diameter of approximately 3/8-inch in one of the 1/2-inch nose radius specimens. The bulk of molten material from the cavity froze near the periphery of the cavity resulting in a complete change in the geometry of the specimen near the stagnation point. It was expected that the molten material would flow back on the cone far enough to cause little change in the geometry of the specimen near the stagnation point. Similar difficulties were experienced with the 1/4-inch nose radius specimens. No useful data were recorded using the cone-hemisphere specimens.

Although not as desirable geometrically as cone-hemispheres, it was found that flat plates of S.C.F.S. placed normal to the flow gave more useful ablation data than did the cone-hemispheres. The flat plates were 1/2-inch thick, 2 inches wide and 6 inches long.\*\* Considering the small diameter of the rocket exhaust stream relative to the width of the plates, these specimens behaved as infinite flat plates. Several specimens were fitted with thermocouples on the backside directly behind the point of exhaust impingement.

---

\*The silica slip was furnished by the High Temperature Materials Branch of the Engineering Experiment Station of the Georgia Institute of Technology.

\*\*The flat plates of S.C.F.S. were obtained from the High Temperature and Materials Branch of the Engineering Experiment Station of the Georgia Institute of Technology.

## Experimental Procedure

### Heat Flux Measurements

Heat flux measurements were made by positioning the calorimeter along the centerline of the rocket exhaust and rapidly starting and stopping the motor. A horizontal blip was started at the bottom left of the scope screen simultaneously with the starting of the motor. The horizontal sweep together with the voltage from the thermocouple on the vertical input gave a trace on the scope of thermocouple emf versus time. A photograph of the stored trace against a lighted grid produced a graph from which the rise in temperature of the backside of the slug with time could be computed.

If the thermal conductivity of the calorimeter slug is infinite, the temperature of the slug will be uniform at any instant of time and the heat flux to the slug is given by the equation (47)

$$-\dot{q}_{o,cw} = \rho_c c_c L_c \frac{dT_{bs}}{dt} \quad (5-1)$$

where

$L_c$  = slug length

$c_c$  = specific heat of slug material

$\rho_c$  = density of slug material

$T_{bs}$  = temperature of the backside

This heat flux is the zero mass transfer cold surface heat flux since the temperature at the surface of the calorimeter is always much lower than the temperature of the exhaust stream. The slug material for the

calorimeter used here was copper. Although the thermal conductivity of copper is very large, it is desirable to have an estimate of the error incurred by using Equation (5-1) to compute the heat flux. An estimate of the error can be obtained by comparing Equation (5-1) with the corresponding equation for a cylindrical slug of length  $L_c$  having a finite thermal conductivity and insulated on the backside. This corresponding equation can be derived from the solution given by Carslaw and Jaeger (48) for the temperature distribution in an infinite flat plate initially at a uniform temperature with one face insulated and the other face suddenly subjected to a constant heat flux. The equation is

$$-\dot{q}_{o,cw} = \rho_c c_c L_c \left[ 1 - 2 \sum_{v=1}^{\infty} (-1)^v e^{-\frac{\alpha_c v^2 \pi^2 t}{L_c^2}} \right]^{-1} \frac{dT_{bs}}{dt} \quad (5-2)$$

where  $\alpha_c$  is the thermal diffusivity of the slug material. It is seen that Equations (5-1) and (5-2) are identical apart from the factor in the brackets in Equation (5-2). A plot of this factor as a function of the parameter  $\alpha_c t / L_c^2$  is shown in Figure 6 on page 73. Using the thermal diffusivity of copper and the length of the slug in the calorimeter used here, it can be shown from Figure 6 that the factor in Equation (5-2) is greater than 0.97 for  $t$  greater than one second. This partially justifies the use of Equation (5-1) for calculating the heat flux from the

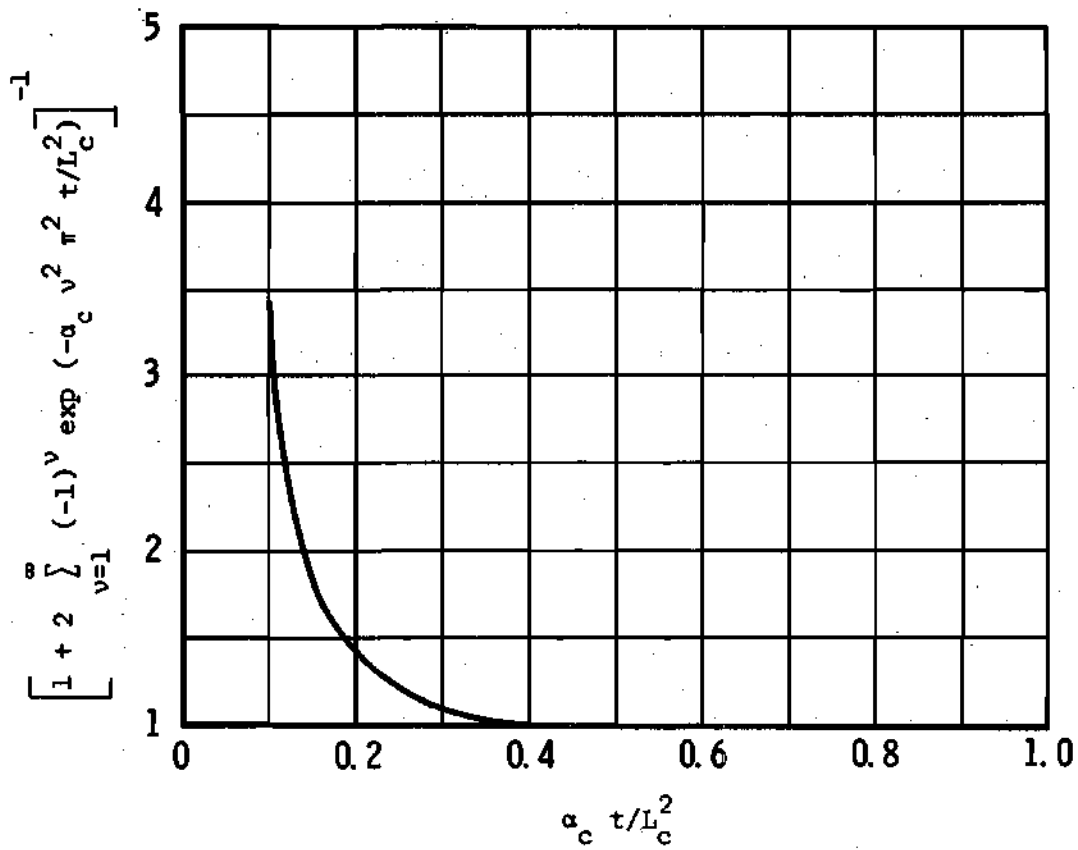


Figure 6. Correction Factor for Finite Thermal Conductivity of Calorimeter Slug

measured rise in backside temperature with time if  $\frac{dT_{bs}}{dt}$  is taken at  $t$  greater than one second.

It was found experimentally that the heat flux results were quite sensitive to correct alignment of the calorimeter in the rocket exhaust. Only slight misalignment from the centerline would result in as much as 50 per cent variation in the measured heat flux.

#### Stagnation Pressure Measurements

Stagnation pressure as a function of position behind the exit of the rocket motor was determined by positioning the water-cooled pressure probe along the centerline of the exhaust and recording the pressure indicated by the Bourdon gage. Since the probe was water cooled, it was possible to make measurements closer to the motor than it was with the transient calorimeter.

#### Ablation Studies

Ablation studies on the flat plates of S.C.F.S. were made at 4, 5, 6 and 7 inches from the exit of the rocket motor. Two samples each were run at each location except at 4 inches where only 1 sample was run. The temperature of the backside of the samples fitted with thermocouples was monitored with an electronic recorder. The ablated depth at the stagnation point was measured with a thread comparing micrometer. The length of the runs varied from 15 to 30 seconds.

### Experimental Results

#### Heat Flux

Figure 7 on page 75 shows the cold surface heat flux as a function of position behind the motor as determined by the transient

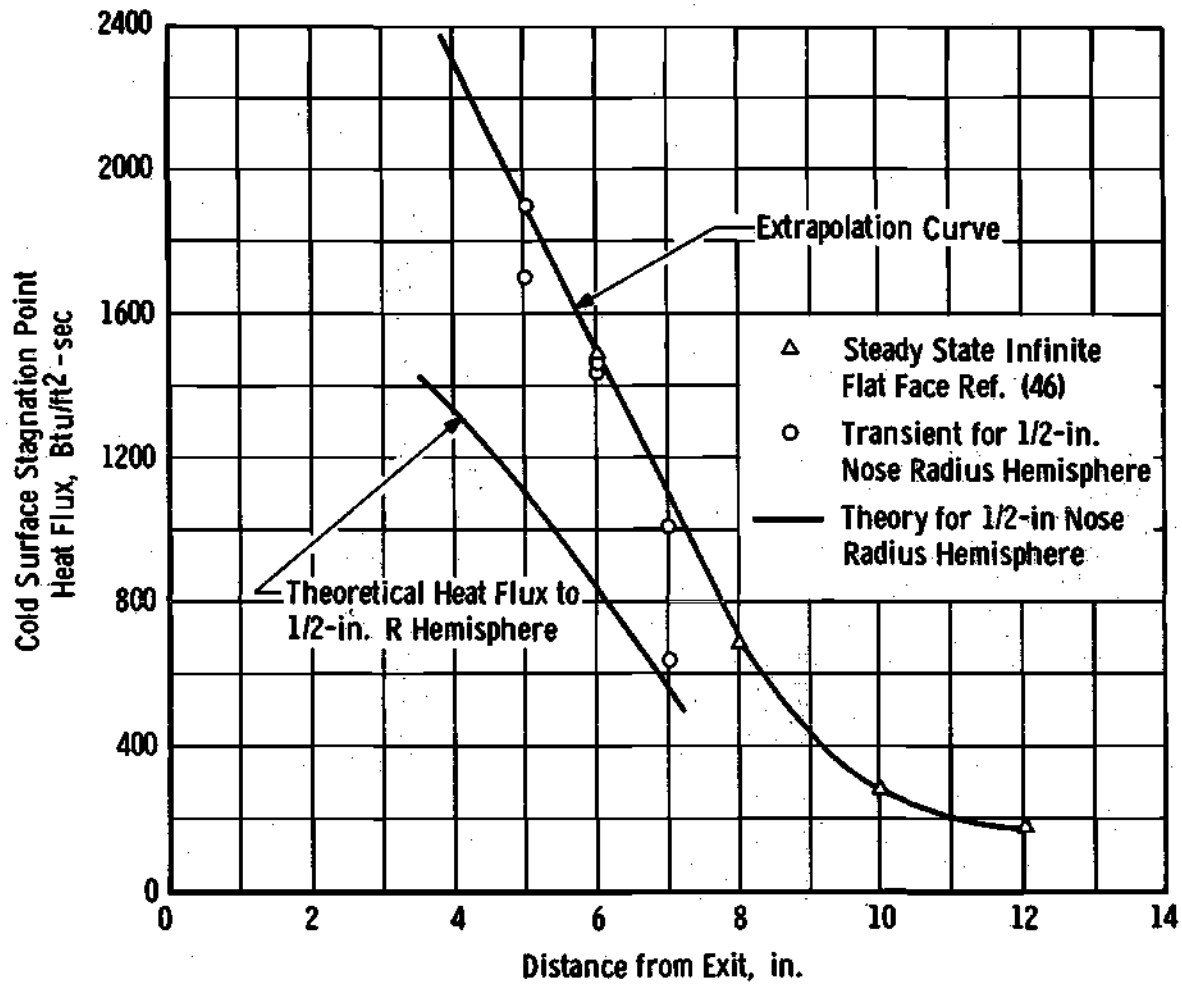


Figure 7. Heat Flux versus Distance from Exit of Rocket Motor

hemispherical calorimeter. Sometime after these heat flux data were obtained in the manner described in the procedure, it was found that the pressure in the combustion chamber of the rocket motor is initially about twice its steady state value. This could certainly account for the disagreement between the theory and experiment indicated in Figure 7 since the heat flux measurements are made within the first few seconds after the motor is ignited. The greater combustion chamber pressure would tend to increase the flow rate and also the stagnation pressure, which in turn would tend to increase the heat flux. Although these heat flux data were not used in the ablation calculations, it was felt that they should be included for the sake of completeness.

Also shown in Figure 7 is the heat flux distribution as measured with a steady state flat face calorimeter. The latter data were not obtained by this author and are reported in reference 48. No direct comparison can be made between the two sets of data since the stagnation point velocity gradients are different for the hemisphere and the flat face.

#### Stagnation Pressure

Figure 8 on page 77 shows a plot of the measured stagnation pressure as a function of position behind the exit of the rocket motor. The estimated stagnation pressure in the exit plane of the motor as computed from the measured chamber pressure is also shown (this calculation assumes that a normal shock stands in the exit plane). It should be noted that the stagnation pressure measured is not the isentropic total pressure of the stream since the stream has passed through a shock wave before reaching the probe.

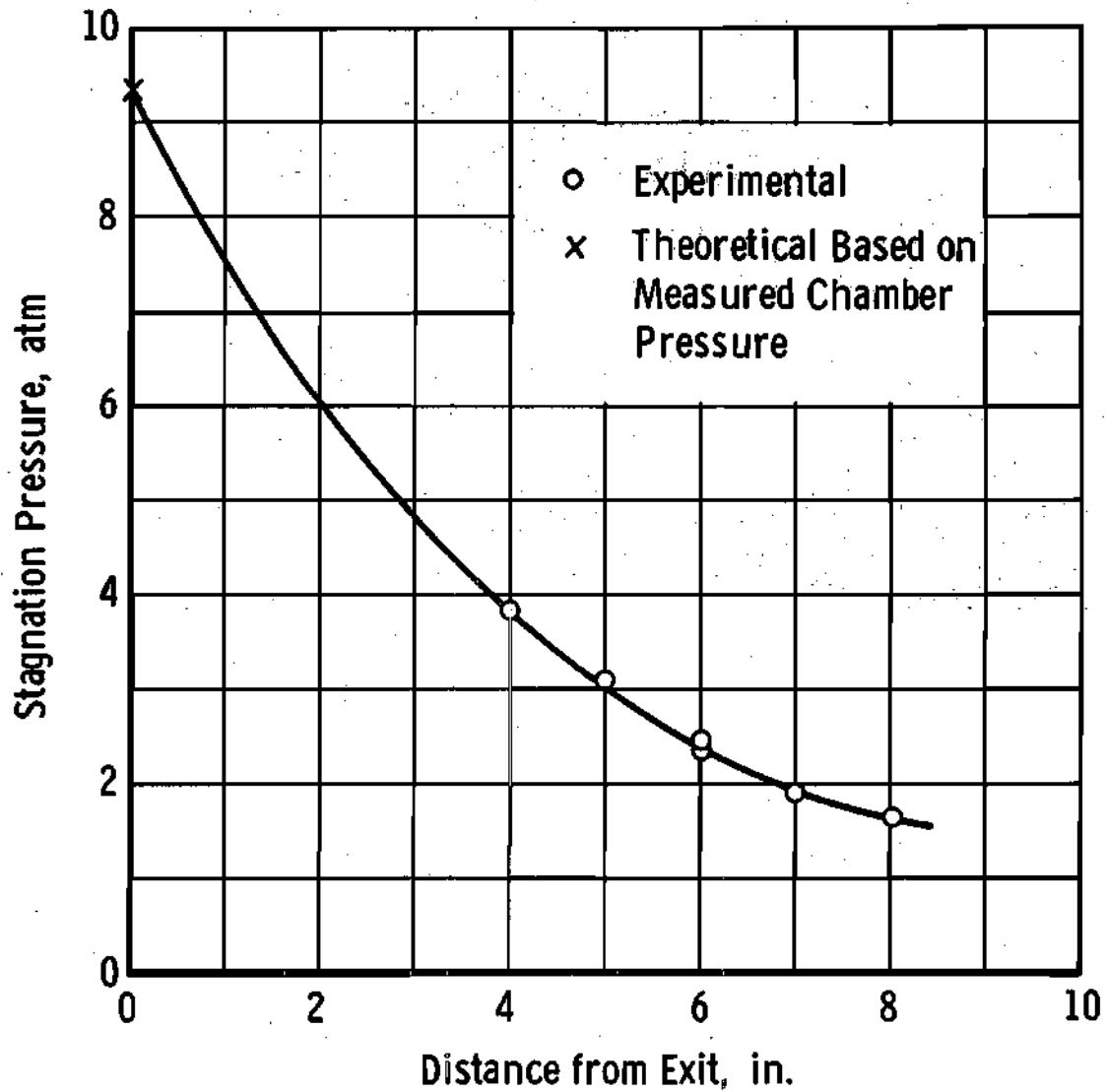


Figure 8. Stagnation Pressure versus Distance from Exit of Rocket Motor

### Ablation of S.C.F.S.

In Figure 9 on page 79 is shown the experimentally determined average ablation rate as a function of position behind the rocket motor. This average ablation rate is computed by dividing the ablated depth at the stagnation point by the time of exposure to the rocket exhaust. Figure 10 on page 80 gives the experimentally determined heat of ablation as a function of position in the rocket exhaust. The heat of ablation here is defined as the cold surface stagnation point heat flux at a particular location divided by the mass ablation rate at the same location (the mass ablation rate is the produce of the density of S.C.F.S. and the average ablation rate). Since the specimens used were flat plates, the cold surface heat flux used in computing the heat of ablation was the heat flux as measured by the flat face steady state calorimeter and given in Figure 7 on page 75. The backside temperature was measured only on those runs of 30 seconds duration. The results of these experimental measurements are given in Figure 11 on page 81.

### Experimental Error

#### Heat Flux

It is not possible to make an accurate assessment of the overall experimental error in the heat flux measured by the transient type calorimeter. However, some of the major errors in individual measurements are discussed below.

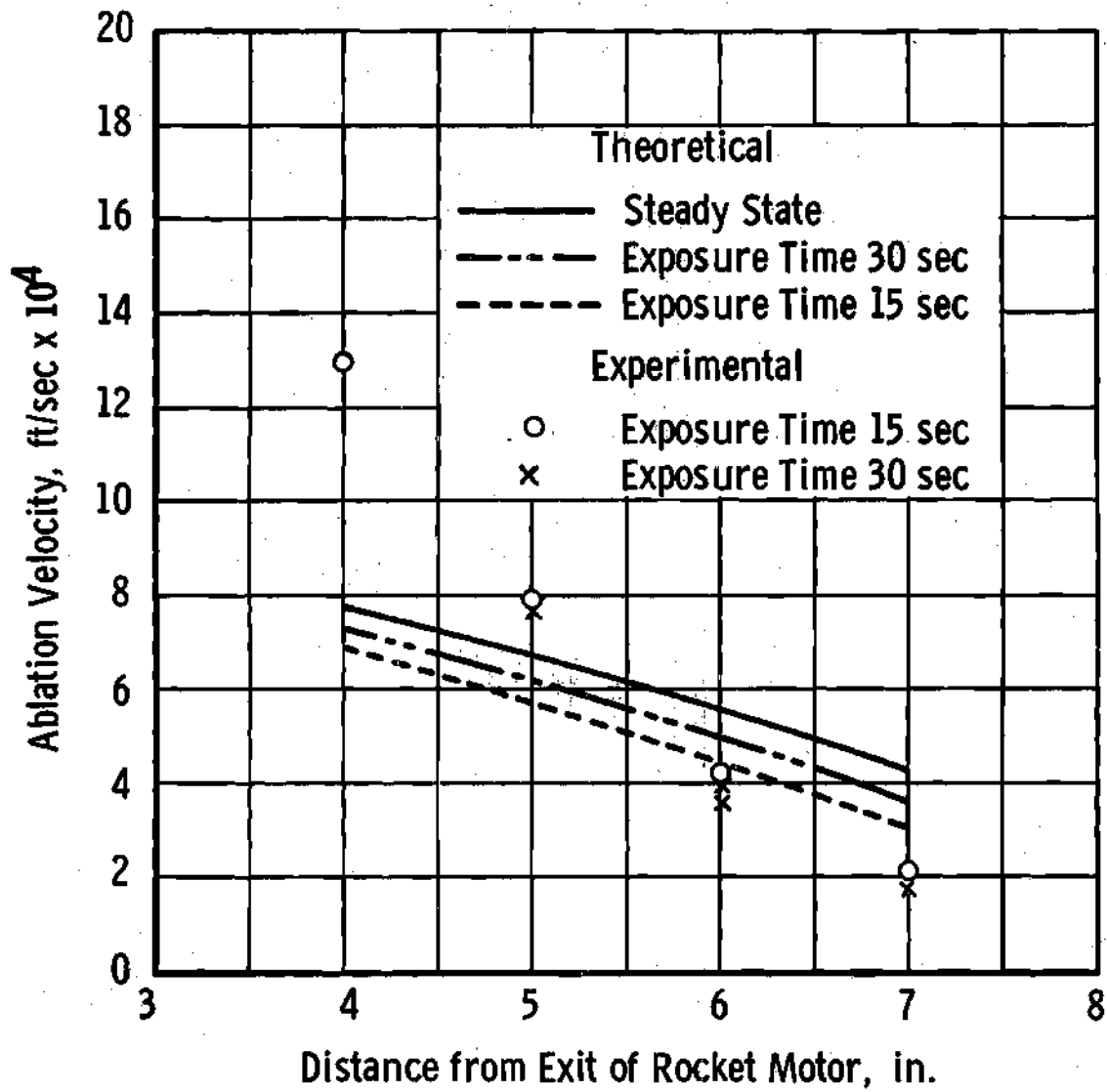


Figure 9. Ablation Velocity versus Position in Rocket Exhaust

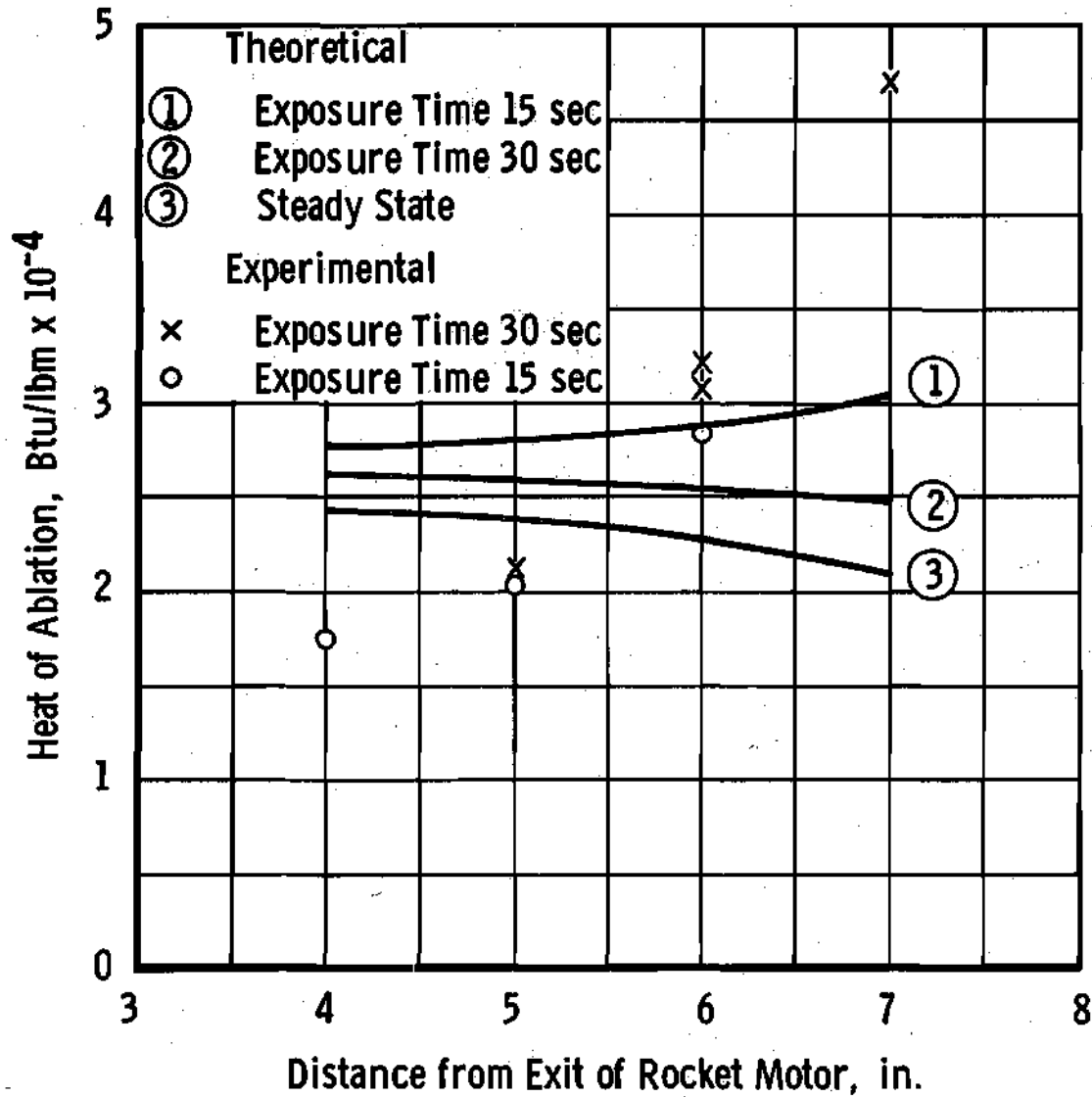


Figure 10. Heat of Ablation of Slip-Cast Fused Silica in Rocket Exhaust

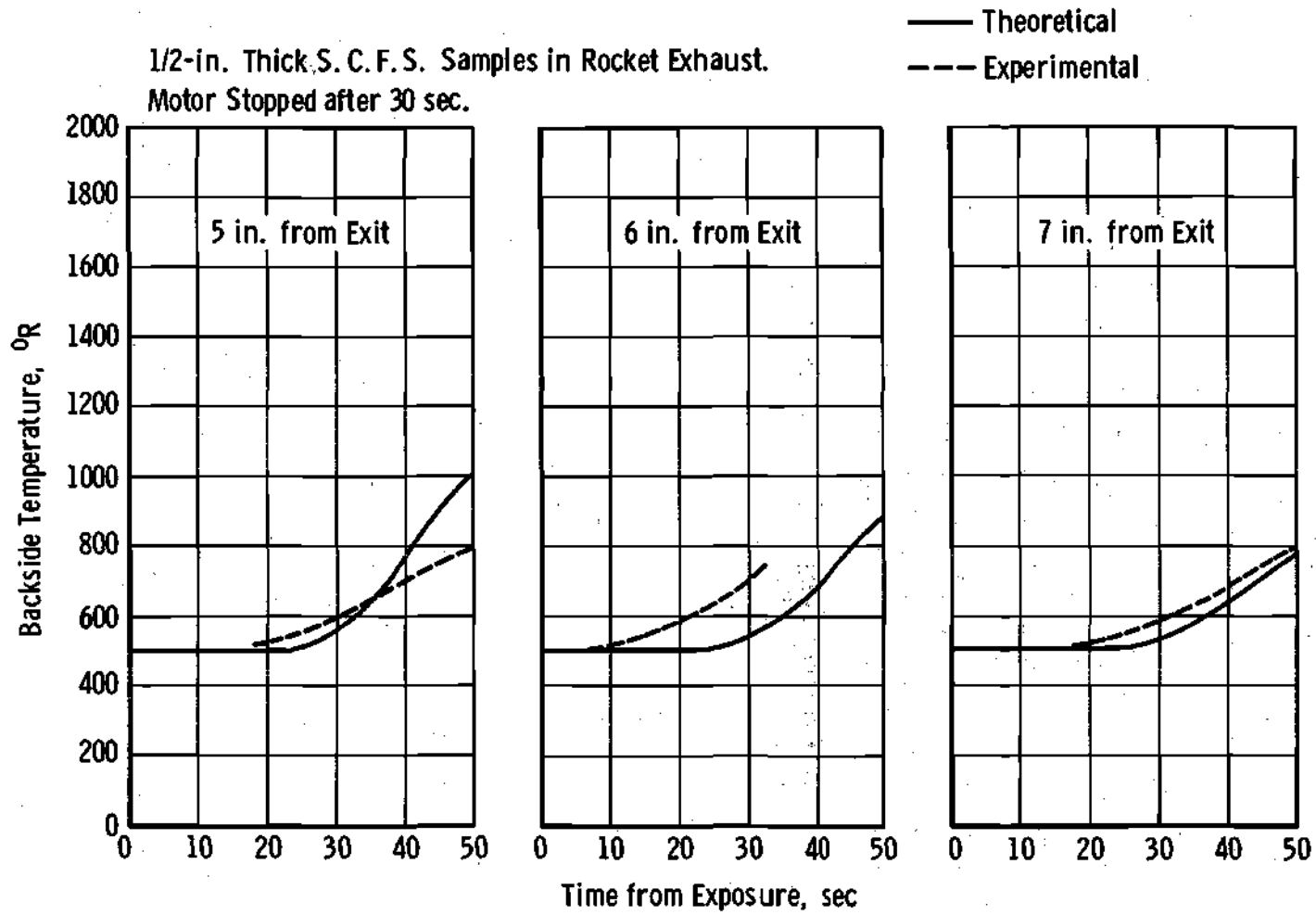


Figure 11. Backside Temperature versus Time

The derivation of Equation (5-1) is predicated on the assumption that the calorimeter slug is cylindrical and has perfectly flat ends normal to the centerline of the cylinder. If the calorimeter slug does not have perfectly flat ends, then an effective length can be used in Equation (5-1). The calorimeter used here did not have perfectly flat ends since the front face was curved and the back face had a thermocouple affixed with a small amount of silver solder (see Figure 4 on page 68). Since the radius of curvature of the front face was much greater than the radius of the slug itself, the effect of curvature there is negligibly small. The maximum thickness of the silver solder joint at the back face was less than 3 per cent of the length of the slug itself. Therefore, it is estimated that the maximum error in the effective slug length is less than 3 per cent if the effective slug length is taken to be the length of the slug itself.

The thermocouple used to measure the temperature at the back face of the calorimeter slug was checked against the steam point and found to have an error of order zero compared to the other possible errors in the measurements.

It is estimated that the slope of the graphs of thermocouple emf versus time could be computed with less than 10 per cent error.

The calorimeter was located along the centerline with less than  $\pm 1/8$ -inch error. It is estimated that the radial tolerance was  $\pm 1/16$ -inch from the centerline.

No error analysis for the heat flux to the flat face steady state calorimeter was given in reference 46; however, on the basis of the raw experimental data given, it is estimated that the experimentally deter-

mined heat flux should not be in error by more than 15 per cent.

#### Stagnation Pressure

The least count on the Bourdon pressure gage used to measure the stagnation pressure was 1 psi; however, in view of the relatively larger pressure fluctuations--less than  $\pm 3$  psi--it is estimated that the error in the measured stagnation pressure is less than  $\pm 3$  psi.

#### Ablation Rate

The ablated depth of the samples was measured using the thread comparing micrometer on two different occasions and the measurements were found to agree within  $\pm 0.005$  inch. Thus, it is reasonable to assume that the measured depth of ablation should be accurate to within  $\pm 0.005$  inch. It is estimated that the maximum error in the exposure time is  $\pm 0.5$  second. The average ablation rate was calculated by dividing the ablated depth by the time of exposure and then the maximum per cent error in the average ablation rate is the sum of the maximum per cent errors in the ablated depth and the time of exposure. On this basis, the maximum per cent error in the average ablation rate at various positions and exposure times is given in Table 2.

Table 2. Estimated Errors in the Experimental Ablation Rate

Exposure Time Seconds	Distance from Exit of Rocket Motor--Inches			
	4	5	6	7
15	$\pm 10$	$\pm 10$	$\pm 10$	$\pm 20$
30		$\pm 5$	$\pm 5$	$\pm 10$

## CHAPTER VI

## THEORETICAL PERFORMANCE OF SLIP-CAST FUSED SILICA

In Chapter IV, a theory was developed for the ablation of S.C.F.S. in air under re-entry or simulated re-entry conditions and also for the ablation of S.C.F.S. in the exhaust of an oxy-hydrogen rocket motor. In this chapter, this theory is used to obtain numerical results for the ablation of S.C.F.S. in the rocket test facility described in Chapter V and along three illustrative ballistic re-entry trajectories. The thermal properties of S.C.F.S. used in the calculations are given in Appendix F, page 156.

Theoretical Behavior of S.C.F.S. in the Rocket Exhaust

Reference to Chapter IV shows that in order to obtain numerical results from the theory, it is necessary to know the environmental conditions at the outer edge of the gas boundary layer at the stagnation point. Appendix A is devoted to the determination of the stagnation conditions as a function of distance from the exit of the rocket motor.

For the environmental conditions described in Appendix A, the applicable equations of Chapter IV were solved simultaneously to determine the theoretical behavior of S.C.F.S. in the rocket exhaust. The numerical calculations were made using a high speed digital computer. A copy of the computer program used is given in Appendix G, page 163.

The heat flux data used in the numerical calculations are the steady state flat face calorimeter data reported in reference 46 and

reproduced here in Figure 7 on page 75. It is seen that experimental heat flux data were obtained at only 6, 8, 10 and 12 inches from the exit of the rocket motor; consequently it was necessary to extrapolate the data given in order to make theoretical calculations at distances less than 6 inches from the nozzle exit. The curve used for the extrapolation is also shown in Figure 7. The extrapolation curve was just sketched in in a manner that appeared to give a reasonable extrapolation of the experimental data at six, eight and ten inches from the exit of the rocket motor.

In order to circumvent certain numerical problems with the computer program, the heat flux was forced to increase exponentially to its steady state value rather than allowing an instantaneous jump from zero to its steady state value. The rate of increase was great enough to insure that the heat flux was virtually constant after 0.1 second. Similarly to some of the experimental tests conducted (see Chapter V), the theoretical exposure time in the rocket exhaust was taken to be 30 seconds. In order to simulate the cooling period after shut down of the rocket motor, the convective heat flux at the front of the sample was forced to decay exponentially at a rate to make it virtually zero after 30.25 seconds.

The Lewis number was taken to be unity in all the calculations for ablation in the exhaust of the rocket motor.

### Results

Figure 12 on page 86 shows the theoretical steady state ablation

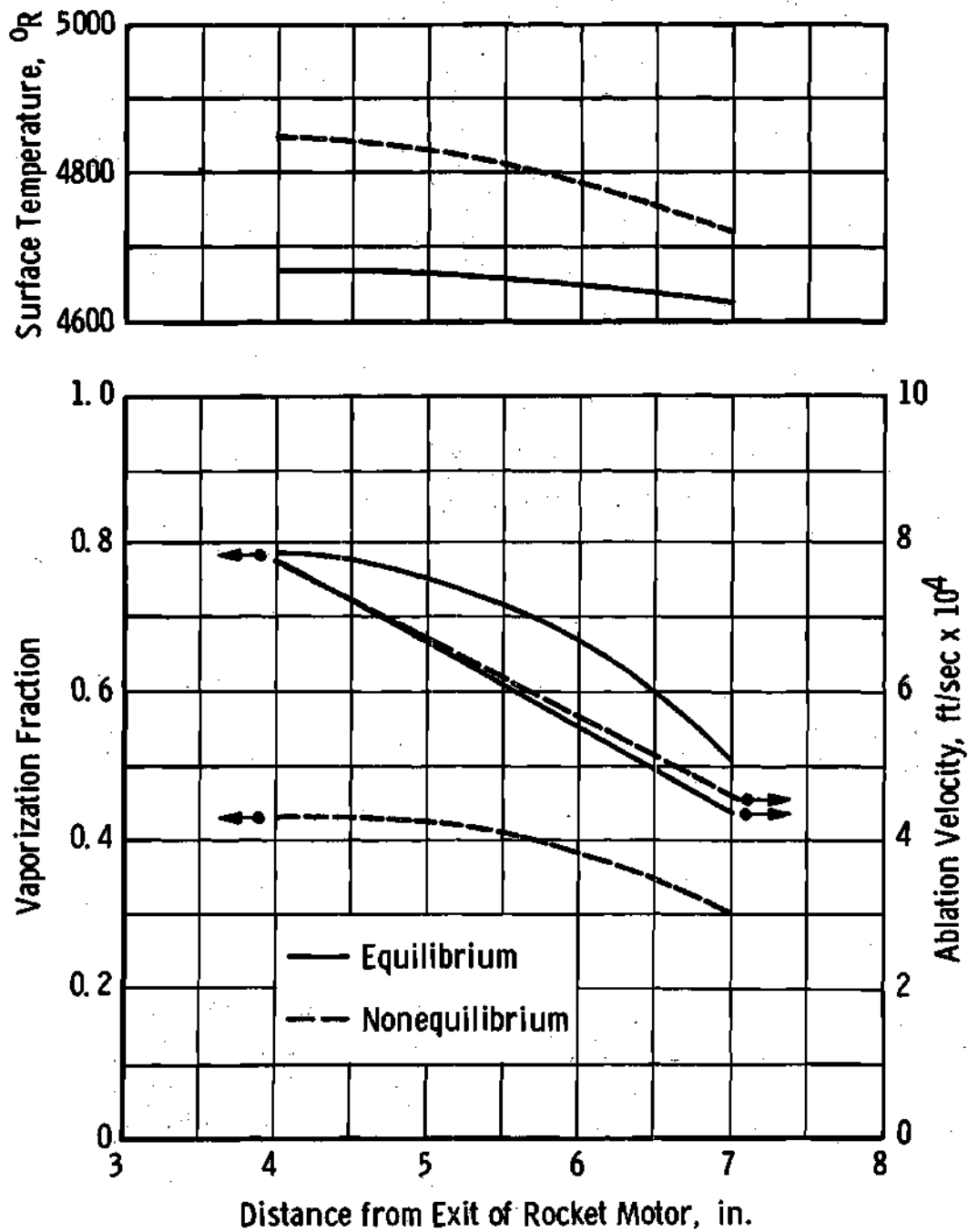


Figure 12. Theoretical Steady State Vaporization Fraction, Surface Temperature and Ablation Velocity versus Distance from Exit of Rocket Motor

rate, surface temperature and vaporization fraction\* of S.C.F.S. for both equilibrium and nonequilibrium vaporization in the rocket exhaust. The accommodation coefficient was taken to be unity in the nonequilibrium calculations. Figure 9 on page 79 gives the theoretical steady state and average ablation rates of S.C.F.S. in the rocket exhaust. The curves shown are for equilibrium vaporization at the surface, but as can be seen from Figure 12, the ablation rate distributions for nonequilibrium at the surface would be virtually the same. Figure 10 on page 80 shows the theoretical heat of ablation of S.C.F.S. in the rocket exhaust for equilibrium vaporization at the surface. Figure 11 on page 81 shows the rise in the temperature of the backside of a specimen with time for three locations in the rocket exhaust. The difference in temperature response of the backside for equilibrium vaporization over nonequilibrium vaporization was so slight that the data given in Figure 11 represent either case. Figure 13 on page 88 illustrates the effect of accommodation coefficient on ablation rate, vaporization fraction and surface temperature.

#### Discussion of Results

Before discussing the theoretical behavior of S.C.F.S. it should be emphasized that the theoretical results are based on the phenomenological models for the mechanisms of vaporization, radiation and melt flow introduced in Chapter III and any conclusions drawn from the results are subject to any shortcomings that the models may have.

---

\*The vaporization fraction is defined as the ratio of the vaporization velocity, that is the axial velocity of the liquid silica at the gas-liquid interface, to the ablation velocity, or  $F_v = v_w/v_{-L}$ .

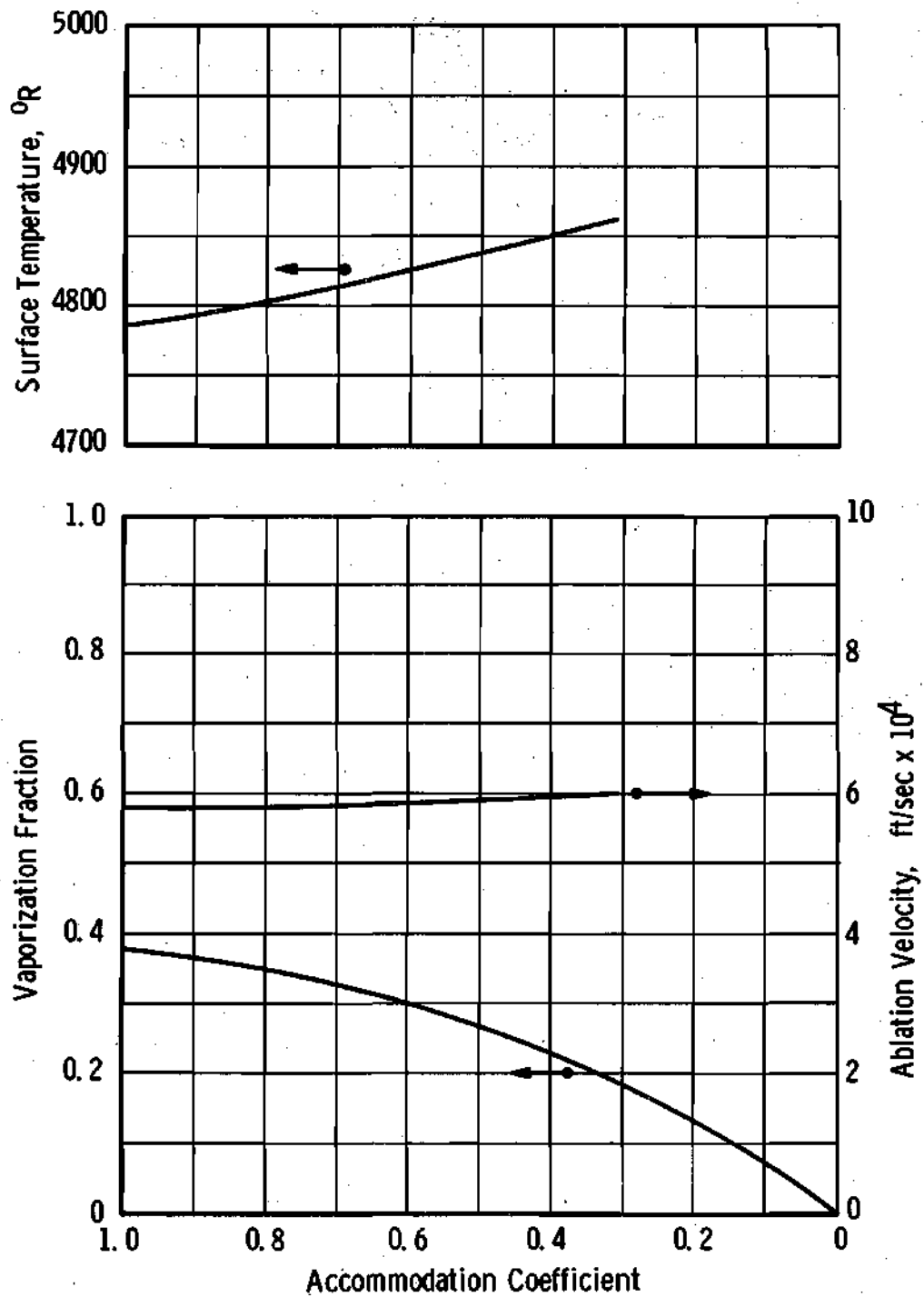


Figure 13. The Effect of Accommodation Coefficient on Surface Temperature, Ablation Velocity and Vaporization Fraction at Six Inches from the Exit of the Rocket Motor

Reference to Figure 12 on page 86 shows that the vaporization fraction for equilibrium vaporization is approximately twice the vaporization fraction for nonequilibrium vaporization, while there is virtually no difference in the ablation rate between the two cases. There is an interplay between the vaporization process and the thermal radiation from the surface and the melt flow which accounts for this behavior. When nonequilibrium is considered in the vaporization process, the concentrations of species and temperature at the surface and the rate of vaporization become intimately connected. As can be seen from Figure 12, nonequilibrium vaporization increases the surface temperature. Clearly an increase in surface temperature is accompanied by an increase in melt flow (through a decrease in the melt viscosity), an increase in thermal radiation from the surface and a decrease in the convective heat flux to the ablating body.

Although the ablation rates for equilibrium and nonequilibrium vaporization are practically equal, it is interesting to note that the ablation rate for nonequilibrium vaporization is slightly less than for equilibrium vaporization. This effect can be attributed to the interaction of S.C.F.S. with this particular environment rather than a characteristic of the material. Since the enthalpy difference across the gas boundary layer is relatively small for this environment, the increase in surface temperature for nonequilibrium vaporization decreases the convective heat flux to the body and increases the thermal radiation from the surface by an amount to more than offset the reduction in energy absorption by the latent heat of vaporization due to the reduction in the amount of material vaporized. This trend in the

ablation rates for the two cases would not be observed in an environment having a stagnation enthalpy much greater than the gas enthalpy at the ablating surface.

Since the definition of the heat of ablation is the quotient of the cold surface heat flux and the mass ablation rate, it is evident that the curves presented in Figure 10 on page 80 for the heat of ablation under the conditions of equilibrium vaporization are, for all practical purposes, valid for nonequilibrium vaporization as well. It is seen in Figure 10 that the theoretical heat of ablation is relatively independent of location in the rocket exhaust and has a nominal value of approximately 25,000 Btu/lbm. The apparent heat of vaporization ( $h_w - h_{SiO_2}(L)$ ) was calculated to be approximately 4,400 Btu/lbm for S.C.F.S. ablating in the rocket exhaust.\*

Figure 13 on page 88 illustrates the effect of accommodation coefficient on the ablation of S.C.F.S. As was pointed out earlier, nonequilibrium vaporization has its least effect when the accommodation coefficient is unity and the departure from equilibrium becomes increasingly greater as the accommodation coefficient is decreased. Reference to Figure 13 shows that a decrease in the accommodation coefficient results in an increase in the surface temperature and a decrease in the vaporization fraction. The ablation rate is seen to be virtually independent of the accommodation coefficient over the range for which calculations were made.

---

\* This effective heat of vaporization in the rocket exhaust compares to approximately 6000 Btu/lbm for the ablation of S.C.F.S. in air.

It is interesting to note that the usual variables which can be conveniently measured in experimental ablation tests cannot be used satisfactorily to determine the credibility of the assumed models for vaporization introduced in Chapter III. Two of the most convenient variables measurable in a stagnation point study are surface temperature and ablation rate. However, as has been previously discussed, the ablation rate is relatively independent of the mechanism of vaporization. Moreover, the difference in surface temperature between the case of equilibrium vaporization and nonequilibrium vaporization is less than 200 °F which is of the same order of magnitude as the uncertainty in surface temperature measurements. Although the vaporization fraction is relatively sensitive to the mechanism of vaporization, it is difficult to measure in a stagnation point analysis. If it were found that the measured vaporization fraction and ablation rate were in agreement with the theory, this would not be sufficient justification to insure the validity of the model of vaporization since there might be compensating effects which would account for the agreement. For example, it can be shown that a realistic adjustment in the constants of the Arrhenius viscosity equation can produce an influence on the vaporization fraction and ablation rate for equilibrium vaporization similar to the effect of nonequilibrium vaporization. This will be discussed further in Chapter VII in the light of the experimental tests discussed in Chapter V.

### Performance of S.C.F.S. Along Illustrative Trajectories

In order to illustrate the performance of S.C.F.S. as an ablative heat shield material on a re-entry vehicle, the theory developed in Chapter IV for the ablation of S.C.F.S. in air was used to determine the behavior of S.C.F.S. along three ballistic re-entry trajectories. The parameters describing the trajectories are given in Appendix E, page 154, along with an analysis for the dynamics of atmospheric re-entry. One trajectory is typical of an ICBM, another of an IRBM and the third is the re-entry trajectory for a Trailblazer II test vehicle (49). Using the analysis presented in Appendix E, calculations were made to determine flight velocity, altitude and stagnation pressure as a function of time from re-entry at 300,000 ft. The results of the calculations are given in Figures 14, 15 and 16. The cold surface zero mass transfer heat flux was calculated from the Fay and Riddell correlation (44) for a unity Lewis number. Correlation formulas for density and transport properties of reference 50 were used in the calculations. The results of the calculations are given in Figures 17, 18 and 19 on pages 96, 97 and 98, respectively.

#### Results

Vaporization from the surface was assumed to be an equilibrium process and the Lewis number was assumed to be unity in all of the trajectory calculations. The latter assumption is discussed in a later section of this chapter. The thermal properties of S.C.F.S. used in the calculations are given in Appendix F.

Figure 20 on page 99 shows the ablation rate and surface temperature while Figure 21 on page 100 shows the vaporization fraction for the

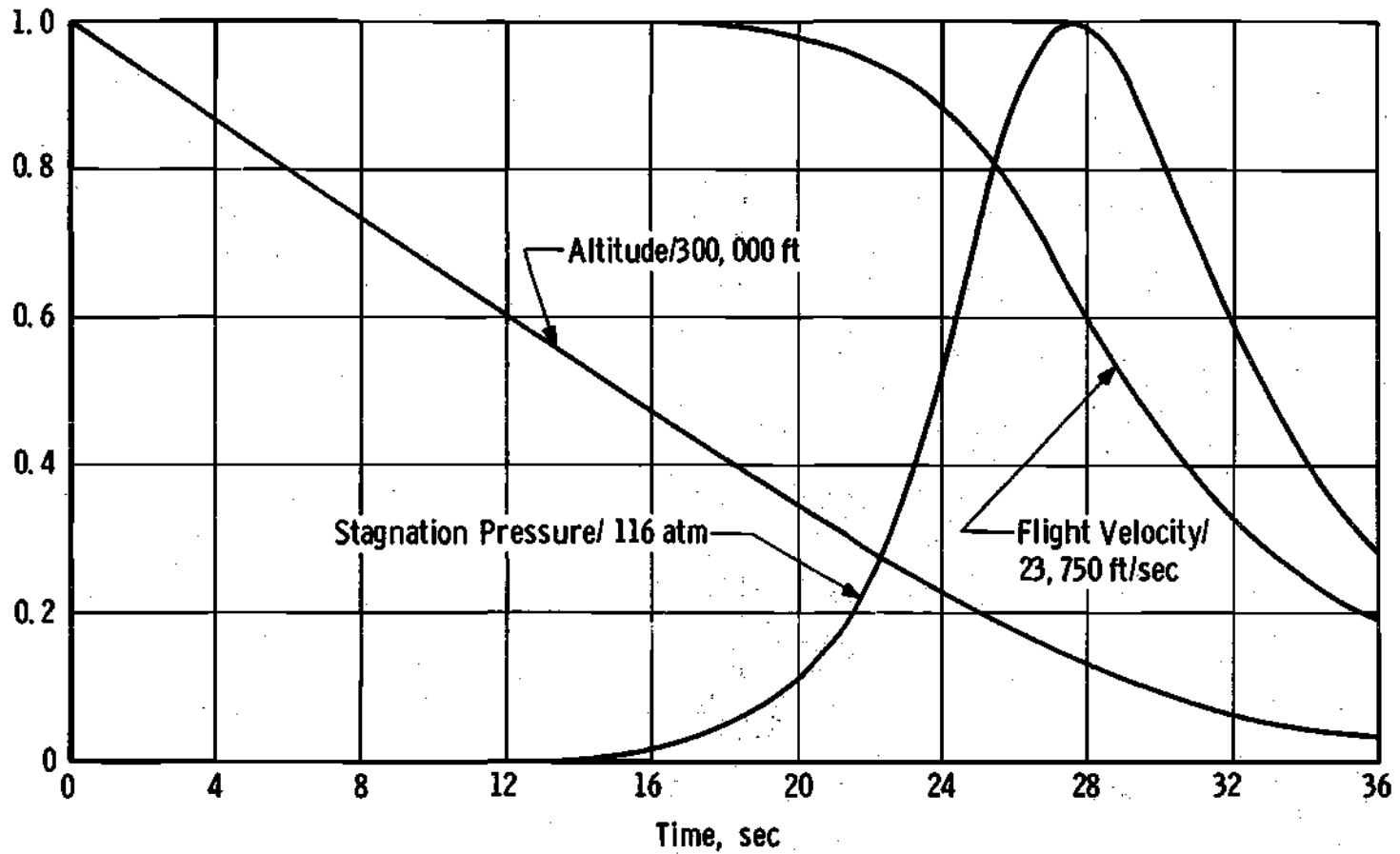


Figure 14. Stagnation Pressure, Flight Velocity and Altitude versus Time from Re-entry at 300,000 ft: ICBM

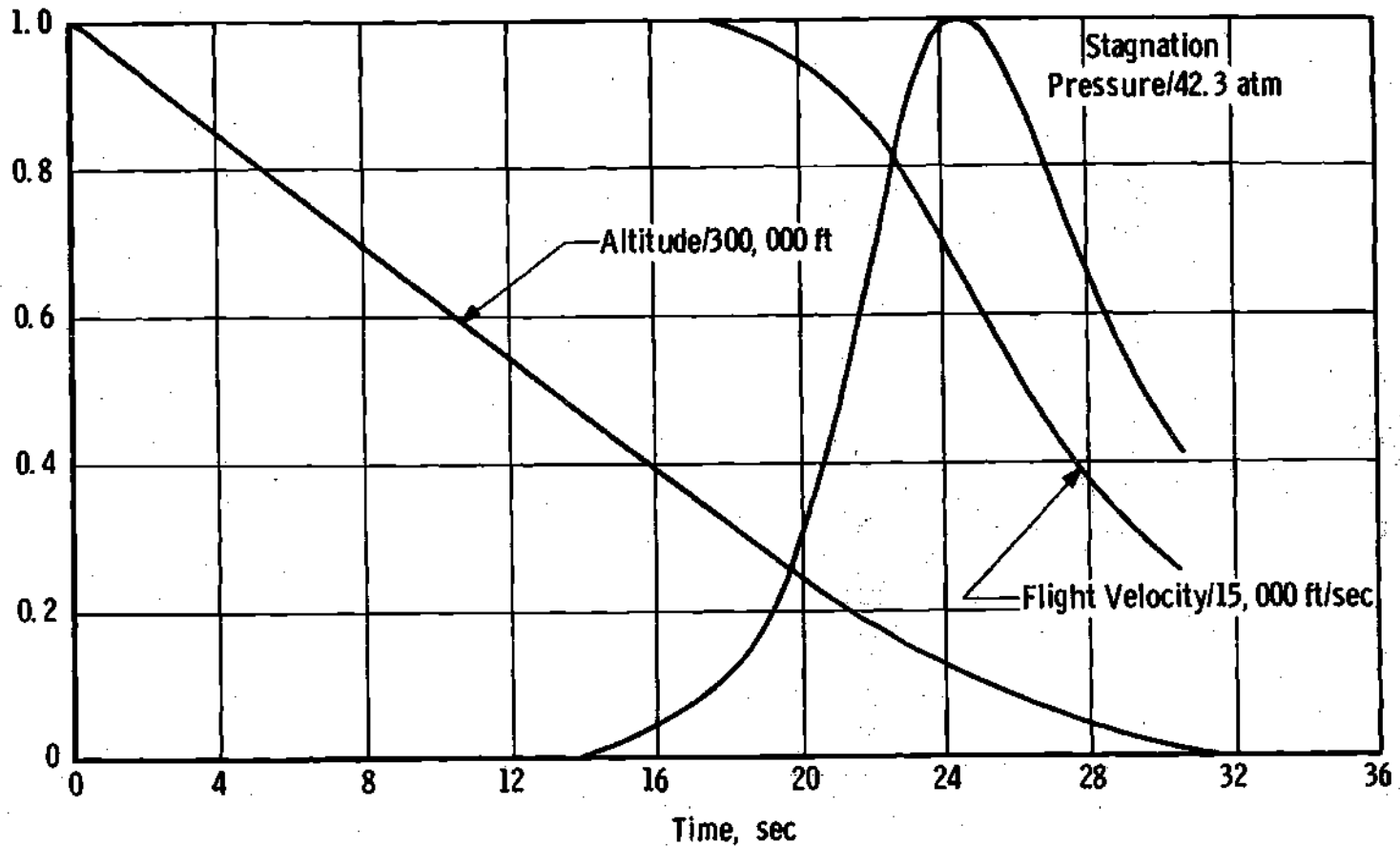


Figure 15. Stagnation Pressure, Flight Velocity and Altitude versus Time from Re-entry at 300,000 ft: IRBM

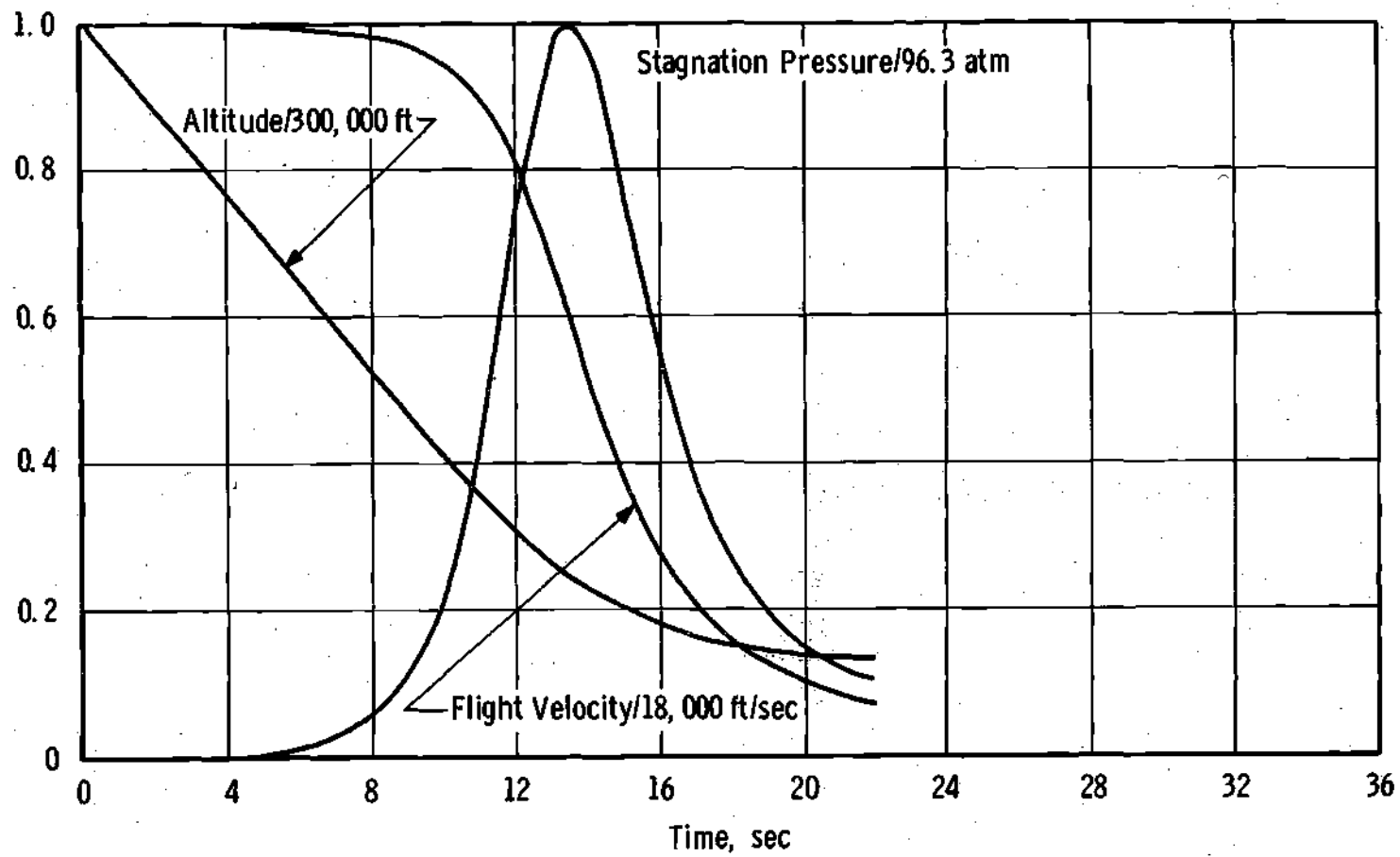


Figure 16. Stagnation Pressure, Flight Velocity and Altitude versus Time from Re-entry at 300,000 ft: Trailblazer II Vehicle

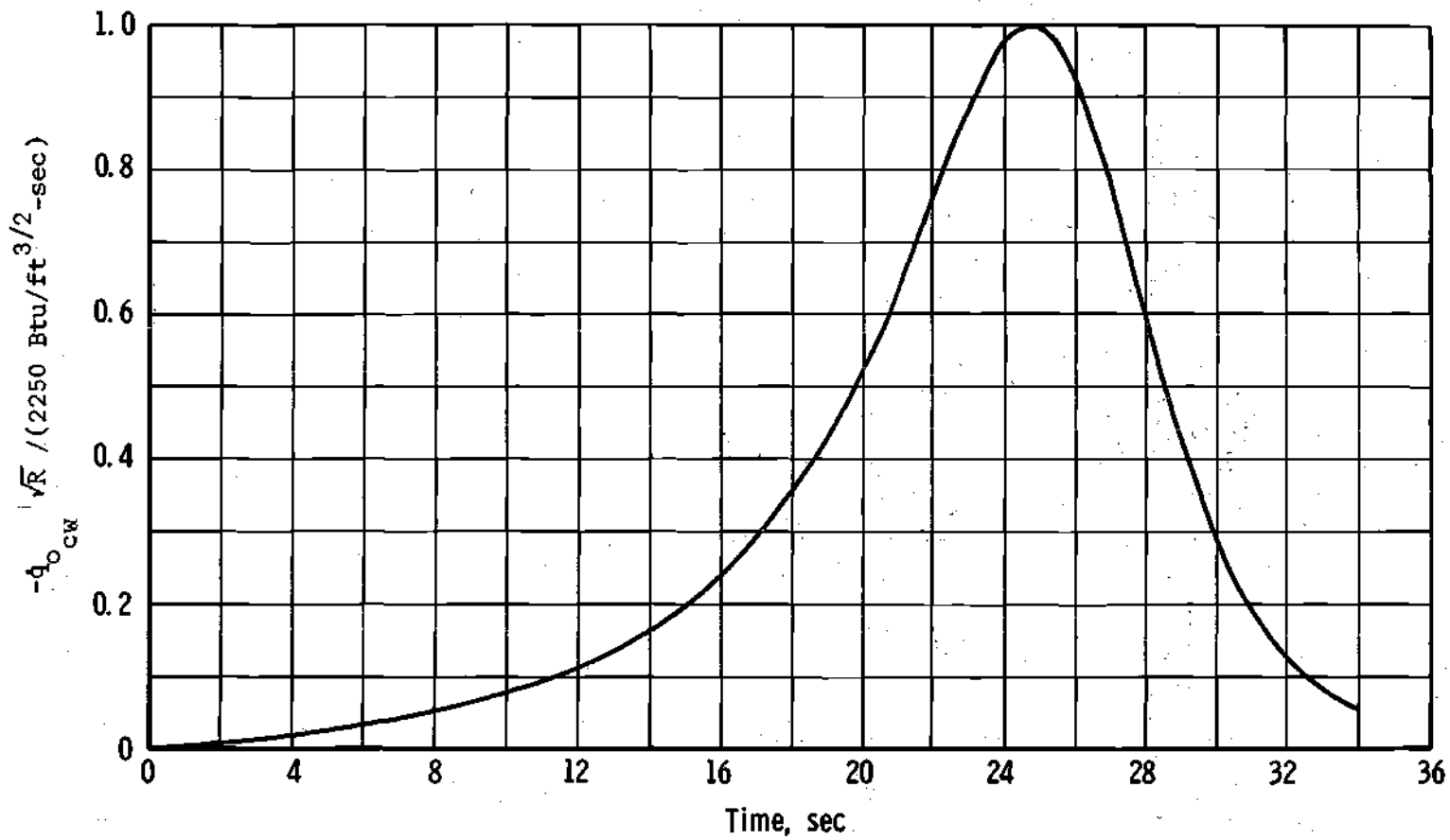


Figure 17. Stagnation Point Heat Flux versus Time from Re-entry at 300,000 ft: ICBM

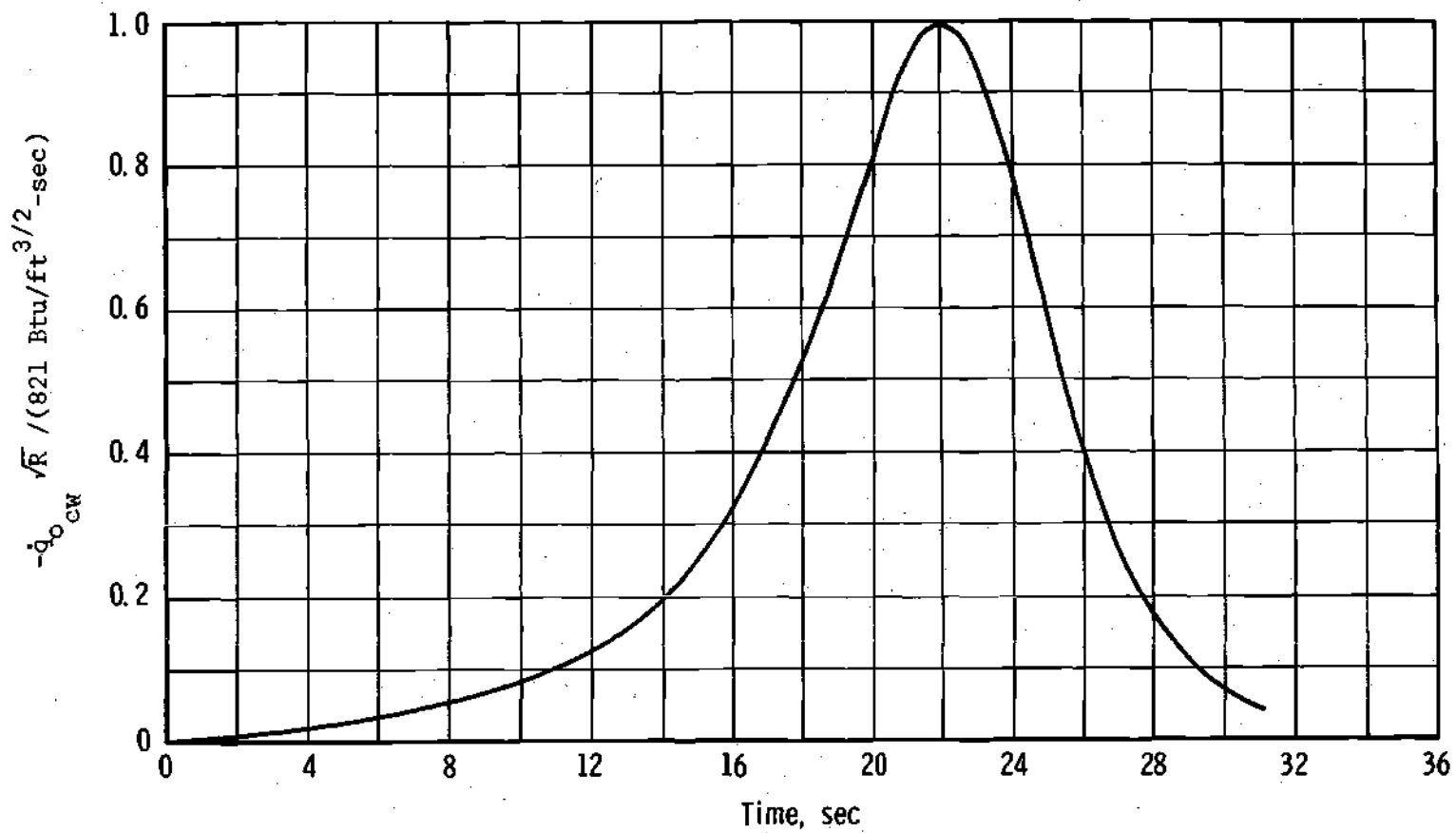


Figure 18. Stagnation Point Heat Flux versus Time from Re-entry at 300,000 ft: IRBM

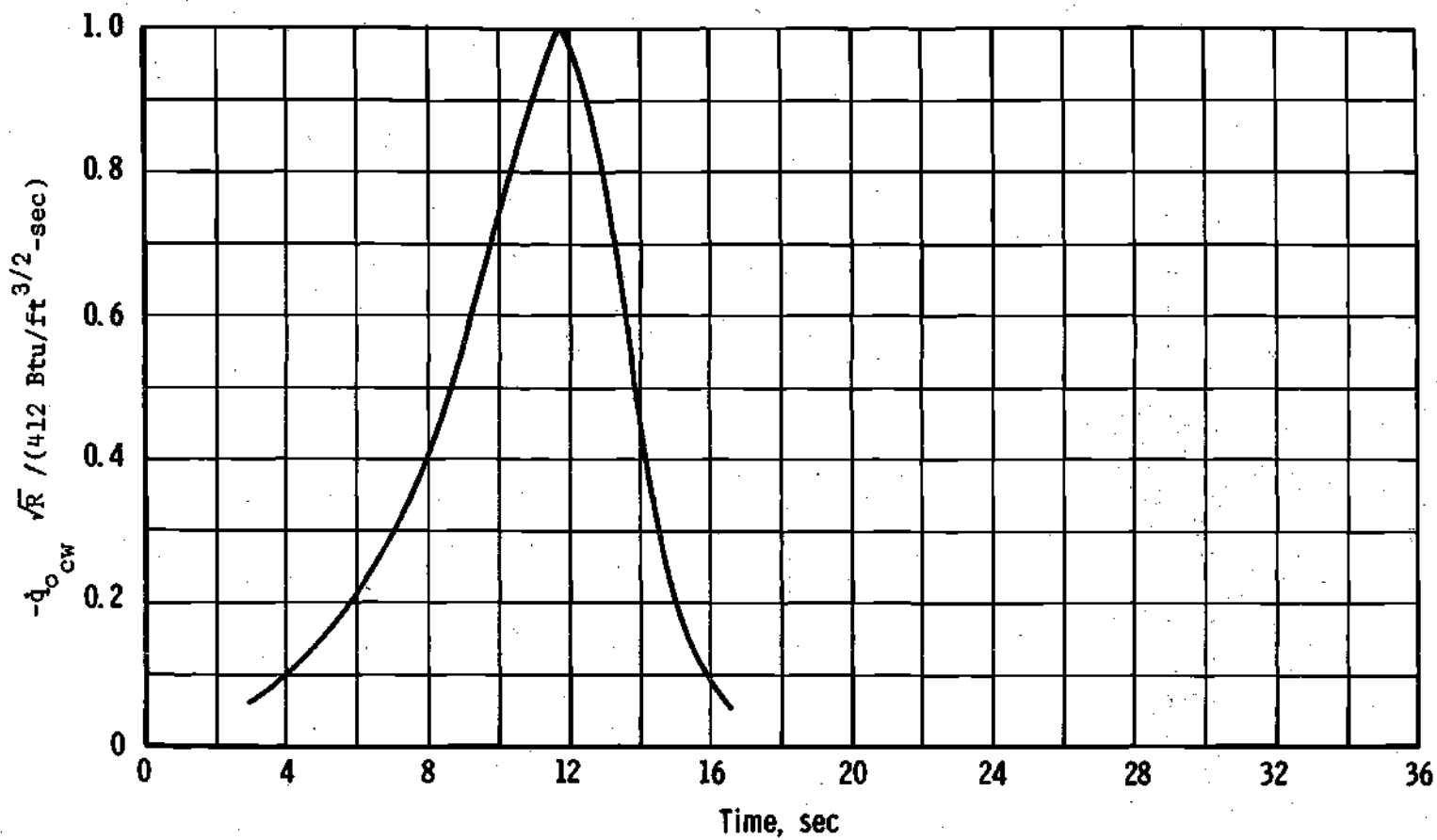


Figure 19. Stagnation Point Heat Flux versus Time from  
Re-entry at 300,000 ft: Trailblazer II Vehicle

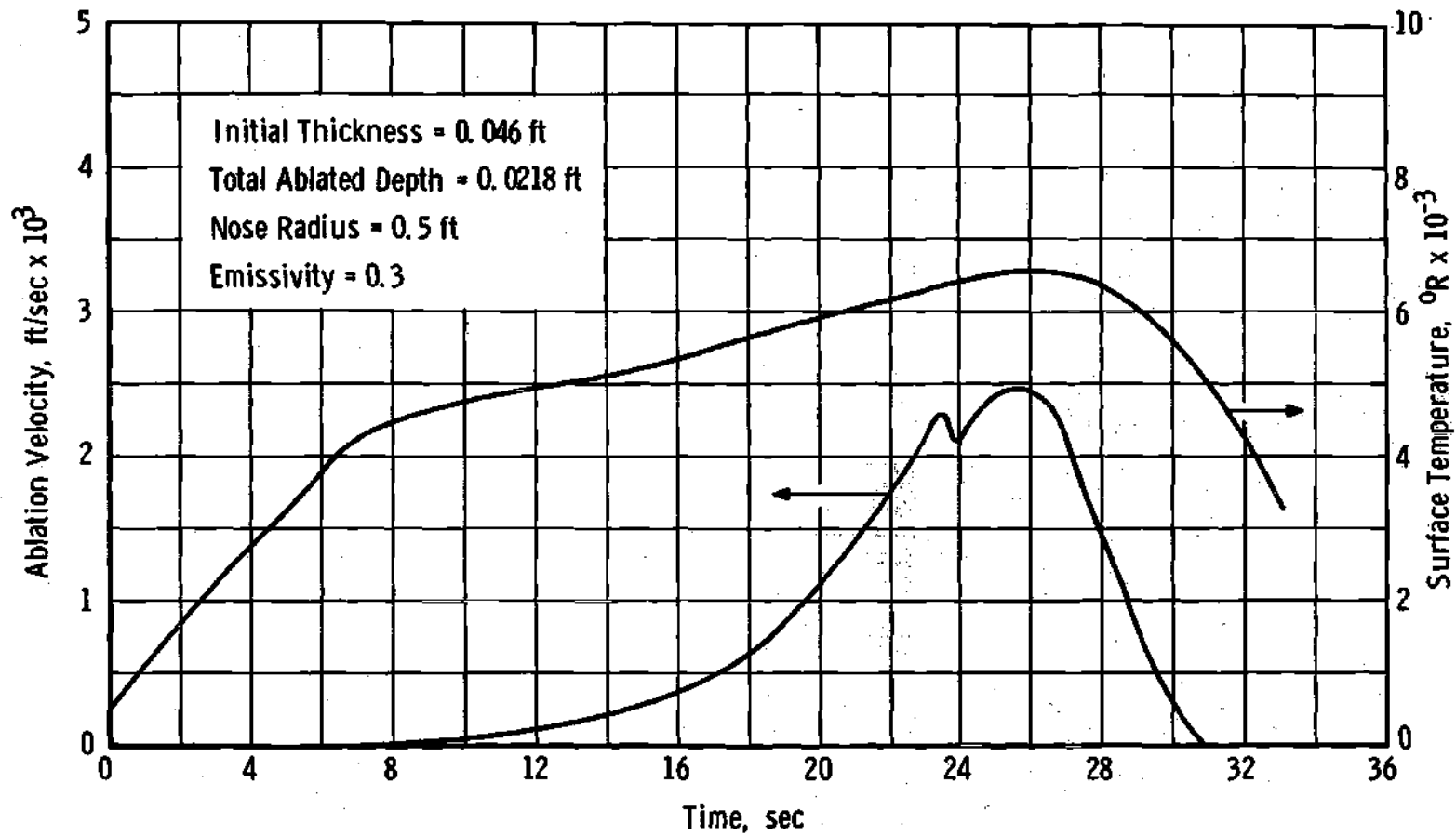


Figure 20. Ablation Velocity and Surface Temperature versus Time from Re-entry at 300,000 ft: ICBM



Figure 21.. Vaporization Fraction versus Time from Re-entry at 300,000 ft: ICBM

ablation of S.C.F.S. along the ICBM trajectory. The stagnation point radius of curvature was taken to be 0.5 ft and the initial thickness was taken to be 0.551 inches.

Figure 22 on page 102 shows the ablation rate and surface temperature for the ablation of S.C.F.S. along the IRBM trajectory. The vaporization fraction for this case is given in Figure 23 on page 103. As with the ICBM, the nose radius was taken to be 0.5 ft and the initial thickness 0.551 inches.

The ablation rate and surface temperature and the vaporization fraction are given in Figures 24 and 25 on pages 104 and 105, respectively, for the trajectory of the Trailblazer II vehicle. As reported in reference 49, the Trailblazer II has a nose radius of 0.51 ft. The initial thickness was assumed to be 0.551 inches.

#### Discussion of Results

For the initial thickness of the S.C.F.S. heat shield selected, it was found that there was practically no rise in temperature of the backside for the duration of flight along the three trajectories considered. This may be attributed to the relatively low thermal diffusivity of S.C.F.S. and also the fact that the flight times were relatively short for all of the trajectories.

Of particular interest are the two peaks in the ablation rate which occur in the ICBM and IRBM trajectories. These peaks occur because of the way in which the heat flux and stagnation pressure vary near the vicinity of the peaks. It is also suspected that transient effects are partly responsible for this phenomenon through the inertia of the surface temperature to the rapidly changing heat flux.

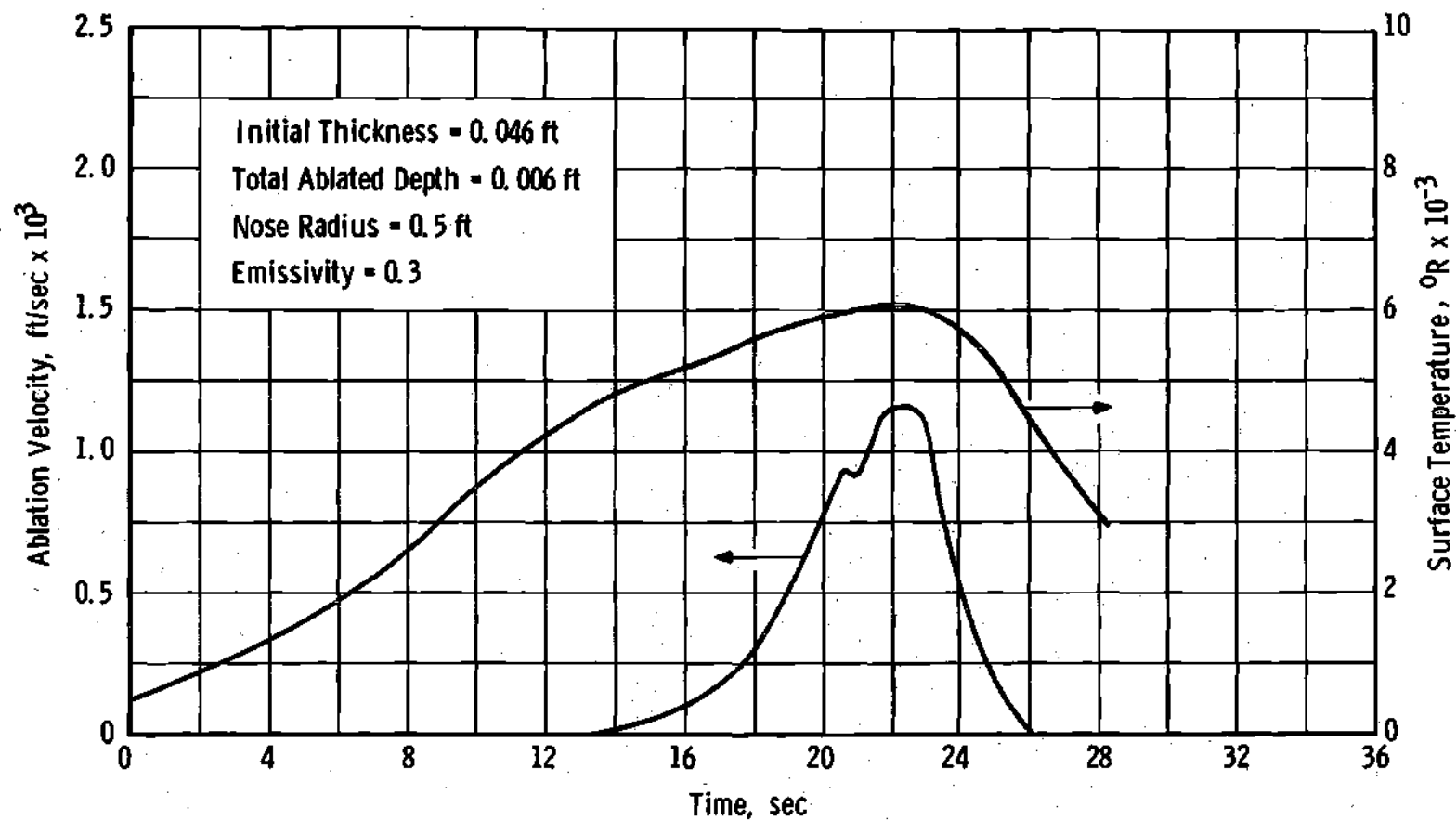


Figure 22. Ablation Velocity and Surface Temperature versus Time from Re-entry at 300,000 ft: IRBM

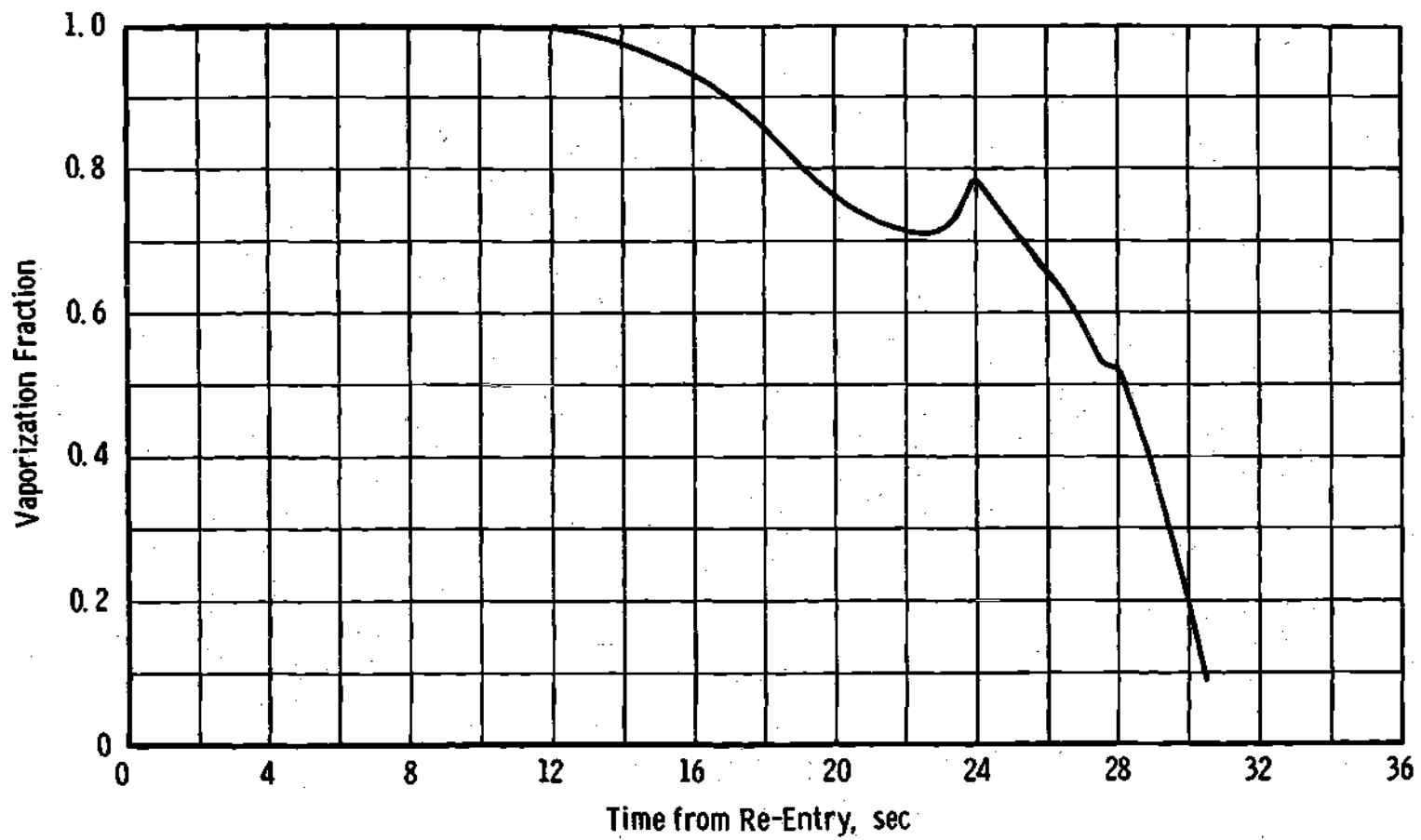


Figure 23. Vaporization Fraction versus Time from Re-entry at 300,000 ft: IRBM

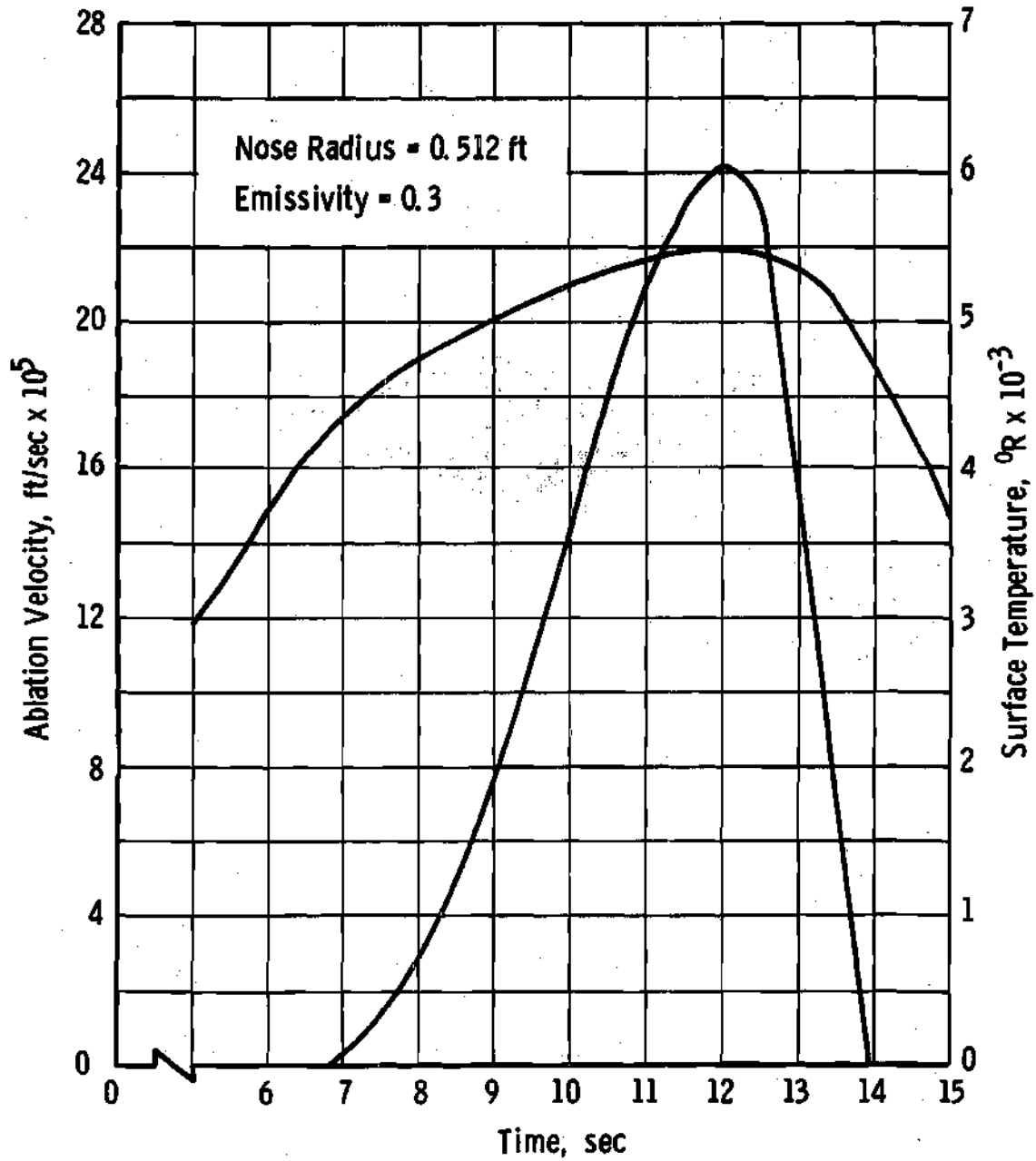


Figure 24. Ablation Velocity and Surface Temperature versus Time from Re-entry at 300,000 ft: Trailblazer II Vehicle

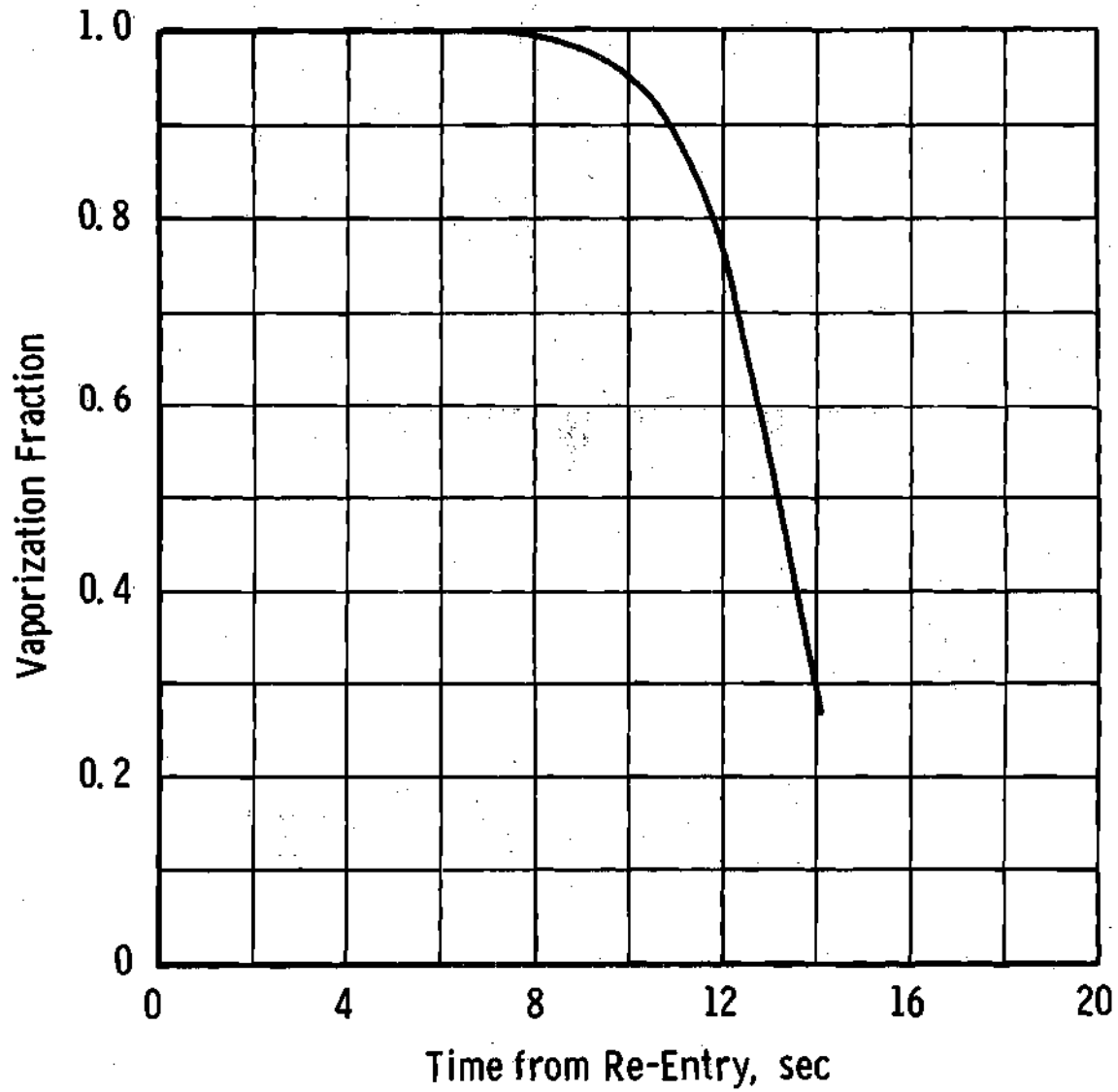


Figure 25. Vaporization Fraction versus Time from Re-entry at 300,000 ft: Trailblazer II Vehicle

For the trajectories selected, it is seen that S.C.F.S. performs quite well at the stagnation point as an ablative heat shield. However, it should not be inferred that S.C.F.S. would be suitable for use as an ablative heat shield on every kind of re-entry vehicle. Although the calculations are not included here, the performance of S.C.F.S. along a trajectory used in reference 51 to illustrate the performance of graphite as an ablative heat shield material was evaluated. For this trajectory the re-entry angle was  $16.5^\circ$ , the re-entry flight velocity 24,500 ft/sec and the ballistic coefficient,  $W/C_D A$ , 3000 lbf/ft<sup>2</sup>. In keeping with the assumed nose radius of the graphite shield (51), the nose radius was taken to be 0.25 inch. For this application it was found that S.C.F.S. would not be suitable. It was found that more than 0.25 inch of S.C.F.S. was ablated even before appreciable flow began. Thus, any generalization regarding the performance of S.C.F.S. as a heat shield material for re-entry vehicles on the basis of the calculations presented in this study would not be justified.

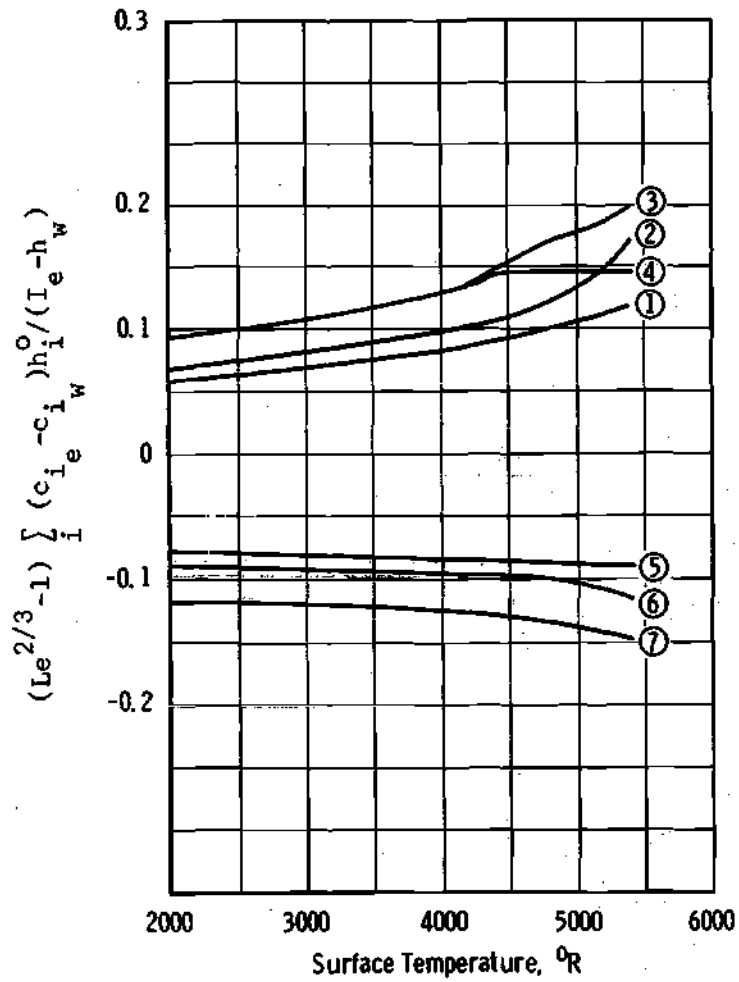
#### The Effect of Lewis Number Different from Unity

Referring to Equations (4-59a) and (4-59c) it can be seen that for the frozen boundary layer, the Lewis number has two separate effects. The effect in Equation (4-59a) is related to the contribution to the energy flux at the surface due to the convection and diffusion of various species to the surface and their recombination there. The effect of Lewis number in Equation (4-59c) can be considered a mass transfer effect which is due to the effect of the Lewis number on the concentration profiles in the boundary layer. The concentration boundary layer thickness decreases as the Lewis number increases.

In order to obtain an estimate of the magnitude of the Lewis number effect in Equation (4-59a) for silica vaporizing into air, the parameter

$$(Le^{2/3} - 1) \frac{\sum_i (c_{i_e} - c_{i_w}) h_i^0}{I_e - h_w}$$

was calculated as a function of surface temperature for a range of stagnation pressures and enthalpies. The Lewis number was taken to be the same as for equilibrium air at the same stagnation enthalpy and pressure and the surface was assumed to be in equilibrium for the calculations. The results of the calculations are presented in Figure 26 on page 108. It is interesting to note that the parameter is less than 0.2 for all of the conditions under which calculations were made. It follows that there is less than 20 per cent error in the heat flux as calculated from Equation (4-59a) for the frozen boundary layer and the heat flux as calculated from Equation (4-60a) for the case of the Lewis number being unity. The reason that the parameter has opposite signs for the high and low enthalpy levels can be attributed to the fact that the Lewis number is greater than unity at the lower enthalpy level and less than unity at the higher enthalpy level where there is considerable dissociation.



Le taken to be the Lewis number of equilibrium air as given in NACA TN-4150 Reference 52.

$P_e$ , atm	0.01	0.1	1.0	10.0
$I_e$ , Btu/lbm				
2,480	④	③	②	①
10,000	⑦	⑥	⑤	

Figure 26. Effect of Lewis Number on Heat Transfer

## CHAPTER VII

## COMPARISON OF EXPERIMENTAL AND THEORETICAL RESULTS

In Chapter V the results of an experimental study on the ablation of S.C.F.S. in the exhaust of an oxy-hydrogen rocket motor were discussed. Then in Chapter VI, the results of a theoretical study on the ablation of S.C.F.S. under environmental conditions corresponding to the environment of the oxy-hydrogen rocket motor exhaust in which the experimental studies were conducted were discussed. The purpose of this chapter is to make a comparison between the results of the experimental and theoretical investigations and to discuss the comparison.

The comparison is made using the theoretical calculations based on equilibrium vaporization from the surface of the ablating S.C.F.S. However, recalling from Chapter VI that the theoretical ablation rate, heat of ablation and backside temperature response for nonequilibrium vaporization are practically the same as for equilibrium vaporization, the comparison also applies to the results of the theoretical calculations based on nonequilibrium vaporization from the surface.

Discussion of the Comparison ofTheoretical and Experimental Results

Figure 9 on page <sup>79</sup>79 shows the theoretical average ablation rate distribution along the centerline of the rocket exhaust along with the experimentally determined values of the average ablation rate. Considering the many assumptions that were necessary in order to obtain a

theoretical solution to the ablation problem in the rocket exhaust, the general agreement between experiment and theory is quite good. The difference in the trends of the theoretical and experimental curves is thought to be the result of the choice of heat flux used in the calculations for the theoretical behavior of the S.C.F.S. It is noted that agreement is very good at the 6-inch location where the measured value of heat flux could be used in the calculations. It is estimated that if the heat flux were increased by about 55 per cent at 4 and 5 inches from the exit of the nozzle for the calculations, the theory would exhibit the same trend as the experiment there. Reference to Figure 7 on page 75 shows that an increase of 55 per cent would certainly not be unrealistic since there is considerable uncertainty in any extrapolation used. Since there is such a large difference in the measured heat flux at 6 and 8 inches from the exit, it would not be unrealistic to choose a much lower heat flux at 7 inches in order to make the theory and experiment agree better there. After careful consideration, it was decided that nothing would be gained by using a posteriori values of heat flux in order to obtain better agreement between the experiment and theory. At a particular location behind the exit of the motor, one would expect the theoretical average ablation rate to increase as the run time is increased since the heat flux is constant and transient effects are less pronounced. Figure 9 on page 79 shows this trend in the theoretical average ablation rate; however, it is interesting to note that the experimental average ablation rate exhibits the opposite trend. It is believed that this is the result of the decrease in heat flux as ablation takes place with the face of the sample moving away

from the exit of the motor.

Figure 10 on page 80 shows the experimental and theoretical heat of ablation of S.C.F.S. in the rocket exhaust. As was defined earlier, the heat of ablation here is simply the stagnation point heat flux divided by the average rate of mass ablation. In general, the comments made regarding the disagreement between theory and experiment for the ablation rate apply also to the heat of ablation. It is interesting to note that the theoretical heat of ablation is virtually independent of location along the centerline of the rocket exhaust, whereas the experimental heat of ablation shows considerable dependence on location. If the heat flux at a particular location behind the exit of the rocket motor is varied arbitrarily while keeping the environmental conditions constant, it can be shown that the theoretical heat of ablation of S.C.F.S. at that location is relatively independent of the heat flux. It follows that a reasonable a posteriori value of heat flux to obtain better agreement between experiment and theory at a particular location could be calculated by multiplying the ratio of the theoretical to experimental heat of ablation by the heat flux used in the calculations at that location.

Figure 11 on page 81 shows the theoretical and experimental temperature response of the backside of the S.C.F.S. specimens upon exposure to the rocket exhaust. Figure 11 shows that the experimentally determined backside temperature rises much faster than the theoretically determined temperature. It may be recalled from Chapter IV that the theoretical calculations were made assuming the backside to be perfectly insulated. However, the thermocouples were affixed to the backsides of

the specimens with a small amount of silica cement and were not insulated otherwise. It is theorized that in addition to the heat received at the backside by conduction through the specimen, there was a back flow of hot gas into the backside region causing additional heating--particularly to the relatively unprotected thermocouple. Clearly this could cause the rapid rise in the experimentally measured backside temperature; however, it would take further testing to establish the validity of this hypothesis.

#### Summary

The general agreement between the experimentally determined ablation rate and heat of ablation in the rocket exhaust is quite good. The difference in the variation of the experimental and theoretical ablation rate, and also heat of ablation, with distance from the exit of the rocket motor is thought to be the result of the choice of heat flux used in the calculations. After careful examination, it is concluded that the validity of the experimentally determined backside temperature is questionable. Additional experiments designed to protect the backside from the possible back flow of hot exhaust gases would be needed to reach a definite conclusion regarding the backside temperature.

## CHAPTER VIII

## CONCLUSIONS AND RECOMMENDATIONS

A theoretical and experimental investigation of the ablation of slip cast fused silica has been made. The theoretical study treated the ablation of S.C.F.S. in the exhaust of an oxy-hydrogen rocket motor and also the ablation of S.C.F.S. in air under re-entry or simulated re-entry conditions. Both equilibrium and nonequilibrium vaporization were considered in the theoretical analysis. Flat plates of S.C.F.S. were tested normal to the flow in the exhaust of a small oxy-hydrogen rocket motor and the results of the study were compared with the numerical results of the theoretical study for ablation in this environment. The variables which were compared were ablation rate, heat of ablation and the backside temperature response. The agreement between the theoretical and experimental results was quite good considering the many assumptions that were necessary in order to obtain the theoretical solution, and it can be concluded that the theory is satisfactory for predicting the ablation rate of S.C.F.S. in the rocket exhaust. The results of the experimental and theoretical study on the ablation of S.C.F.S. in the rocket exhaust indicate that S.C.F.S. is a very good ablator for the environmental conditions found in the rocket exhaust.

In order to give proper consideration to the interaction of S.C.F.S. with the environment of the oxy-hydrogen rocket motor, an analysis of the oxy-hydrogen rocket motor test facility was made.

Separate analyses for flow in the rocket motor itself, mixing of the rocket exhaust with the atmosphere and flow through the shock that stands ahead of a body placed in the exhaust were made. The combined analyses made possible the determination of the variables which characterize the environment of the rocket exhaust, such as stagnation point enthalpy, temperature and species concentrations, from only the experimentally determined stagnation pressure distribution along the centerline of the rocket exhaust. The environmental conditions determined in this manner were used as input to the theoretical solution for the ablation of S.C.F.S. in order to obtain the theoretical predictions regarding the behavior of S.C.F.S. in the rocket exhaust. This approach to the determination of the effect of the environment, particularly the chemistry of the environment, on the material being tested appears to be both reasonable and desirable.

With regard to the suitability of the oxy-hydrogen rocket motor as a test facility for conducting ablation studies, it can be said that it gives a relatively severe thermal environment with moderate stagnation pressures and temperatures. However, from the standpoint of the geometry and size of the specimens that can be tested, it is concluded that a larger rocket motor than used in this study would be more desirable for testing purposes.

On the basis of the model introduced to represent the mechanism of nonequilibrium vaporization, it can be concluded for ablation in the rocket exhaust that nonequilibrium vaporization has considerable influence on the fraction of ablating material that vaporizes but almost no influence on the ablation rate itself. However, it should be mentioned

that no conclusion can be reached regarding the validity of the model for nonequilibrium on the basis of the experimental studies conducted.

For the illustrative trajectories and nose radii selected to study the performance of S.C.F.S. as an ablative heat shield material, it was found that S.C.F.S. performed very well.

The following recommendations are made regarding further research on the ablation of S.C.F.S. and the oxy-hydrogen rocket motor as a test facility:

1. The ablation of S.C.F.S. should be investigated experimentally over a large range of conditions. Testing over a range of operating conditions for the oxy-hydrogen rocket motor and testing over a range of operating conditions in an arc plasma wind tunnel would be desirable.

2. Stagnation point heat flux measurements should be made at distances less than six inches from the exit of the rocket motor so that ablation calculations could be made using measured heat flux rather than extrapolated heat flux data as was used in this study.

3. Further study should be devoted to the investigation of the separate phenomena which occur during the ablation of S.C.F.S. such as surface vaporization and melt flow. Surface vaporization could probably be studied by observing the behavior of S.C.F.S. at elevated temperatures in a vacuum. Melt flow might be studied by designing an experiment in which the mechanism of melt removal could be well defined, for example, a rotating disk of S.C.F.S. exposed to a high temperature environment, and in which the vaporization would be negligibly small.

4. Theoretical analyses similar to those developed for the ablation of S.C.F.S. in the rocket exhaust should be performed for other ablative materials and compared with experimental data.

## APPENDIX A

## ROCKET TEST FACILITY

The Rocket Motor

An analysis of flow in the rocket motor based on isentropic flow of a perfect gas having constant specific heats is reported in reference 46. The following analysis is similar to the analysis given there; however, variable specific heats are considered and justifications for a number of simplifying assumptions are given.

The gas mixture in the rocket motor combustion chamber is assumed to be in chemical equilibrium. For the oxy-hydrogen ratio and chamber pressure at which the motor is operated, it can be seen from reference 53 that there is little dissociation in the combustion chamber and it is reasonable to assume that the only species present are molecular hydrogen and water vapor. It will be assumed that the flow through the nozzle is frozen at the nondissociated combustion chamber composition. This is a reasonable assumption since it can be shown that there is not a great deal of difference in the frozen and equilibrium composition throughout the nozzle.

Although the combustion chamber and nozzle are water cooled, it will be assumed that the flow is adiabatic. This assumption is justified in the following manner. The total heat transfer rate to the water cooled nozzle calculated from an energy balance on the cooling water (54) is less than 5 Btu/sec or approximately 180 Btu per pound of

gas flowing through the nozzle. Since the stagnation enthalpy\* of the gas in the nozzle is in excess of 5400 Btu/lbm, it follows that the stagnation enthalpy of the gas flowing through the nozzle changes by less than 3-1/2 per cent due to cooling which justifies the assumption of adiabatic flow.

For one dimensional reversible, frozen and adiabatic flow of a perfect gas having temperature dependent specific heats, the following differential equations can be written:

Energy

$$UdU + dh_T = 0 \quad (A-1)$$

Momentum

$$UdU + \frac{dp}{\rho} = 0 \quad (A-2)$$

Continuity

$$\frac{dU}{U} + \frac{dA}{A} + \frac{d\rho}{\rho} = 0 \quad (A-3)$$

---

\* Stagnation enthalpy here refers to the sum of the kinetic energy and the sensible enthalpy of the gas in the nozzle with the reference state for the enthalpy being 0 °R.

State

$$p = \rho \frac{\bar{R}_u}{\bar{M}_f} T \quad (\text{A-4})$$

It is assumed that the gaseous molecular oxygen and hydrogen both enter at 77 °F--the base state temperature for thermodynamic data in reference 55. Since gaseous molecular oxygen and hydrogen are in their base states, it follows that the chemical enthalpy of the gas mixture is zero everywhere in the nozzle and Equation (A-1) can be integrated to give

$$\frac{U^2}{2} + h_T = - c_{H_2O_f} h_{H_2O}^o \quad (\text{A-5})$$

Combining Equations (A-1), (A-2) and (A-4) and integrating yields

$$\int_{T_c}^T \frac{\bar{M}_f c_{P_f}}{\bar{R}_u} \frac{dT}{T} = \ln \frac{P}{P_c} \quad (\text{A-6})$$

Assuming that the flow in the diverging section of the rocket nozzle is supersonic, the throat velocity must be the sonic velocity there and

$$U_t = \sqrt{\gamma_f \frac{\bar{R}_u}{\bar{M}_f} T_t} \quad (\text{A-7})$$

where  $\gamma_f$  is the ratio of the specific heats of the mixture at the throat temperature. From Equations (A-5) and (A-7) it follows that the throat temperature is given by the implicit relationship

$$\gamma_f \frac{\bar{R}_u}{\bar{M}_f} \frac{T_t}{2} + \int_{T_r}^{T_t} c_{P_f} dT = -c_{H_2O_f} h_{H_2O}^{\circ} \quad (A-8)$$

Now combining the integrated form of the continuity Equation (A-3) with Equations (A-5) and (A-6) gives

$$A_E^2 \left( -2c_{H_2O_f} h_{H_2O}^{\circ} - 2 \int_{T_r}^{T_E} c_{P_f} dT \right) \left( \frac{T_t}{T_E} \right)^2 = A_t^2 \gamma_t \frac{\bar{R}_u}{\bar{M}_f} T_t e^{-2 \int_{T_t}^{T_E} \frac{\bar{M}_f c_{P_f}}{\bar{R}_u T} dT} \quad (A-9)$$

The chamber temperature can be calculated from Equation (A-5) with  $U$  taken to be zero. That is

$$\int_{T_r}^{T_c} c_{P_f} dT = -c_{H_2O_f} h_{H_2O}^{\circ} \quad (A-10)$$

For the molar oxy-hydrogen ratio of one-to-four at which the motor is operated, it follows that no dissociation  $c_{H_2O_f} = 0.9$  and  $c_{H_2f} = 0.1$ . Using the data in Appendix F, the combustion chamber temperature calculated from Equation (A-10) is found to be 5925 °R from Equation (A-8), and for the area ratio given in Table 1 on page 65, the exit temperature given by Equation (A-9) is 3360 °R. If it is assumed that the flow expands to atmospheric pressure, the theoretical chamber pressure is calculated from Equation (A-6) to be 308 psia which compares favorably with the measured value of 275 psia given in reference 46. For the exit temperature of 3360 °R, the exit velocity as

calculated from Equation (A-5) is 12,500 ft/sec with a corresponding exit Mach number of 2.74.

#### Turbulent Mixing of the Rocket Motor Exhaust with the Atmosphere

This analysis essentially follows that of Libby (56); the actual rocket exhaust being idealized by the turbulent mixing of an axisymmetric, uniform and homogeneous supersonic jet with a quiescent atmosphere at a uniform pressure.\* The exhaust is assumed to be free of shocks. The flow is assumed to be frozen in composition and the turbulent Prandtl, Lewis and Schmidt numbers equal to unity. Thus, the equations describing the flow as taken from reference (56) are

##### Momentum

$$\rho U \frac{\partial U}{\partial z} + \rho V \frac{\partial U}{\partial r} = \frac{1}{r} \frac{\partial}{\partial r} (\rho \epsilon_T r \frac{\partial U}{\partial r}) \quad (A-11)$$

##### Energy

$$\rho U \frac{\partial \bar{h}}{\partial z} + \rho V \frac{\partial \bar{h}}{\partial r} = \frac{1}{r} \frac{\partial}{\partial r} (\rho \epsilon_T r \frac{\partial \bar{h}}{\partial r}) \quad (A-12)$$

##### Continuity

$$\frac{\partial(\rho U)}{\partial z} + \frac{1}{r} \frac{\partial(r \rho V)}{\partial r} = 0 \quad (A-13)$$

---

\*The Reynolds number for turbulence of a jet based on the efflux velocity and exit diameter of the jet is of the order of 2000 (57). Since the Reynolds number at the exit of the nozzle is of the order of 100,000, there is good reason to suppose that the rocket exhaust is turbulent.

Species Continuity

$$\rho U \frac{\partial c_i}{\partial z} + \rho V \frac{\partial c_i}{\partial r} = \frac{1}{r} \frac{\partial}{\partial r} \left( \rho \epsilon_T r \frac{\partial c_i}{\partial r} \right) \quad (\text{A-13})$$

The coordinate system for the above equations is shown in Figure 27 on page 123. For convenience the following nondimensional variables are defined:

$$\bar{U} = U/U_E \quad (\text{A-14a})$$

$$\bar{H} = \frac{\bar{h} - \bar{h}_\infty}{\bar{h}_E - \bar{h}_\infty} \quad (\text{A-14b})$$

$$\bar{K}_i = \frac{c_i - c_{i_\infty}}{c_{i_E} - c_{i_\infty}} \quad (\text{A-14c})$$

The subscript  $\infty$  denotes conditions at the outer edge of the jet where the atmosphere is relatively unaffected by mixing.

It should be noted that  $\bar{U}$ ,  $\bar{H}$ , and  $\bar{K}_i$  all satisfy the same differential operator.

$$\rho U \frac{\partial}{\partial z} + \rho V \frac{\partial}{\partial r} = \frac{1}{r} \frac{\partial}{\partial r} \left( \rho \epsilon_T r \frac{\partial}{\partial r} \right) \quad (\text{A-15})$$

The boundary conditions on  $\bar{U}$ ,  $\bar{H}$  and  $\bar{K}_i$  are  
at  $z = 0$

$$\bar{U} = \bar{H} = \bar{K}_i = 1 \quad 0 \leq r \leq d/2$$

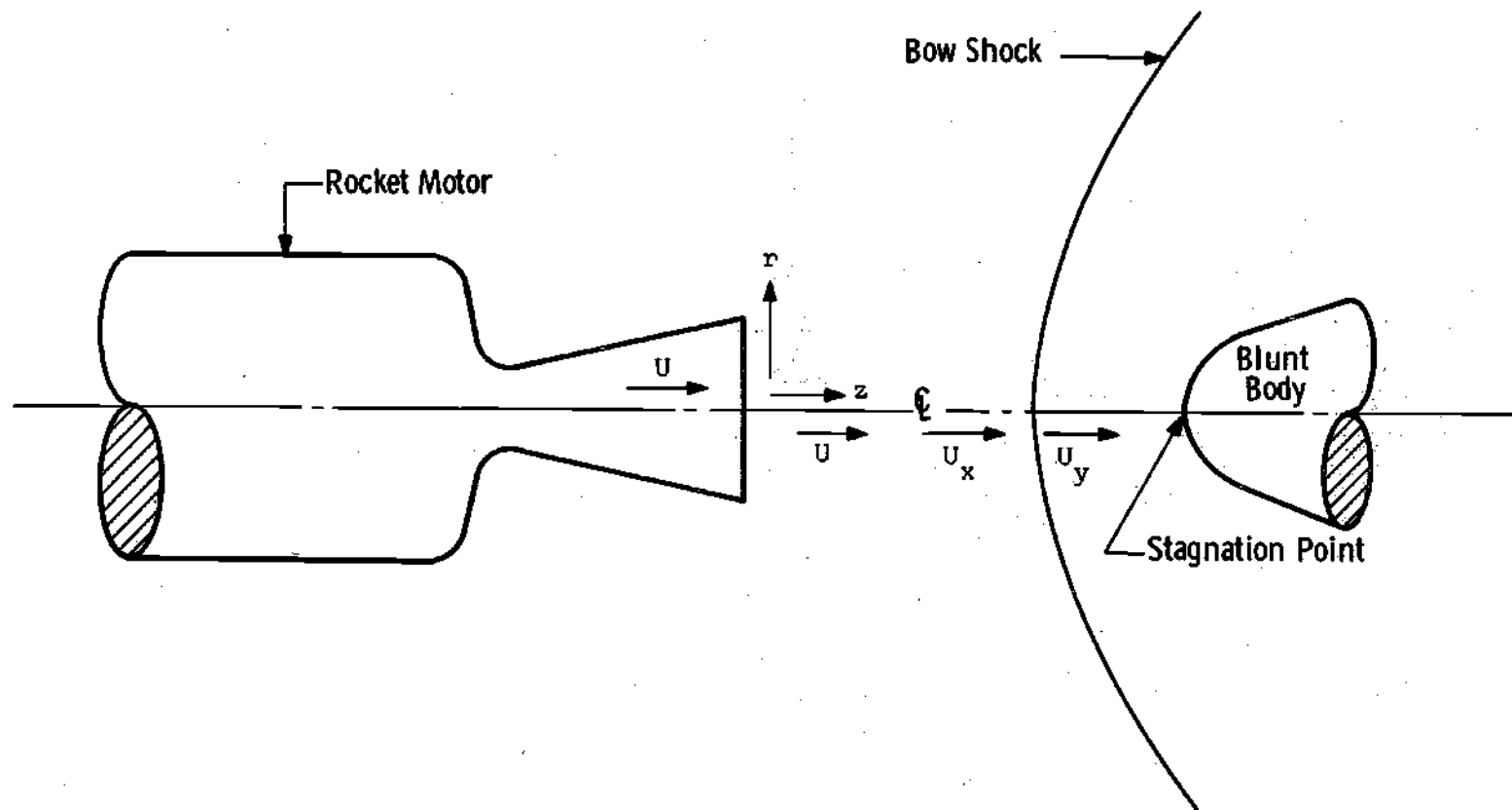


Figure 27. Sketch of Flow Regimes in Rocket Exhaust

$$\bar{U} = \bar{H} = \bar{K}_i = 0 \quad d/2 < r < \infty$$

as  $z \rightarrow \infty$

$$\bar{U} = \bar{H} = \bar{K}_i = 0 \quad 0 < z < \infty$$

Since  $\bar{U}$ ,  $\bar{H}$  and the  $\bar{K}_i$ 's satisfy the same differential equation and the same boundary conditions, they must be equal in the entire region of mixing. That is

$$\bar{U} = \bar{H} = \bar{K}_i \quad \begin{array}{l} 0 \leq r < \infty \\ 0 \leq z < \infty \end{array} \quad (\text{A-16})$$

According to the analysis of flow in the rocket motor given above, molecular hydrogen and water vapor are the only species which leave the exit of the motor. It follows that

$$\bar{K}_{\text{H}_2\text{O}} = c_{\text{H}_2\text{O}}/c_{\text{H}_2\text{O}_F} = \bar{U} \quad (\text{A-17})$$

$$\bar{K}_{\text{H}_2} = c_{\text{H}_2}/c_{\text{H}_2F} = \bar{U} \quad (\text{A-18})$$

$$\bar{K}_{\text{N}_2} = c_{\text{N}_2}/c_{\text{N}_2\infty} = \bar{U} \quad (\text{A-19})$$

$$\bar{K}_{\text{O}_2} = 1 - c_{\text{O}_2}/c_{\text{O}_2\infty} = \bar{U} \quad (\text{A-20})$$

Now

$$\bar{h} = \frac{U^2}{2} + c_{H_2} \int_{T_r}^T c_{p_{H_2}} dT + c_{H_2O} \int_{T_r}^T c_{p_{H_2O}} dT + \quad (A-21)$$

$$c_{N_2} \int_{T_r}^T c_{p_{N_2}} dT + c_{O_2} \int_{T_r}^T c_{p_{O_2}} dT$$

or

$$\bar{h} = \bar{U}^2 \frac{U_E^2}{2} + \bar{U} h_{T_f} + (1 - \bar{U}) h_{T_{air}} \quad (A-22)$$

where

$$h_{T_f} = c_{H_2O_f} \int_{T_r}^T c_{p_{H_2O}} dT + c_{H_2f} \int_{T_r}^T c_{p_{H_2}} dT \quad (A-23)$$

and

$$h_{T_{air}} = c_{N_2\infty} \int_{T_r}^T c_{p_{N_2}} dT + c_{O_2\infty} \int_{T_r}^T c_{p_{O_2}} dT \quad (A-24)$$

It is sufficiently accurate to assume that the temperature  $T_r$  is equal to the reference temperature, that is 77 °F. It follows that the total enthalpy which includes chemical effects is

$$h = \bar{h} + \bar{U} c_{H_2O_f} h_{H_2O}^{\circ} \quad (A-25)$$

or

$$\bar{U}^2 \frac{U_E^2}{2} + \bar{U} h_{T_f} + (1 - \bar{U}) h_{T_{air}} + \bar{U} c_{H_2O_f} h_{H_2O}^o = 0 \quad (A-26)$$

Equation (A-26) effectively gives the temperature distribution in the mixing region as a function of the nondimensional velocity  $\bar{U}$  since  $h_{T_f}$  and  $h_{T_{air}}$  can be formulated as functions of temperature alone.

Figure 28 gives the concentration distribution of species along the centerline of the rocket exhaust as a function of nondimensional velocity for the molar oxy-hydrogen ratio of one-to-four. For the data given in Appendix F, the temperature and Mach number variation along the centerline as a function of nondimensional velocity is given in Figure 29 on page 128.

#### Conditions Downstream of Normal Shock

Since the exhaust of the rocket motor is supersonic at the exit, placing a blunt body in the stream will result in the formation of a detached shock in front of the body. If the body is a body of revolution placed so that its axis coincides with the centerline of the exhaust, the shock will be a symmetric bow shock. In the vicinity of the centerline the shock is virtually normal and the flow is one dimensional.

In view of the relatively high pressure and temperature behind the shock, it is reasonable to assume that the flow behind the shock is in chemical equilibrium. If flow through the shock is assumed to be adiabatic, the following equations relate conditions just upstream of the shock, which are known, to conditions just downstream of the shock:

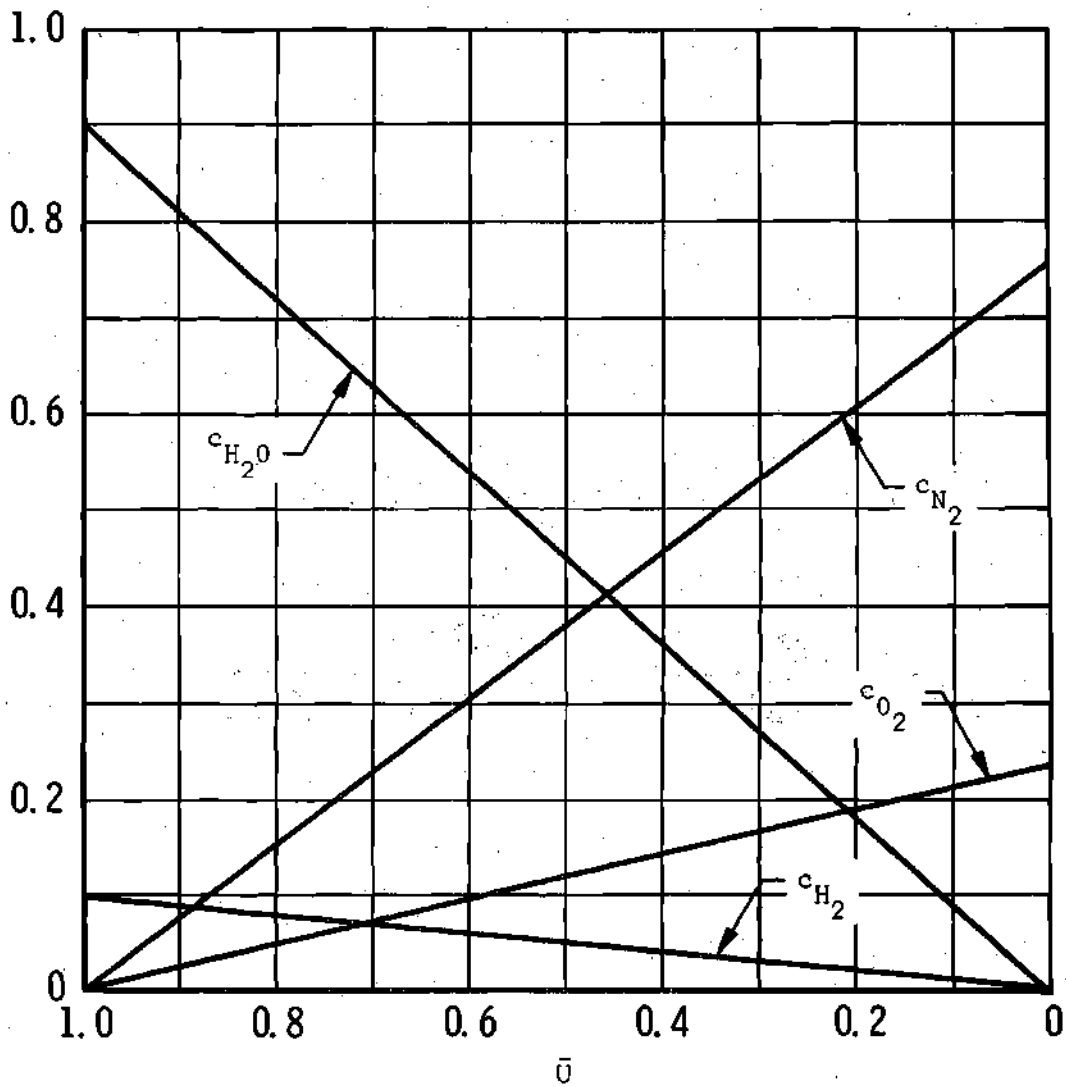


Figure 28. Mass Fractions of Species versus Nondimensional Centerline Velocity in Rocket Exhaust for Frozen Mixing

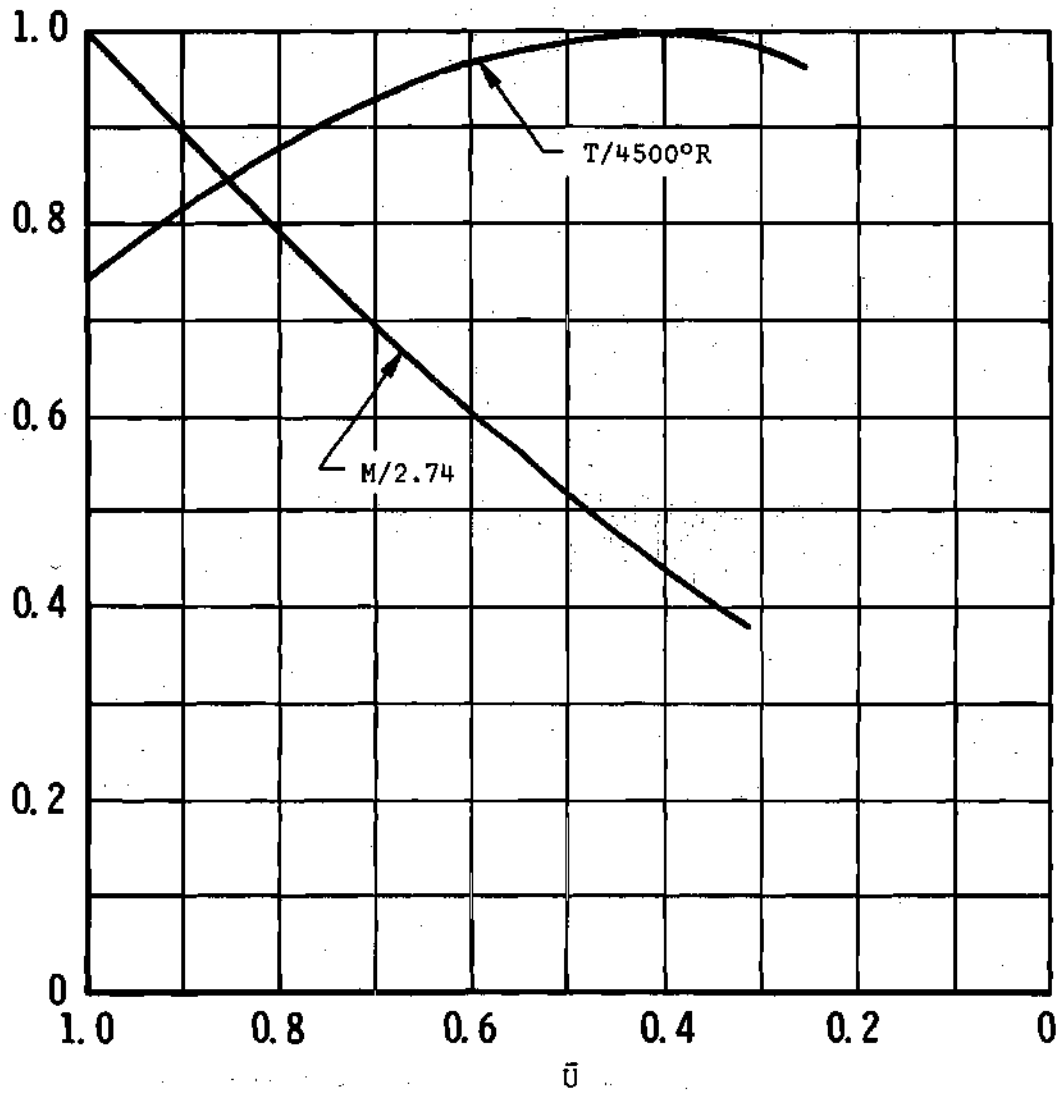


Figure 29. Mach Number and Temperature Distribution Along Centerline of Rocket Exhaust versus Nondimensional Centerline Velocity

Energy

$$h_x + \frac{U_x^2}{2} = h_y + \frac{U_y^2}{2} = 0 \quad (\text{A-27})$$

Momentum

$$p_x - p_y = \rho_x U_x (U_y - U_x) \quad (\text{A-28})$$

Continuity

$$\rho_x U_x = \rho_y U_y \quad (\text{A-29})$$

Conservation of Elements

$$\bar{c}_{N_x} = \bar{c}_{N_y} \quad (\text{A-30})$$

$$\bar{c}_{O_x} = \bar{c}_{O_y} \quad (\text{A-31})$$

$$\bar{c}_{H_x} = \bar{c}_{H_y} \quad (\text{A-32})$$

Chemical Equilibrium

$$\frac{p_{O_1}}{\sqrt{p_{O_2}}} = K_{P_3} \quad (\text{A-33})$$

$$\frac{P_H}{\sqrt{P_{H_2}}} = K_{P_4} \quad (\text{A-34})$$

$$\frac{P_{OH}}{\sqrt{P_{O_2}} \sqrt{P_{H_2}}} = K_{P_5} \quad (\text{A-35})$$

$$\frac{P_{H_2O}}{P_{H_2} \sqrt{P_{O_2}}} = K_{P_6} \quad (\text{A-36})$$

The equilibrium constants given in the equations of chemical equilibrium above are defined in terms of their respective chemical reaction equations in Chapter IV.

The equations of chemical equilibrium can be combined with Dalton's law of partial pressures and the equations of conservation of elements to give the following two polynomials in the square roots of the partial pressures of molecular hydrogen and oxygen:

$$\alpha \bar{X} \bar{Y}^2 + K_{P_4} \frac{\alpha}{2} \bar{X} \bar{Y} + K_{P_5} \frac{\alpha-1}{2} \bar{X}^2 \bar{Y} + K_{P_6} \frac{2\alpha-1}{2} \bar{X}^2 \bar{Y}^2 - \bar{X}^3 - \frac{1}{2} K_{P_3} \bar{X}^2 = 0 \quad (\text{A-37})$$

$$(1+\beta)(\bar{X} \bar{Y}^2 + K_{P_6} \bar{X}^2 \bar{Y}^2) + (1+\beta/2)(K_{P_4} \bar{X} \bar{Y} + K_{P_5} \bar{X}^2 \bar{Y}) + \bar{X}^3 + K_{P_3} \bar{X}^2 = p_e \bar{X} \quad (\text{A-38})$$

where for simplicity

$$\bar{X} = \sqrt{P_{O_2}}$$

and

$$\bar{Y} = \sqrt{p_{H_2}}$$

For a given temperature and pressure, these equations can be solved simultaneously to obtain  $P_{O_2}$  and  $p_{H_2}$  which can be used to determine the partial pressures of all of the other species.

#### Flow from the Normal Shock to the Stagnation Point

It is assumed that the flow from the normal shock to the stagnation point is adiabatic and in a state of shifting chemical equilibrium. In addition to the equations of chemical equilibrium (A-33) -- (A-38), the following differential equations can be written for the flow behind the shock:

##### Energy

$$UdU + dh = 0 \quad (A-39)$$

##### Momentum (Euler's Equation)

$$UdU + \frac{dp}{\rho} = 0 \quad (A-40)$$

Normally these equations must be integrated numerically together with the equations of chemical equilibrium. However, it was found by direct numerical integration that there is little error in calculating the stagnation pressure from the equation

$$p_e = p_y \left( 1 + \frac{\gamma_y - 1}{2} M_y^2 \right)^{\frac{\gamma_y}{\gamma_y - 1}} \quad (\text{A-41})$$

which can be derived by assuming reversible adiabatic flow of a non-reacting gas having constant specific heats. Since the adiabatic stagnation temperature under the condition of chemical equilibrium is dependent only on the stagnation pressure, it can be calculated once the stagnation pressure has been obtained from Equation (A-41). It is therefore not necessary to consider in detail the flow from the shock to the stagnation point in order to obtain the conditions at the stagnation point.

#### Conditions at the Stagnation Point

The gas mixture at the stagnation point is assumed to be in chemical equilibrium. Since the flow from just up stream of the shock to the stagnation point is assumed to be adiabatic, it can be seen from Equation (A-25) that the stagnation point total enthalpy is zero. It follows that

$$\sum_i \int_{T_r}^{T_e} c_{i,e} c_{p,i} dT + \sum_i c_{i,e} h_i^{\circ} = 0 \quad (\text{A-42})$$

The subscript e is used here since the conditions at the stagnation point are taken to be identical to the conditions at the edge of the gas boundary layer. Since the element mass fractions at the stagnation point are identical to the element mass fractions just down stream of

the shock, the mass fractions at the stagnation point are related to the stagnation point temperature and pressure by Equations (A-33) -- (A-38). Thus, for any given value of  $\bar{U}_x$ , the stagnation pressure can be calculated from Equation (A-41) and the stagnation point temperature and gas composition can be calculated by solving Equations (A-33) -- (A-38) and (A-42) simultaneously.

### Numerical Results

The numerical calculations were made by writing routines for a digital computer. Since the basic principles of the calculating procedure are straightforward, copies of the programs are not given; however, the rudiments of the procedure are outlined below. For a given value of  $\bar{U}_x$ , the element mass fractions just ahead of the shock were calculated from Equations (A-17) -- (A-20). Clearly these will be the element mass fractions just below the shock and along the centerline to the stagnation point also. Equations (A-27) -- (A-38) were solved simultaneously to give the conditions just down stream of the shock. Equation (A-41) was used to calculate the stagnation pressure. Finally, Equations (A-33) -- (A-38) and (A-42) were solved together to give the stagnation point temperature and gas composition.

Figures 30 and 31 show the variation of the stagnation point temperature, pressure and molecular weight with  $\bar{U}_x$ . From the experimentally determined variation of stagnation pressure with distance from the exit of the rocket motor, the theoretical variation of stagnation pressure with  $\bar{U}_x$  was used to determine the variation of  $\bar{U}_x$  with distance behind the motor's exit. This variation is shown in Figure 32.

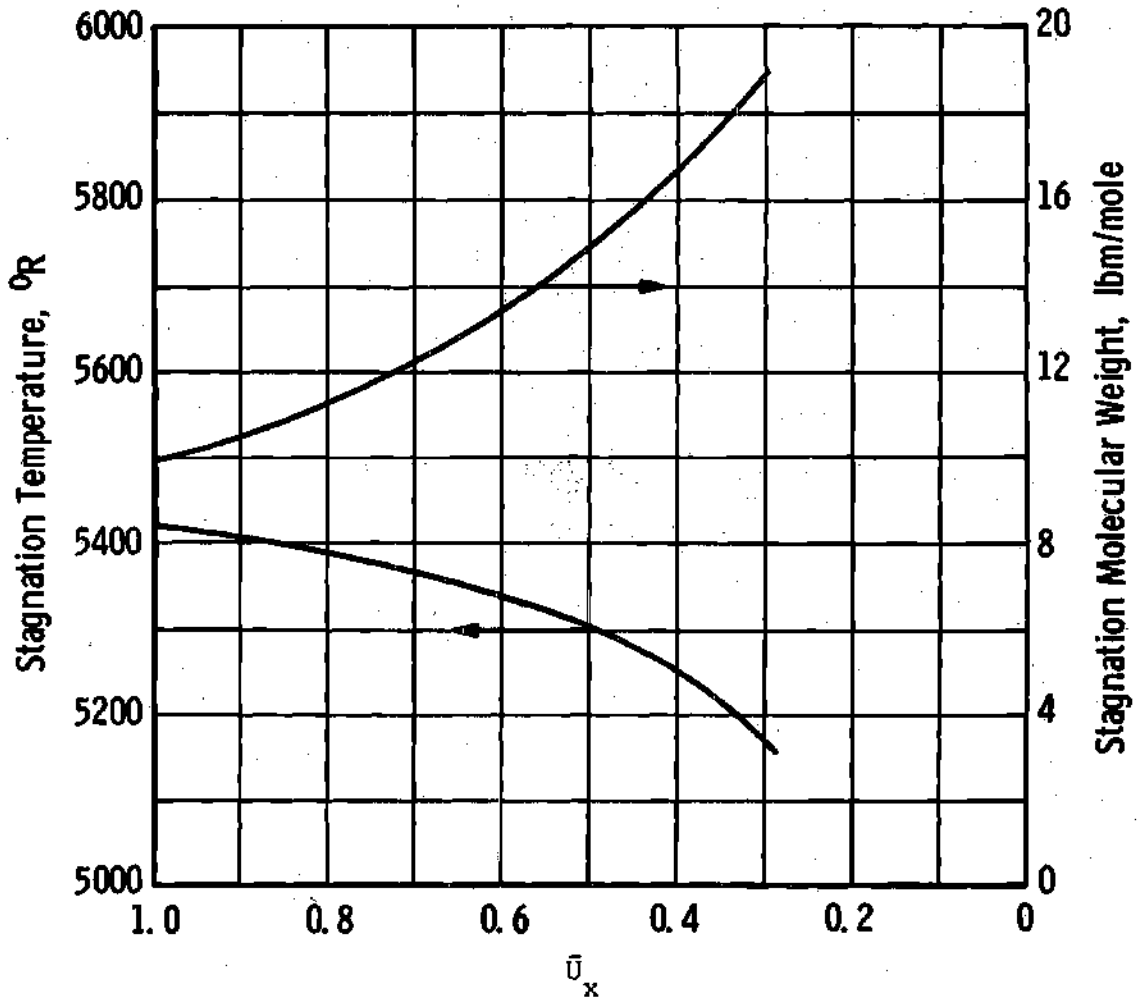


Figure 30. Stagnation Temperature and Molecular Weight versus Nondimensional Centerline Velocity Immediately Ahead of Shock

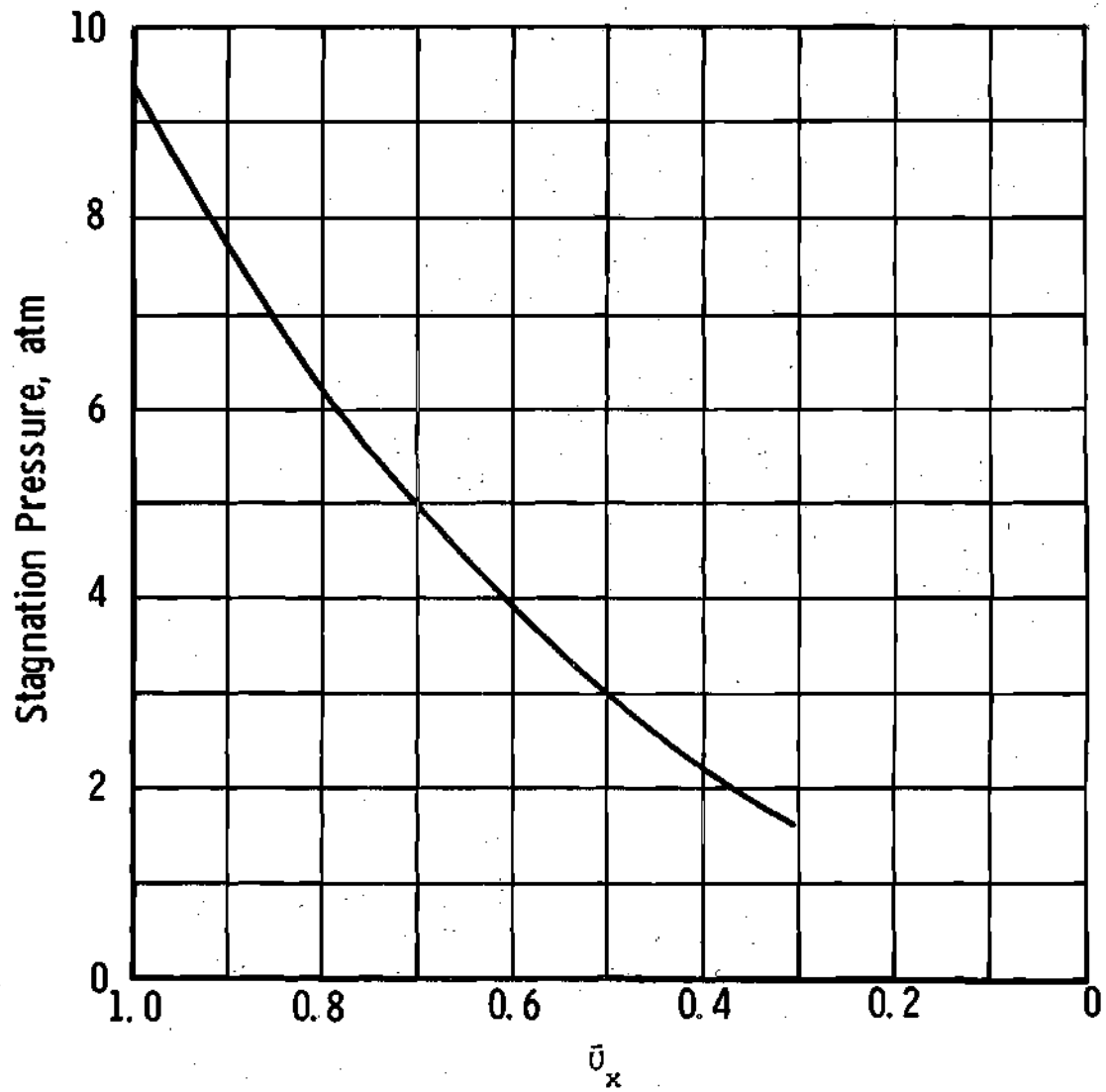


Figure 31. Stagnation Pressure versus  
Nondimensional Centerline Velocity

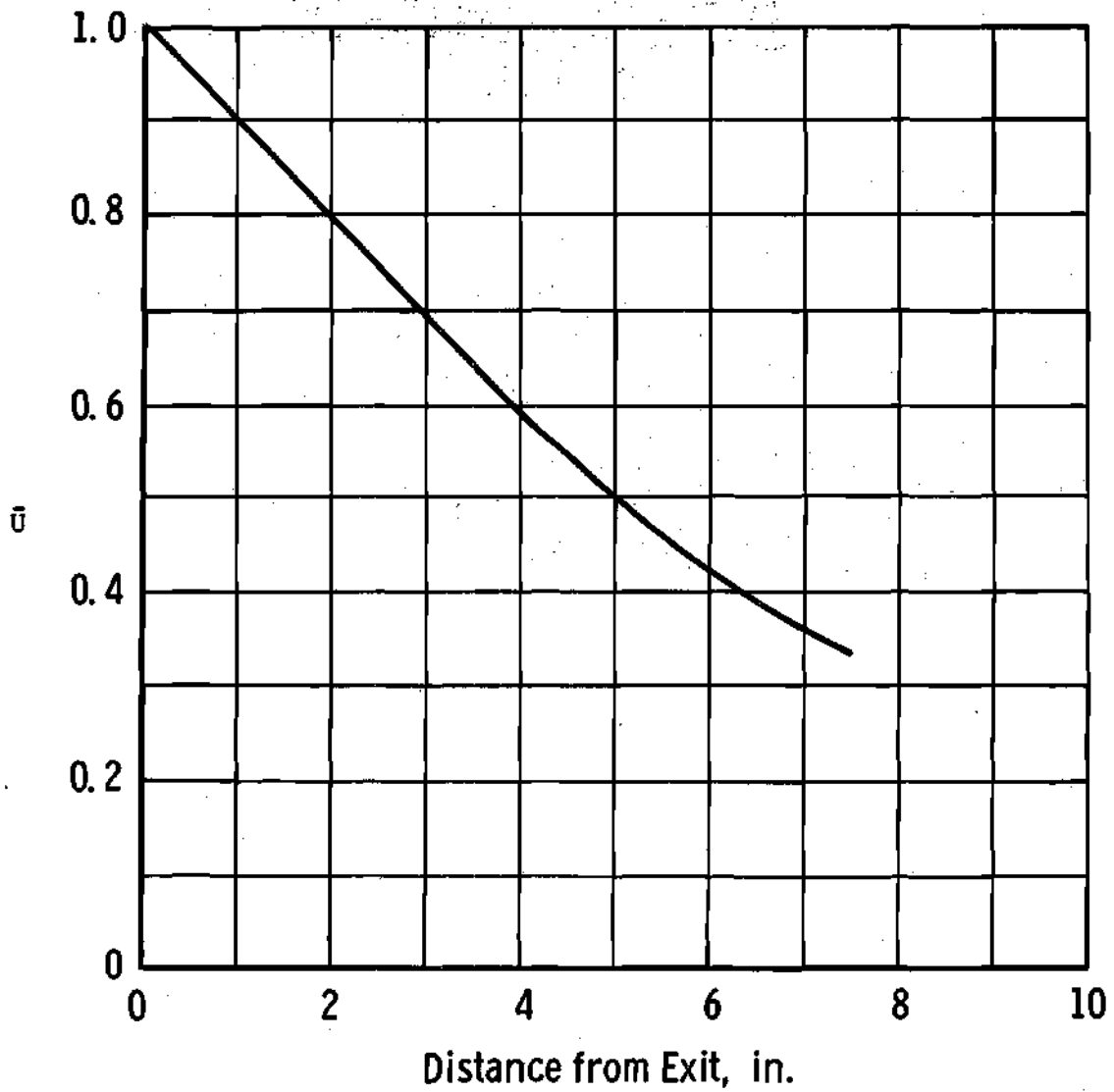


Figure 32. Nondimensional Centerline Velocity versus Distance from Exit of Rocket Motor

### Heat Transfer

The correlation formula of Fay and Riddell (44) for a Lewis number of unity is used in the theoretical prediction of the stagnation point heat transfer to a nonablating body in the rocket exhaust--a calorimeter for example. This formula is

$$-\dot{q}_{o,cw} / \sqrt{\left. \frac{dU_e}{ds} \right|_{sp}} = 0.76 \text{Pr}^{-0.6} \sqrt{\rho_e \mu_e} (I_e - h_{cw}) \quad (\text{A-43})$$

Although this formula was derived for air, it agrees quite well with heat transfer experiments conducted in methane-air combustion products (45) which to some extent justifies its use here.

The parameter on the left-hand side of Equation (A-43) is shown as a function of  $\bar{U}_x$  in Figure 33. The thermodynamic and transport property data used in the calculations are given in Appendix F. Figure 7 shows the theoretical cold surface heat transfer to a hemispherical body with the stagnation point velocity gradient calculated from the Newtonian approximation (Equation (4-68)).

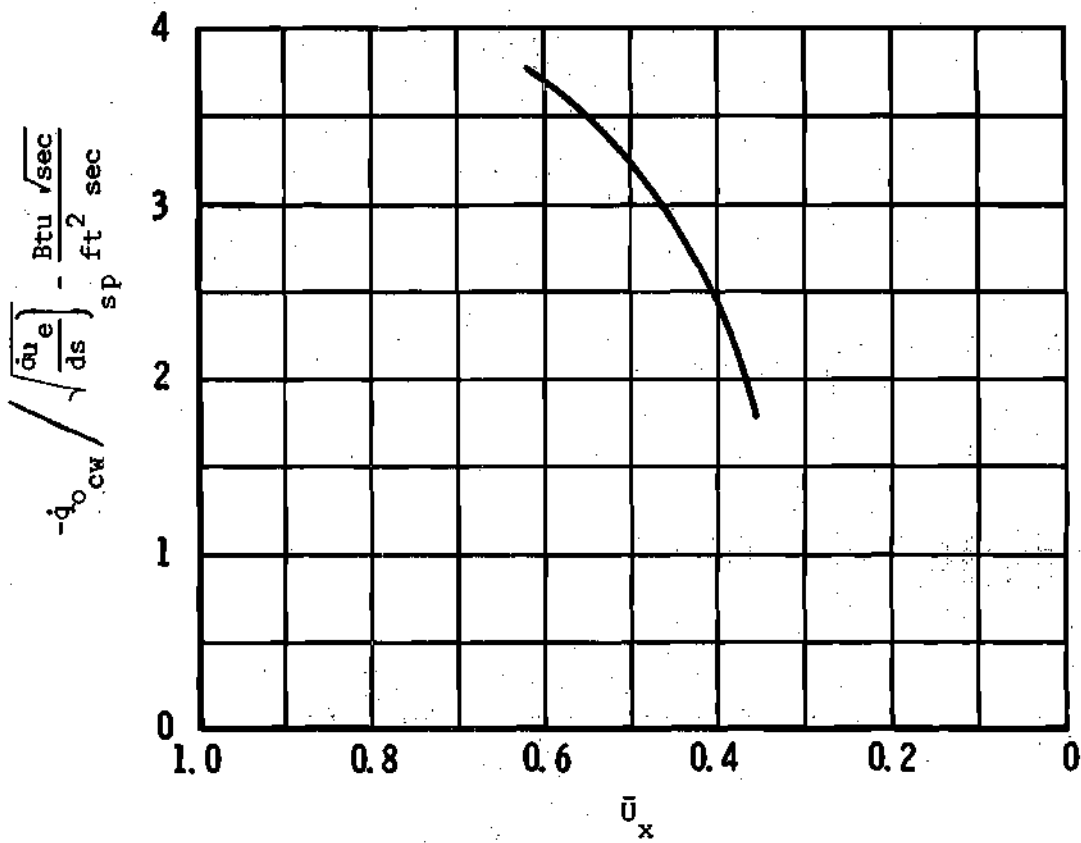


Figure 33. Stagnation Point Heat Flux Parameter versus Nondimensional Centerline Velocity in the Rocket Exhaust

## APPENDIX B

## CONVERGENCE AND STABILITY OF THE DIFFERENCE EQUATIONS

The numerical solution of partial differential equations by finite difference techniques is subject to two different kinds of errors. The first of these errors is the truncation error,<sup>\*</sup> which is the result of replacing a partial derivative by a finite difference quotient. Clearly the size of the truncation error is a function of the step sizes chosen for the independent variables of the partial differential equation; and, if the numerical solution is to converge to the exact solution, the truncation error must vanish as the step size is made to approach zero. Another error inherent in the numerical solution is numerical or "round off" error<sup>\*</sup> due to the fact that only a finite number of significant figures can be handled practically in the numerical computations. Numerical error is not usually a problem if the calculations are performed on a high speed digital computer.

For a partial differential equation having one dependent variable and two independent variables, it might appear that the choice of step sizes for the independent variables would be completely arbitrary. However, if the numerical solution is to remain stable, as is shown below, there is a relationship of the step size of one variable to the

---

<sup>\*</sup>Since there is no standard definition for these errors, it should be noted that the definitions used here are the same as used by Schneider (47).

step size of the other variable which must be satisfied.

#### Derivation of a Stability Criterion

The partial differential equation of concern in the present study is Equation (4-3a) of the text

$$\frac{\partial T}{\partial t} + v \frac{\partial T}{\partial y} = \alpha_s \frac{\partial^2 T}{\partial y^2} \quad (\text{B-1})$$

It is noted that if  $v = 0$ , Equation (B-1) is the one-dimensional heat conduction equation and as shown by Carslaw and Jaeger (48), a sufficient stability criterion is

$$\frac{\alpha_s \Delta t}{\Delta y^2} < \frac{1}{2} \quad (\text{B-2})$$

Following an approach similar to the one used by Carslaw and Jaeger (48) in the derivation of the above stability criterion, a stability criterion is derived for Equation (B-1). Replacing the derivatives in Equation (B-1) by finite difference quotients (see reference 36) yields

$$\frac{T_y^{t+\Delta t} - T_y^t}{\Delta t} + v \frac{T_{y+\Delta y}^t - T_{y-\Delta y}^t}{2\Delta y} = \alpha_s \frac{T_{y+\Delta y}^t - 2T_y^t + T_{y-\Delta y}^t}{\Delta y^2} \quad (\text{B-3})$$

Solving Equation (B-3) for  $T_y^{t+\Delta t}$  yields

$$T_y^{t+\Delta t} = M'(T_{y+\Delta y}^t + T_{y-\Delta y}^t) - (2M'-1)T_y^t - \frac{v^t \Delta y}{2\alpha_s} (T_{y+\Delta y}^t - T_{y-\Delta y}^t) \quad (B-4)$$

where

$$M' = \frac{\alpha_s \Delta t}{\Delta y^2} \quad (B-5)$$

Now if  $\delta T_y^{t+\Delta t}$  is a small change in  $T_y^{t+\Delta t}$  due to small changes  $\delta T_y^t$ ,  $\delta T_{y+\Delta y}^t$  in  $T_{y+\Delta y}^t$ ,  $T_{y-\Delta y}^t$  and  $T_{y+\Delta y}^t$ , respectively, then

$$\delta T_y^{t+\Delta t} = M'(1 - \frac{v^t \Delta y}{2\alpha_s}) \delta T_{y+\Delta y}^t + M'(1 + \frac{v^t \Delta y}{2\alpha_s}) \delta T_{y-\Delta y}^t - (2M'-1)\delta T_y^t \quad (B-6)$$

Supposing that the maximum error in  $T_{y+\Delta y}^t$ ,  $T_y^t$  and  $T_{y-\Delta y}^t$  is  $e'$  then the maximum error that is propagated to  $T_y^{t+\Delta t}$  is

$$|\delta T_y^{t+\Delta t}| \leq e' (M' |1 - \frac{v^t \Delta y}{2\alpha_s}| + M' |1 + \frac{v^t \Delta y}{2\alpha_s}| + |2M'-1|) \quad (B-7)$$

Now if the solution is to remain stable, the propagated error must not increase; thus,

$$M' |1 - \frac{v^t \Delta y}{2\alpha_s}| + M' |1 + \frac{v^t \Delta y}{2\alpha_s}| + |2M'-1| \leq 1 \quad (B-8)$$

Obviously a necessary condition on Equation (B-8) is

$$M' \leq \frac{1}{2} \quad (B-9)$$

If  $\frac{v^t \Delta y}{2 \alpha_s} \leq 1$ , it follows that

$$M' \leq \frac{1}{2} \quad (\text{B-10})$$

is a sufficient condition on Equation (B-8), and a sufficient, but not necessary, condition on the stability of the solution. If  $\frac{v^t \Delta y}{2 \alpha_s} > 1$ , then

$$M' \leq \frac{1}{1 + \frac{v^t \Delta y}{2 \alpha_s}} \quad (\text{B-11})$$

is the sufficient condition of stability of the numerical solution. The results are summarized in Table 3.

Schneider (47) pointed out that step sizes which do not satisfy the inequality (B-2) for the unsteady one-dimensional heat conduction equation without convection result in a violation of the First Law of Thermodynamics. This can also be shown to be the case for step sizes which do not satisfy the stability requirements in Table 3.

Table 3. Stability Criteria for  
the Numerical Solution

$\frac{v^t \Delta y}{2 \alpha_s}$	$M'$
0	$< \frac{1}{2}$
$< 1$	$< \frac{1}{2}$
$\geq 1$	$\leq \frac{1}{1 + \frac{v^t \Delta y}{2 \alpha_s}}$

## APPENDIX C

## HYPOTHETICAL ABLATION PROBLEM

In order to provide a check on the accuracy of the digital computer program used for the actual ablation calculations, a closed form solution to a hypothetical ablation problem was obtained and compared to the numerical computer solution of the same problem.

Formulation of the Problem

The vaporization of a semi-infinite slab having constant thermal properties and subjected to a heat input  $\dot{q}(t)$  from its environment is considered. The heat of vaporization of the material  $L_v$  is assumed to be constant. The temperature distribution must satisfy Equation (4-3a) of the text

$$\frac{\partial T}{\partial t} + v \frac{\partial T}{\partial y} = \alpha_s \frac{\partial^2 T}{\partial y^2} \quad (C-1)$$

where  $v$  is a function of time alone since there is no melting ablation. The initial temperature distribution is assumed to be

$$T(0,y) = T_0 e^{y/\delta_c} \quad (C-2)$$

where  $\delta_c$  is a constant and  $T_0$  is the initial surface temperature. The following boundary conditions are now imposed:

at  $y = 0$

$$k_s \frac{\partial T}{\partial y} = \dot{q}(t) - \rho_s L_v v$$

as  $y \rightarrow -\infty$

$$T = 0$$

$$\frac{\partial T}{\partial y} = 0$$

The ablation velocity  $v$  is assumed to vary with the surface temperature in the manner

$$v = v_o \left[ 1 - \left( \frac{T_o}{T(t,0)} \right)^{\frac{\bar{a} \delta_c}{v_o}} \right] \quad (C-3)$$

where  $v_o$  and  $\bar{a}$  are constants. It is assumed that the heat input  $\dot{q}(t)$  is of the form

$$\dot{q}(t) = C_1' \frac{t}{1 + C_2' t} + C_3' (1 + C_2' t)^{C_4'} \quad (C-4)$$

where  $C_1'$ ,  $C_2'$ ,  $C_3'$  and  $C_4'$  are constants. In order to obtain the solution, only two of these four constants may be chosen independently.

#### Closed Form Solution

It can be verified by direct substitution that

$$T(t,y) = T_o (1 + \bar{a} t) \frac{v_o}{\bar{a} \delta_c} e^{y/\delta_c} \quad * \quad (C-5)$$

is a solution to Equation (C-1) and the prescribed boundary and initial conditions if

$$\bar{a} = C'_2 \quad (C-6)$$

$$v_o = \frac{C'_1}{\rho_s L_v C'_2} \quad (C-7)$$

$$\delta_c = \frac{k_s T_o}{C'_3} \quad (C-8)$$

and

$$\delta_c = \frac{C'_1}{C'_4 (C'_2)^2 \rho_s L_v} \quad (C-9)$$

If  $C'_1$  and  $C'_2$  are the constants to be chosen independently, then

$$C'_3 = \frac{C'_1 k_s T_o}{C'_2 \rho_s L_v \alpha_s} \quad (C-10)$$

and

---

\* Although this solution was found by trial and error, it could be obtained through the use of the Laplace transformation.

$$C_4' = \frac{C_1'}{(C_2')^2 \delta_c \rho_s L_v} \quad (C-11)$$

#### Numerical Results

For the following numerical values of the constants, the exact closed form solution is compared to the numerical computer solution in Figures 34 and 35 on pages 148 and 149, respectively:

$$L_v = 5500 \text{ Btu/lbm}$$

$$K_s = 0.000097 \text{ Btu/ft-sec-}^\circ\text{R}$$

$$\alpha_s = 0.00000323 \text{ ft}^2/\text{sec}$$

$$\rho_s = 120 \text{ lbm/ft}^3$$

$$C_1' = 1.1 \text{ Btu/ft}^2\text{-sec}^2$$

$$C_2' = 0.01 \text{ sec}^{-1}$$

Clearly the agreement is very good between the two solutions.

It should be remarked that for certain other numerical values for the above constants, there was considerable difference between the closed form and numerical solutions. However, it was found that these numerical values gave unrealistically high heat fluxes at the vaporizing surface and correspondingly large temperature gradients which could not be handled accurately by the finite difference equations for the numerical solution.

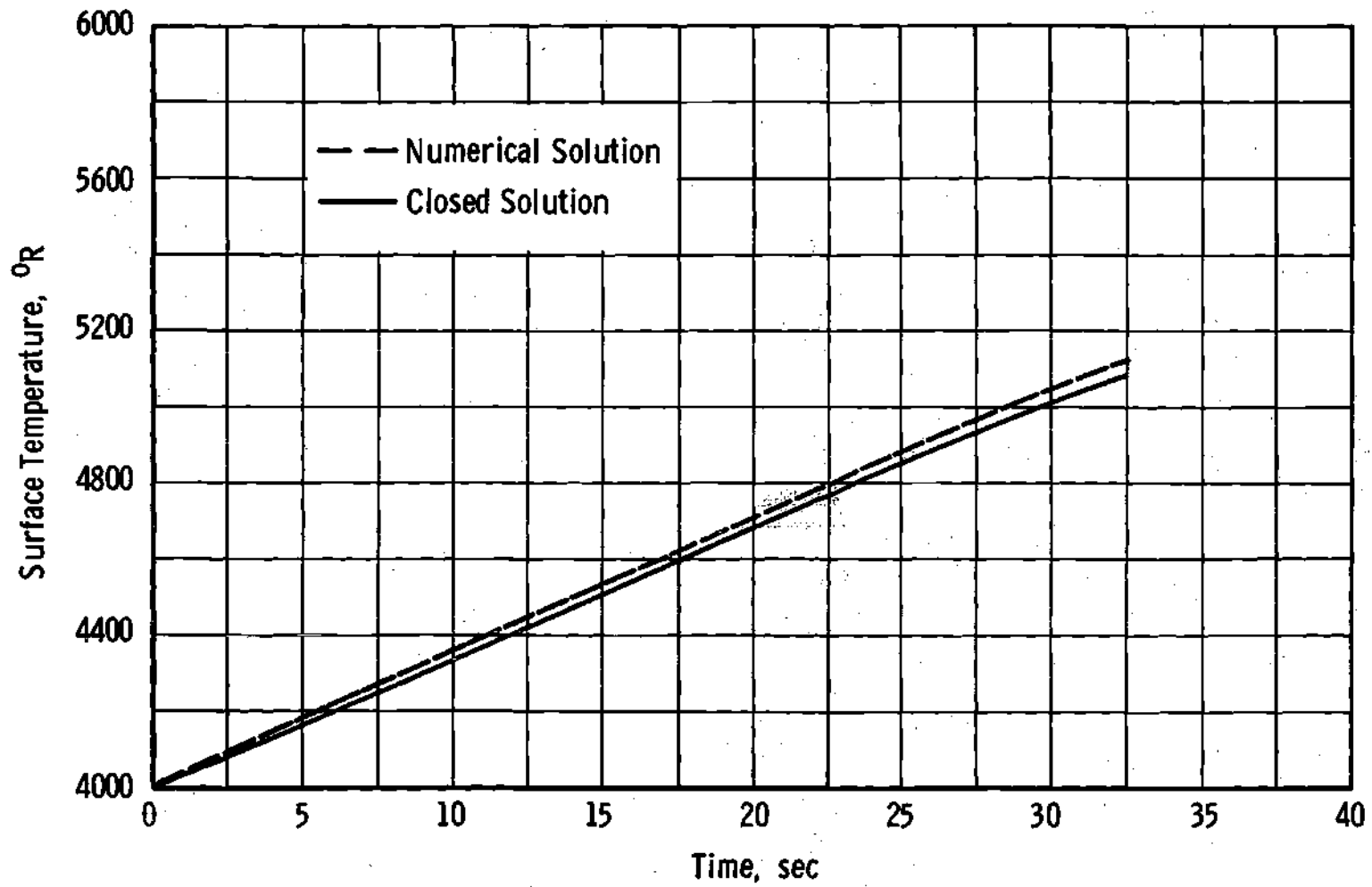


Figure 34. Surface Temperature versus Time for Hypothetical Ablation Problem

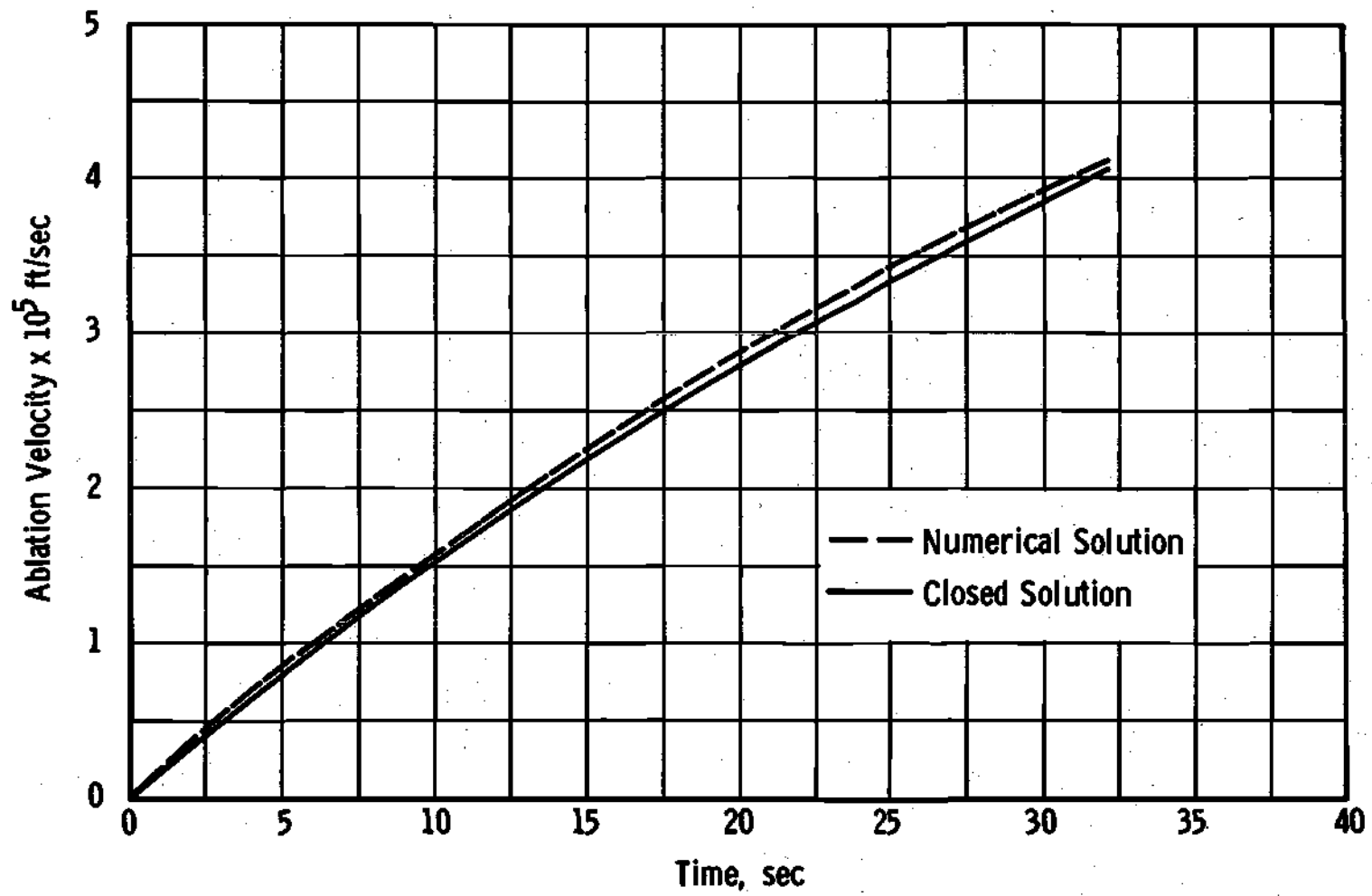
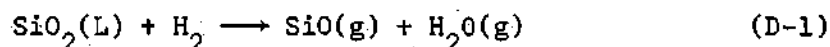


Figure 35. Ablation Velocity versus Time  
for Hypothetical Ablation Problem

## APPENDIX D

JUSTIFICATION FOR NEGLECTING Si AND SiH<sub>4</sub> VAPOR

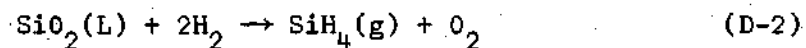
Studies of the reduction of silica by hydrogen gas by Grube and Speidel (58) and Tombs and Welch (40) indicate that the most important chemical reaction is



with SiO and H<sub>2</sub>O being the principle products of reaction. However, SiH<sub>4</sub> gas and Si vapor have also been observed (see reference 59) to be products of reaction when hydrogen gas is allowed to react with silica. This appendix is devoted to showing that the mole fractions of SiH<sub>4</sub> and Si are negligible compared to the mole fractions of the species considered in the oxy-hydrogen environment.

An Upper Bound on the Mole Fraction of SiH<sub>4</sub>

Considering the chemical reaction equation



it follows that

$$\frac{P_{\text{SiH}_4} P_{\text{O}_2}}{P_{\text{H}_2}^2} = K_{p7} \quad (\text{D-3})$$

where  $K_{P_7}$  is the equilibrium constant for the chemical reaction given by Equation (D-2). Combining Equation (4-121) with Equation (D-3) yields

$$P_{\text{SiH}_4} = P_{\text{H}_2}^2 \left( \frac{P_{\text{H}_2}}{P_{\text{H}_2\text{O}}} \right)^2 K_{P_7} K_{P_6}^2 \quad (\text{D-4})$$

Now

$$\frac{P_{\text{H}_2}}{P_{\text{H}_2\text{O}}} < 1 \quad (\text{D-5})$$

and

$$P_{\text{H}_2} < P_e \quad (\text{D-6})$$

Thus,

$$X_{\text{SiH}_4} < P_e K_{P_7} K_{P_6}^2 \quad (\text{D-7})$$

From the data given in Appendix F,

$$X_{\text{SiH}_4} < P_e \exp(-6.36 - 81000 \text{ }^\circ\text{R}/T) \quad (\text{D-8})$$

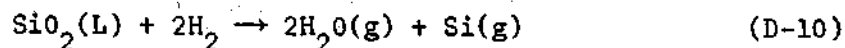
It is known that  $p_e < 10 \text{ Atm.}$  and  $T < 5400 \text{ }^\circ\text{R.}$ ; therefore

$$X_{\text{SiH}_4} < 10 \exp(-21.36) \quad (\text{D-9})$$

which is small enough to justify neglecting  $\text{SiH}_4$  in the analysis.

An Upper Bound on the Mole Fraction of Si

Considering the chemical reaction equation



it follows that

$$\frac{P_{\text{Si}} P_{\text{H}_2\text{O}}^2}{P_{\text{H}_2}^2} = K_{P_8} \quad (\text{D-11})$$

where  $K_{P_8}$  is the equilibrium constant for the chemical reaction given by Equation (D-10). Equation (D-11) can be rewritten to give

$$X_{\text{Si}} = \frac{1}{P_e} \left( \frac{P_{\text{H}_2}}{P_{\text{H}_2\text{O}}} \right)^2 K_{P_8} \quad (\text{D-12})$$

Now using Equation (D-5), it follows that

$$X_{\text{Si}} < \frac{K_{P_8}}{P_e} \quad (\text{D-13})$$

Using the equilibrium constant data in Appendix F, Equation (D-13) can be written

$$X_{\text{Si}} < \frac{1}{P_e} \exp(9.6 - 177000 \text{ } ^\circ\text{R}/\text{T}) \quad (\text{D-14})$$

Now it is known that  $p_e > 1 \text{ Atm.}$  and  $T < 5400 \text{ }^\circ\text{R};$  thus

$$X_{\text{Si}} < \exp(-23.0) \quad (\text{D-15})$$

which is small enough to justify neglecting Si vapor in the analysis.

## APPENDIX E

## DYNAMICS OF ATMOSPHERIC RE-ENTRY

Upon entering the earth's atmosphere, a vehicle will experience a number of forces which determine its subsequent motion. If the vehicle is nonlifting, the predominant force will be the aerodynamic drag caused by the air resistance.

If the weight component is small compared with the drag force, Newton's law for a nonlifting ballistic vehicle is (see reference 60).

$$-W \frac{dv_F}{dt} = \frac{1}{2} \rho_a V_F^2 C_D A_D \quad (E-1)$$

where

$W$  = mass of vehicle

$A_D$  = drag reference area

$C_D$  = drag coefficient

$t$  = time

$V_F$  = velocity along the direction of flight

$\rho_a$  = local density of atmosphere

If drag is the only force acting on the vehicle, the flight path angle  $\theta$  to the horizontal is constant and

$$\frac{dy_a}{dt} = -V_F \sin \theta \quad (E-2)$$

where  $Y_a$  is the altitude. The density is a known function of the altitude; thus, Equations (E-1) and (E-2) can be integrated numerically if the initial conditions of entry are specified.

For the study of the performance of slip-cast fused silica along typical trajectories, the following trajectories were selected:

<u>Type</u>	<u>W/C, A</u> <u>D-D</u> <u>lbm/sq ft</u>	<u>Altitude</u> <u>ft</u>	<u>Velocity</u> <u>ft/sec</u>	<u>Angle</u> <u>deg</u>
ICBM	1000	250,000	23,750	24.2
IRBM	1000	250,000	15,600	47.0
Trailblazer	80	250,000	18,000	80.0

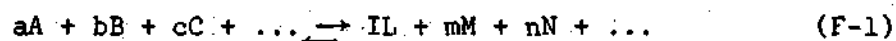
The Trailblazer is a test vehicle and is discussed in reference 49. Figure 16 shows the flight velocity, stagnation pressure and altitude versus time for re-entry from 300,000 ft for the ICBM, IRBM and Trailblazer II trajectories, respectively. The 1962 U. S. Standard Atmosphere (61) was used in the integration of Equations (E-1) and (E-2).

## APPENDIX F

## THERMODYNAMIC AND TRANSPORT PROPERTY DATA

Equilibrium Constant Data

Considering the chemical reaction equation:



the equilibrium constant in terms of partial pressures for this reaction is defined by the equation

$$K_p = \exp(-\Delta F_f^\circ / \bar{R}_u T) \quad (F-2)$$

where  $\Delta F_f^\circ$  is the change in free energy for the reaction. The free energy changes for the chemical reactions considered in Chapter IV are given in Table 4 along with the sources of the data. The data are given in terms of linear correlation equations in the absolute temperature. The data from the JANAF (62) tables were correlated by the present author, whereas the data given by Schick (24) were already given in equation form.

Gas Viscosity

As was stated in the text, the viscosity data for air were obtained from the correlation formulas of reference 50. These viscosity data were used in the calculations for the typical trajectories.

Table 4. Free Energy Data

Reaction	$\Delta F_f^\circ$ Btu	Source
$\text{SiO}_2(\text{L}) \rightarrow \text{SiO}_2(\text{g})$	229,000 - 36.0 T/°R	Schick (24)
$\text{SiO}_2(\text{g}) \rightarrow \text{SiO}(\text{g}) + \frac{1}{2} \text{O}_2$	82,500 - 18.2 T/°R	Schick (24)
$\frac{1}{2} \text{O}_2 \rightarrow \text{O}$	110,400 - 16.11 T/°R	Schick (24)
$\frac{1}{2} \text{H}_2 \rightarrow \text{H}$	97,400 - 14.37 T/°R	JANAF (62)
$\text{H}_2 + \frac{1}{2} \text{O}_2 \rightarrow \text{H}_2\text{O}(\text{g})$	-108,700 + 13.98 T/°R	JANAF (62)
$\frac{1}{2} \text{H}_2 + \frac{1}{2} \text{O}_2 \rightarrow \text{OH}$	15,730 - 3.29 T/°R	JANAF (62)
$\text{SiO}_2(\text{L}) + 2\text{H}_2 \rightarrow \text{SiH}_4(\text{g}) + \text{O}_2$	388,500 - 15.76 T/°R	JANAF (62)
$\text{SiO}(\text{g}) \rightarrow \text{Si}(\text{g}) + \frac{1}{2} \text{O}_2$	232,000 - 16.31 T/°R	Schick (24)

The viscosity of the gas mixture in the oxy-hydrogen environment was calculated from the viscosities of the individual species by using the viscosity equation developed by Wilke (63). It can be written in the form

$$\mu = \sum_i \mu_i \left[ 1 + \sum_{\substack{k=1 \\ k \neq i}} G_{ik} \frac{X_k}{X_i} \right]^{-1} \quad (\text{F-3})$$

where

$$G_{ik} = \frac{1}{\sqrt{8}} \left( 1 + \frac{\bar{M}_i}{\bar{M}_k} \right)^{-\frac{1}{2}} \left[ 1 + \left( \frac{\mu_i}{\mu_k} \right)^{\frac{1}{2}} \left( \frac{\bar{M}_k}{\bar{M}_i} \right)^{\frac{1}{4}} \right] \quad (\text{F-4})$$

Although this equation was derived for gas mixtures containing only nonpolar molecules, it has been used satisfactorily to estimate the viscosity of gas mixtures containing water vapor (64).

The viscosities of the individual species were calculated from the data given in reference 65. From reference 65 it follows that

$$\mu_i = 1.338 \times 10^{-6} \frac{\sqrt{\bar{M}_i T}}{\sigma_i^2 \Omega_{\mu_i}} \quad (\text{F-5})$$

where  $\mu_i$  is the viscosity in lbm/ft-sec,  $T$  the absolute temperature in  $^{\circ}\text{R}$ ,  $\sigma_i$  the molecular diameter in  $\text{\AA}$ , and  $\Omega_{\mu_i}$  is the collision integral for viscosity. Equation (F-5) has its foundations in statistical mechanics and theoretically applies only to nonpolar gases; however, as pointed out in reference 65 it is reasonably accurate for polar gases at high temperatures. For convenience the collision integrals of the species of interest here were correlated to an equation of the form

$$\Omega_{\mu_i} = A_i + B_i/T \quad (\text{F-6})$$

where  $A_i$  and  $B_i$  are constants. If Equation (F-6) is combined with Equation (F-5) it will be seen that the resulting equation for viscosity

has the same form as Sutherland's equation. The molecular diameters and constants  $A_i$  and  $B_i$  for the species considered are given in Table 5.

Table 5. Some Parameters for Predicting Transport Properties

Species	$\sigma_i$ Å	$A_i$	$B_i$ -°R	$\bar{M}_i$	$E_i$
H <sub>2</sub>	2.827	0.577	393.0	2.00	1.911
O <sub>2</sub>	3.467	0.660	302.0	32.00	1.705
H <sub>2</sub> O	2.641	0.767	1180.0	18.00	2.440
H	2.708	0.525	400.0	1.00	1.000
O	3.050	0.660	302.0	16.00	1.000
OH	3.147	0.582	501.0	17.00	1.565
N <sub>2</sub>	3.798	0.610	352.0	28.00	1.687

#### Gas Thermal Conductivity

The thermal conductivity of the gas mixture in the oxy-hydrogen environment was calculated from the equation

$$\lambda = \sum_{i=1} \lambda_i \left[ 1 + \sum_{\substack{k=1 \\ k \neq i}} G_{ik} \frac{X_k}{X_i} \right]^{-1} \quad (\text{F-7})$$

where  $G_{ik}$  is given by Equation (F-4). This equation is given in reference 66. It is identical to the equation developed by Mason and

Saxena (67) apart from the empirical constant 1.065 which appears in the expression for  $G_{ik}$  used by Mason and Saxena. Like the corresponding equation for viscosity, this equation was derived for nonpolar gas mixtures but will be used here even though water vapor is present.

It can be shown that the thermal conductivity of a gas is related to the viscosity in the manner (66)

$$\lambda_i = 7.45 (\mu_i / \bar{M}_i) E_i \quad (\text{F-8})$$

where  $E_i$  is the Eucken correction factor for polyatomic gases. The Eucken factor suggested by Hirschfelder (68) is

$$E_i = 0.115 + 0.354 \gamma / (\gamma - 1) \quad (\text{F-9})$$

where  $\gamma$  is the ratio of specific heats. The Eucken factor is approximately constant for the species and range of temperatures of interest here and the values used in the numerical calculations are given in Table 5.

#### Specific Heats and Enthalpies of Gases

The equations for the constant pressure specific heats and the equations for the chemical enthalpies of the species considered in this work are given in Table 6 along with the sources for the data. Where reference is made to the JANAF tables (62), the correlation equations were obtained by this author.

Table 6. Specific Heats and Enthalpies of Individual Species

Species	$\tilde{C}_p$ Btu/mole-°R	Reference
H <sub>2</sub>	$5.76 + 5.78 \times 10^{-4} T + 20.0/\sqrt{T}$	(68)
O <sub>2</sub>	$11.515 - 1770.0/\sqrt{T} + 1530.0/T$	(68)
H <sub>2</sub> O	$19.85 - 597.0/\sqrt{T} + 7500.0/T$	(68)
H	4.968	(62)
O	5.00	(62)
OH	8.28	(62)
N <sub>2</sub>	$9.47 - 3470.0/T + 1.16 \times 10^6/T^2$	(68)
SiO	8.98	(62)
SiO <sub>2</sub>	14.7	(62)

Species	$\tilde{H}$ Btu/mole*
H <sub>2</sub>	$5.76T + 2.89 \times 10^{-4} T^2 + 40.0\sqrt{T} - 452.36$
O <sub>2</sub>	$11.515T - 354.0\sqrt{T} + 1530.0 \ln(T/460.0) + 5498.7$
H <sub>2</sub> O	$19.85T - 1194.0\sqrt{T} + 7500.0 \ln(T/1800.0) - 72393.3$
H	$4.968T + 93115.2$
O	$5.00T + 107000.0$
OH	$8.28T + 13692.0$
N <sub>2</sub>	$9.47T - 3470.0 \ln(T/460.0) - 1.16 \times 10^6/T + 1361.0$
SiO	$8.98T - 41728.0$
SiO <sub>2</sub>	$14.7T - 13420.0$
SiO <sub>2</sub> (L)	$21.66T - 397776.0$

\* Obtained by integrating the specific heat equations between the limits of T and a reference temperature and adding the result to the chemical enthalpy at the reference temperature as given in the JANAF tables (62).

Density, Specific Heat, Thermal Conductivity and Viscosity of S.C.F.S.

As was stated in the text, the density of S.C.F.S. in the theoretical analysis was assumed to be constant and equal to the density of S.C.F.S. at room temperature. From reference 46 the density is found to be approximately 120 lbm/ft<sup>3</sup>. It was also assumed that the thermal conductivity and specific heat are constant. The values of thermal conductivity and specific heat used in the numerical calculations were obtained from reference 30 and are respectively  $9.7 \times 10^{-5}$  Btu/ft-sec-°R and 0.25 Btu/lbm-°R. The viscosity of S.C.F.S. is discussed in Chapter III; however, for completeness, the viscosity equation used is repeated below.

$$\mu_s = \exp(109500^\circ\text{R}/T - 16.7) \frac{\text{lbm}}{\text{ft-sec}} \quad (\text{E-10})$$

## APPENDIX G

## COMPUTER PROGRAMS

Nomenclature Translation

<u>Computer Program</u>		<u>Text</u>	<u>Computer Program</u>		<u>Text</u>
ALFA	=	$\alpha$	HN2	=	$h_{N_2}$
BETA	=	$\beta$	HO	=	$h_O$
C	=	$c_{Ps}$	HO <sub>2</sub>	=	$h_{O_2}$
C1	=	$C_1$	HOH	=	$h_{OH}$
C2	=	$C_2$	HSIO	=	$h_{SiO}$
DELTA	=	$\delta_T/n'$	HSIO2	=	$h_{SiO_2}$
DT	=	$\Delta t$	HSIO2L	=	$h(L)$
DY	=	$\Delta y$	HW	=	$h_w$
EPSILON	=	$\epsilon_R$	K	=	$k_s$
HCW	=	$h_{cw}$	K1	=	$K_{P_1}$
HE	=	$I_e$	K2	=	$K_{P_2}$
HH	=	$h_H$	K3	=	$K_{P_3}$
HH2	=	$h_{H_2}$	K4	=	$K_{P_4}$
HH2O	=	$h_{H_2O}$			

<u>Computer Program</u>		<u>Text</u>	<u>Computer Program</u>		<u>Text</u>
K5	=	$K_{P_5}$	PE	=	$P_e$
K6	=	$K_{P_6}$	PGG	=	$\frac{d^2 p}{ds^2}$
K7	=	$K_{P_7}$	PR	=	$Pr$
K8	=	$K_{P_8}$	PSI	=	$\psi(1)$
KHE	=	$\bar{c}_{H_e}$	PSIPR	=	$\psi(Pr)$
KHW	=	$\bar{c}_{H_w}$	PSISC	=	$\psi(Sc)$
KNE	=	$\bar{c}_{N_e}$	QCW	=	$\dot{q}_{o_{cw}}$
KNW	=	$\bar{c}_{N_w}$	QRAD	=	$\dot{q}_R$
KOE	=	$\bar{c}_{O_e}$	QSTAR	=	$Q^*$
KOW	=	$\bar{c}_{O_w}$	RHO	=	$\rho_s$
L	=	$L_o$	RHOE	=	$\rho_e$
LE	=	$L_e$	RHOV	=	$(\rho v)_w$
L1	=	$L(t)$	SC	=	$Sc$
L2	=	$L(t+\Delta t)$	TAUG	=	$\frac{d\tau_w}{ds}$
LV	=	$L_v$	TIM	=	$t$
MA/MV	=	$\bar{M}_v$	T1	=	$T_y^t$
MU	=	$\mu_s$	T2	=	$T_y^{t+\Delta t}$
MW	=	$\bar{M}_w$	TO	=	$T_I$
			U	=	$y$

<u>Computer Program</u>	=	<u>Text</u>
UX	=	$\bar{U}_x$
VG	=	$\frac{du_e}{ds}$
XH	=	$X_H$
XH2	=	$X_{H_2}$
XH2O	=	$X_{H_2O}$

<u>Computer Program</u>	=	<u>Text</u>
XN2	=	$X_{N_2}$
XO	=	$X_O$
XO2	=	$X_{O_2}$
XOH	=	$X_{OH}$
XSiO	=	$X_{SiO}$
XSiO2	=	$X_{SiO_2}$

GEORGIA TECH RECC R-5500 ALGOL COMPILER THURSDAY, 4/27/67, 11:17 PM.

REGIN

```

INTEGER III
INTEGER N, Q, J, I, JJ, KKK
ARRAY U(0:500)
ARRAY M(0:500)
ARRAY T1(0:501), T2(0:501), V1(0:501), V2(0:501)
REAL K2F
REAL KOF, KNE, U1
REAL C1, C2, TIME1, TIME2, TAU1, TAU2, L, L1, L2, D1, DX, EX, MV, MA, TM, TO, C, RHO,
AA, RB, CC, DD, HCW, TH, TA, EE, PSI, PSIPR, PSISC, Y1, Y2, YY, QSTAR, PSTAR,
IL, PS, PT, K1, K2, K3, K4, K5, K6, K7, K8, HS102, H02, HN2, HS10, H0, HH, HH20,
HH2, HS102L, AX, DAX, BX, DRX, CX, DCX, X, XT, ALFA, BETA, W, SRDSC, Y, A1Y,
LV, NW, M1, M2, DWN, DELTA, TAU, PXX, TAUR, UX, HOM, KK, R, RHOMUE, H, K, OL,
XS102, XS10, XN2, MW, KNH, KNE, LE, SC, PR, RHUV, QCW, HS, HW, EPSILON, QRAD,
BA1Y, B1Y, DB1Y, C1Y, DC1Y, D1Y, UD1Y, DY, Z, DZ, XH2, XH, X02, X0, X0H, XH20,
RHHS
REAL VG, TAUG, PGG, PE, HE
REAL DY1
REAL RHDE
REAL TIM
LABEL DOG, BNR, HUSS, ZOT, ANN, SHELLEY, DUTCH, TINA, GENE
FILE/DUT CEW 6(2,15)
LIST ANS1(TIM)
      ANS3(TAUR)
      ANS5(H)
      ANS8(QSTAR)
      ANS9(LV)
      ANS0(KK, TAUG)
      ANS6(PGG, VG)
      ANS7(L1)
      AN1(HE)
      AN2(PE)
      AN3(QCW)
      AN4(RHDE)
      AN5(RHDMUE)
      AN6(H)
      AN7(EPSILON)
      ANS10(XH, XH2, X0, X02, XN2)
      ANS11(XH20, XS10, XS102, X0H)
      ANS12(HY)
      ANS13(PSISC, PSIPR, PSI)
      ANS14(KNE, KNH)
      ANS2(U[J], T1[J], V1[J])
FORMAT OUT
FMT(X20, "RUN TIME = ", X1, F7.1, X2, "SEC")
FMT1(X14,
      "TIME = ", F6.2, X2, "SEC")
FMT3(X14,
      "KK = ", F5.2, X2, "TAUG = ", E15.5, "LBF/FT*3")
TITLE1(X14,
      "STA FT", X4, "TEMP DEG R", X4, "VEL FT/SEC")
TITLE2(X6, "X1", X7, "XH2", X7, "XU", X7, "XU2", X7, "XN2")
TITLE3(X3, "XH20", X6, "XS10", X5, "XS102", X6, "X0H")
FMT5(
      X14, "HEAT XFER COEF = ", F5.3, X2,
      "HTU/(DEG R-SEC)")
FMT7(X14,
      "THICKNESS = ", F7.5, X2, "FET")
FMT8(X14, "HEAT OF ABLATION = ", X2, F11.2, X2, "BTU/LBM")

```

```

FMT9(X14,"HEAT OF VAP. = ",X2,F10.1,X2,"BTU/LBM")
FMT4(X20,"INDEX OF PERFORMANCE",X1,F8.2)
FMT6(X14,
"PGG = ",E15.5,"LBF/FT*4",X2,"VG = ",E15.5," 1/SEC")
F1(X20,"HF = ",X2,F10.1,X2,"BTU/LHM")
F2(X20,"PF = ",X2,F7.3,X2,"ATM")
F3(X20,"GCM = ",X2,F8.1,X2,"BTU/FT*2")
F4(X20,"RHHDC = ",X2,E15.5,X2,"SLUGS/FT*3")
F5(X20,"RHHHUE = ",X2,E15.5,X2,"LBM*2/F1*4*SEC")
F6(X20,"R = ",X2,F7.3,X2,"FT")
F7(X20,"EPSILON = ",X2,F7.3)
FMT10(5(F8.4,X2))
FMT11(4(F8.4,X2))
FMT12
(X20,"HW = ",X2,F10.1,X2,"BTU/LBM")
FMT13(X5,"PSISC = ",F8.4,X5,"PSIPR = ",F8.4,X5,"PSI = ",
F9.4)
FMT14(X5,"KNE = ",E12.5,X5,"KNW = ",E12.5)
FMT2(X12,
F8.5,X6,F10.1,X6,F15.13)

```

```

COMMENT ASSIGNMENT OF STEP SIZES AND INITIAL NUMBER OF STATIONS
N + 82
DY + 0.0005
DT + 0.01

```

```

COMMENT INITIAL SAMPLE THICKNESS
L + 0.041
FOR J + 0 STEP 1 UNTIL 0 DO
J(J) + -J*DY

```

```

COMMENT ASSIGNMENT OF INITIAL CONDITIONS
L2 + L
L1 + L
TIM + 0.0
FOR J + 0 STEP 1 UNTIL 0 DO
V1(J) + 0.0
T0 + 500.0
FOR J + 0 STEP 1 UNTIL 0 DO
T1(J) + T0
T2(J) + T0
T2(J) + 3000.0
T1(J) + 3000.0
PSI + 1.0

```

```

COMMENT ASSIGNMENT OF PROPERTY DATA FOR S.C.F.S.
C1 + EXP (-16.7)/32.2

```

```

C2 + 109500.0      )
MV + 40.0          )
TM + 3200.0        )
C + 0.25           )
MHD + 120.0        )
K + 0.000097       )
EPSILON + 0.3      )

```

```

COMMENT ASSIGNMENT OF ENVIRONMENTAL CONDITIONS      )

```

```

COMMENT DISTANCE FROM EXIT OF MOTOR IS 6 INCHES      )

```

```

PR + 0.500        )
SC + 0.500        )
LE + 1.0           )
HCW + 2835.4      )
UX + 0.42         )
VG + 1.04# 5      )
VG + 1.75*1.75*VG )
QCM + 840.0       )
QCM + 1.75*QCM    )
HE + 155.0        )
RHOE + 0.0107/32.2 )
PE + 2.4          )
KNE + (1.0 - UX)*(0.765) )
KHE + 0.1*UX + 0.1*UX )
KOE + (1.0 - UX)*(0.235) + 0.8*UX )
ALFA + KUE/(16.0*KHE) )
BETA + KNE/(14.0*KHE) )
MA + 15.0         )

```

```

III + 0           )
TAUT + TIME(2)    )
N + 5             )
WRITE(CEW(N))     )

```

```

COMMENT SOME CONVENIENT GROUPS OF VARIABLES THAT APPEAR IN THE FINITE
DIFFERENCE EQUATIONS      )

```

```

AA + 0.25*DT/DY   )
BB + 0.5*MHD*C*DY/K )
TH + K*DT/(RHO*C*(DY+2)) )

```

```

WRITE(CEW(DPL),F1,AN1) )
WRITE(CEW(DBL),F2,AN2) )
WRITE(CEW(DBL),F3,AN3) )
WRITE(CEW(DBL),F4,AN4) )
WRITE(CEW(DBL),F5,AN5) )
WRITE(CEW(DBL),F6,AN6) )
WRITE(CEW(PAGE),F7,AN7) )
Y1 + T2(0)           )
Y2 + T2(0)           )

```

```

DOG1
  QCW + 840.0*(1.0 + 0.75*(1.0 - EXP(-99.0*TIM )))
  TIM + TIM + DT
  IF TIM > 30.0 THEN
  QCW + QCW*EXP( - 10.0*(TIM - 30.0) )
  III + III + 1
  T2(0) + T1(0)
  PGG + -(VG*2)*RHOC
ROB1
  Y1 + Y2
  FOR JJ + 1 , 2 DO
BEGIN
  IF JJ = 1 THEN
  YY + Y1
  IF JJ = 2 THEN
  YY + Y1 + 1.0
  T2(0) + YY
  IF T2(0) < TM THEN
  GO TO ROSS
  TM + 3200.0 - 500.0
  IF V1(N) > 0.000000001 THEN
  QSTAR + QCW/(RHO*V1(N))
  DL + V1(N)*DT
  L2 + L1 - DL

  COMMENT Q IS THE NUMBER OF THE LAST STATION THAT LIES IN THE
  ABLATING BODY
  Q + ENTIER (L2/DY )

  PSTAR + EXP( - 104000.0/T2(0) + 16.48 )
  IF PSTAR >= PE THEN
BEGIN
  T2(0) + T2(0) - 1.0
  GO TO ROB END

  COMMENT EQUILIBRIUM CONSTANTS AS FUNCTIONS OF TEMPERATURE
  K1 + EXP(18.15-115300.0/T2(0))
  K2 + EXP( 9.15 - 41700.0/T2(0) )
  K3 + EXP(8.13-55500.0/T2(0))
  K4 + EXP( (14.37 - 97702.2/T2(0) )/1.986)
  K5 + EXP( (3.29 - 15748.2/T2(0) )/1.986 )
  K6 + EXP(-( 13.98 - 108774.0/T2(0) )/1.986 )

  COMMENT ENTHALPIES OF SPECIES AS FUNCTIONS OF TEMPERATURE
  HS(H2 + 14.7*( T2(0) - 3600.0) - 85500.0
  HD2 + 11.515*(T2(0)-460.0) - 354.0*(SQRT(T2(0)) - 21.4)
  + 1530.0*LN(T2(0)/460.0) + 7.0*460.0
  HN2 + 9.47*(T2(0)-460.0) - 3470.0*LN(T2(0)/460.0)
  + (1.16*6)*(1.0/T2(0) - 0.00217) + 6.96*460.0
  HS(H) + 4.94*(T2(0)-3600.0) - 9400.0
  HD + 5.4*(T2(0) - 3600.0) + 125000.0
  HH + 8.28*(T2(0) - 3600.0) + 43500.0
  HH + 4.968*(T2(0) - 3600.0) + 111000.0
  HH2O + 19.85*(T2(0) - 1800.0) -
  1191.0*(SQRT(T2(0)) - SQRT(1800.0) ) +

```

```

7500.0*LN(T2[0]/1800.0) = 87348.6
HH2 + 5.76*(T2[0] - 1800.0) +
0.000289*( T2[0]*T2[0] - 3.24*1800.0 ) +
40.0*(SQRT(T2[0]) - SQRT(1800.0)) + 12550.0
HSIO2L + 0.361*(T2[0] - 3240.0) = 5460.0

```

COMMENT THE DETERMINATION OF MOLE FRACTIONS OF SPECIES AT THE SURFACE )

X + 0.04\*PE )

ZOT:

AX + (X + XXXXK6)\*(BETA + 1.0) )

DAX + (1.0 + 2.0\*XXXK6)\*(BETA + 1.0) )

BX + (X\*K4 + XXXXK5)\*(BETA/2.0 + 1.0) )

DBX + (K4 + 2.0\*XXXK5)\*(BETA/2.0 + 1.0) )

CX + K2\*K1 + X\*(K1 - PE) + XXXXK3 + XXXX )

DCX + ( K1 - PE) + 2.0\*XXK3 + 3.0\*XXX )

W + 4.0\*AX\*CX/(BX\*BX) )

IF ABS(W) > 0.1 THEN )

SRDSC + BX\*SQRT(1.0 - W) ELSE )

SRDSC + 4X\*(1.0 - 0.5\*W - 0.125\*W\*W - 0.0625\*W\*W\*W - )

0.0391\*W\*W\*W\*W ) )

Y + ( - BX + SRDSC )/(2.0\*AX) )

A1Y + - 1.0 )

D1Y + 0.0 )

H1Y + -0.5\*K3 + 0.5\*(ALFA - 1.0)\*Y\*K5 + )

(ALFA - 0.5)\*Y\*Y\*K6 ) )

DB1Y + 0.5\*(ALFA - 1.0)\*K5 + 2.0\*(ALFA - 0.5)\*Y\*K6 )

C1Y + 0.5\*ALFA\*K4\*Y + ALFA\*Y\*Y )

DC1Y + 0.5\*ALFA\*K4 + 2.0\*ALFA\*Y )

D1Y + 0.5\*K2\*K1 )

DD1Y + 0.0 )

DY1 + - ( DAX\*Y\*Y + DBX\*Y + DCX )/(2.0\*AX\*Y + BX) )

Z + A1Y\*XXX\*Y + B1Y\*XXX + C1Y\*Y + D1Y )

DZ + 3.0\*A1Y\*XXX + 2.0\*B1Y\*Y + C1Y + )

(DA1Y\*XXX\*Y + DB1Y\*XXX + DC1Y\*Y + DD1Y)\*DY1 )

XT + X )

X + X = Z/DZ )

IF ABS(XT - X) > 0.0001\*XT THEN )

GO TO ZOT )

XH2 + Y\*Y/PE )

XH + K4\*Y/PE )

XO2 + X\*Y/PE )

XO + K3\*Y/PE )

XOH + K5\*Y\*Y/PE )

XH2O + K6\*Y\*Y\*Y/PE )

XSIO2 + K1/PE )

XSIO + K2\*K1/(X\*PE) )

XN2 + BETA\*(XH2O + XH2 + 0.5\*XH + 0.5\*XOH ) )

MW + 1.0\*XH + 2.0\*XH2 + 28.0\*XN2 + 16.0\*XO + 32.0\*XO2 + )

44.0\*XSIO + 60.0\*XSIO2 + 18.0\*XH2O + 17.0\*XOH )

KNW + XN2\*28.0/MW )

COMMENT BLOWING CORRECTIONS )

```

PSISC + KNW/(KNW*0.67*(SC+(-0.267))*(LE*0.667)*( (NA/MV)*0.25)
*(KNW - KNE) )
PSIPR + 1.0 + (PSISC - 1.0)*(LE*0.267)
PSI + 1.0 + (PSISC - 1.0)*(SC*0.267)

COMMENT SURFACE SHEAR STRESS GRADIENT AND VAPORIZATION RATE
RHOV + (KNE + KNW)*PSISC*QCM*(LE*0.667)/( (HE-HCW)*KNW)
TAUG + - (PR*(-0.667))*QCM*VG*PSI/((HE-HCW)*32.2)

RDS$
BEGIN
IF T2(0) < TM THEN
PSISC + 1.0
PSIPR + 1.0
PSI + 1.0
END

COMMENT ENTHALPY OF MIXTURE AT SURFACE
IF T2(0) < TM THEN
HW + HCA
ELSE
HW + (HH*XH + HM2*XM2 + MN2*XM2 + HO*XD + MO2*XD2 +
HM2O*XM2O + HS1O*XS1O + HS1O2*XS1O2 + HON*XON )/MW

COMMENT EFFECTIVE HEAT OF VAPORIZATION
LV + HW - HS1O2L

COMMENT NET HEAT TRANSFER RATE JUST BELOW THE GAS-LIQUID INTERFACE
QRAO + (0.0760-12)*EPSILON*(T2(0)+4)
QL + QCM*PSIPR
*(HE-HW)/(HE-HCW) = RHOV*(HW-HS1O2L) = QRAO

FOR J + 1 DO
T2(J) + T1(J) + TH*(T1(J+1) - 2.0*T1(J) + T1(J-1))
+ V1(J)*2.0*AA*(T1(J+1) - T1(J-1))
HW + (T2(0) + T2(J) + 0.5*QL/K)
IF JJ = 1 THEN
M1 + HW
ELSE
M2 + MW*END
DMW + M2 - M1
Y2 + Y1 - M1/DMW
IF ABS(Y2 - Y1) > 0.001*ABS(Y1) THEN
GO TO HUR

```

```

COMMENT CALCULATION OF FUTURE TEMPERATURE DISTRIBUTION FROM PRESENT
TEMPERATURE DISTRIBUTION
FOR J + 1 STEP 1 UNTIL Q=1 DO
T2(J) + T1(J) + TM*(T1(J)+1) - 2.0*T1(J) + T1(J-1)
+ V1(J)*2.0*AA*(T1(J+1) - T1(J-1))
FOR J + Q DO
T2(J) + T2(J-2) + (2.0*(T2(J-1) - T2(J-2))/(DY/2.0 - L2 +
Q*DY - 2*DY))*(Q*DY - L2 - DY)

```

```

IF III = 100 THEN
BEGIN
III + 0
WRITE(CLN(DHL),FMT1,ANS1)
WRITE(CEN(DBL),FMT7,ANS7)
WRITE(CEN(DBL),FMT8,ANS8)
WRITE(CEN(DHL),FMT9,ANS9)
WRITE(CEN(DBL),FMT3,ANS0)
WRITE(CLN(DHL),FMT6,ANS6)
WRITE(CLN(DHL),FMT5,ANS5)
WRITE(CEN(DBL),FMT12,ANS12)
WRITE(CEN(DBL),FMT13,ANS13)
WRITE(CEN(DHL),FMT14,ANS14)
WRITE(CEN(DBL),TITLE2)
WRITE(CEN(DBL),FMT10,ANS10)
WRITE(CEN(DBL),TITLE3)
WRITE(CEN(DHL),FMT11,ANS11)
WRITE(CEN(DBL),TITLE1)
FOR J + 0 STEP 1 UNTIL N DO
WRITE(CEN,FMT2,ANS2)
FOR J + N+1 STEP 4 UNTIL Q = 4 DO
WRITE(CEN,FMT2,ANS2)
FOR J + Q DO
WRITE(CEN,FMT2,ANS2)
END
IF (T1(0) - T2(0)) > 0.0 AND V1(N) < 0.00005 THEN
BEGIN
FOR J + 0 STEP 1 UNTIL Q DO
V1(J) + 0.0
FOR J + 0 STEP 1 UNTIL Q DO
T1(J) + T2(J)
GO TO SHELLEY END
FOR J + 0 STEP 1 UNTIL Q DO
T1(J) + T2(J)
IF T1(0) < TM THEN
GO TO SHELLEY

```

```

COMMENT VELOCITY DISTRIBUTION IN Y DIRECTION IN LIQUID LAYER
V1(0) + RHOV/RHO
NU(0) + C1*EXP(C2/T1(0))
IF QL < 1.0 THEN
DELTA + 0.0 ELSE
DELTA + (T1(0)*T1(0)**K)/(C2*QL)
V1(0) + V1(0) + 2.0*DELTA*DELTA*(TAUG - 2.0*PBG*DELTA)/NU(0)
IF QL < 1.0 THEN

```

```

FOR J + 1 STEP 1 UNTIL 0 DO
V(I,J) + V(I) ELSE
FOR J + 1 STEP 1 UNTIL 0 DO
V(I,J) + V(I) - 2.0*DELTA*DELTA*(EXP(U(I,J)/DELTA))*
(-TAUG - DELTA*PGG*(2.0 - U(I,J)/DELTA))/MU(I)

```

SHELLEY

```

L1 + L2
IF TIM 5 60.0 THEN
GO TO DNG
TAUF + TIME(2)
TAUR+ (TAUF - TAUI)/60.0
WRITE(CAN(D9L),FMT,ANS)
END.

```

```

EXP IS SEGMENT NUMBER 0005,PRT ADDRESS IS 0273
LN IS SEGMENT NUMBER 0006,PRT ADDRESS IS 0300
SQRT IS SEGMENT NUMBER 0007,PRT ADDRESS IS 0277
OUTPUT(N) IS SEGMENT NUMBER 0008,PRT ADDRESS IS 0275
BLOCK CONTROL IS SEGMENT NUMBER 0009,PRT ADDRESS IS 0005
X TO THE I IS SEGMENT NUMBER 0010,PRT ADDRESS IS 0301
ALGOL WRITE IS SEGMENT NUMBER 0011,PRT ADDRESS IS 0014
ALGOL READ IS SEGMENT NUMBER 0012,PRT ADDRESS IS 0015
ALGOL SELECT IS SEGMENT NUMBER 0013,PRT ADDRESS IS 0016

```

```

NUMBER OF ERRORS DETECTED = 0, COMPILATION TIME = 64 SECONDS,
PRT SIZE = 194) TOTAL SEGMENT SIZE = 1193 WORDS) DISK SIZE = 53 SEGS)
ESTIMATED CORE STORAGE REQUIREMENT = 5285 WORDS, NO. PGM. SEGS = 14

```

## APPENDIX H

## NEWTON'S METHOD

Newton's Method

As was pointed out in Chapter IV, Newton's method for solving for the zeros of an equation is a convenient method for solving Equation (4-72). The details of Newton's method may be found in reference 70. It is sufficient here to say that Newton's method is an iterative scheme making use of the approximating formula

$$x_{n+1} = x_n - \bar{f}(x_n)/\bar{f}'(x_n) \quad (\text{H-1})$$

to numerically determine the zeros of the equation  $y = \bar{f}(x)$ . Here the prime denotes differentiation with respect to  $x$  and  $n$  the order of approximation. Normally  $\bar{f}'(x)$  is determined as an explicit function of  $x$ . Since the left-hand side of Equation (4-72) is a polynomial, it is a simple matter to obtain its derivative explicitly.

A Numerical Newton's Method

As was pointed out above, the normal use of Newton's method depends on the knowledge of  $\bar{f}'(x)$  as an explicit function of  $x$ . If  $\bar{f}'(x)$  cannot be obtained practically as an explicit function of  $x$ , then formula (H-1) can be replaced by the formula

$$x_{n+1} = x_n - \bar{f}(x_n)\delta/(\bar{f}(x_n+\delta) - \bar{f}(x_n)) \quad (\text{H-2})$$

where  $\delta$  is a small change in  $x_n$ . If

$$\left| \frac{x_{n+1} - x_n}{x_n} \right| < \bar{\epsilon} \quad (\text{H-3})$$

is the criterion for acceptable accuracy of  $x_{n+1}$ , then for obvious reasons  $\delta/x_n$  should be at least an order of magnitude lower than  $\bar{\epsilon}$ . This method was found to be quite successful in calculating the temperature at the ablating surface. By reference to Chapter IV, it can be shown that the energy flux to the ablating body just below the gas-liquid interface can be formulated as a function of the surface temperature alone. Moreover, the heat transfer by conduction into the body at the gas-liquid interface is also only a function of the surface temperature. However, the energy flux below the surface must be equal to the heat conducted into the body at the surface. The temperature which makes the energy flux equal to the conduction heat transfer is the correct surface temperature. The numerical Newton's method can be used as follows: An initial guess of the surface temperature is made. The energy flux just below the surface and the conduction heat transfer are calculated for this temperature. In addition, these heat transfer rates are calculated for the assumed temperature plus one degree. Equation (H-2) can then be used to get a second approximation to the surface temperature if  $\bar{F}(x)$  is taken to be the difference in the energy flux and the conduction heat transfer,  $\delta$  one degree and  $x$  the surface temperature. Iteration is continued until the desired degree of accuracy in the surface temperature is obtained.

## REFERENCES

1. Sutton, G., "The Hydrodynamics and Heat Conduction of a Melting Surface," J.A.S. vol. 25, no. 1, January 1958, pp. 29-32.
2. Bethe, H. A. and Adams, M. C., "A Theory for the Ablation of Glassy Materials," J. Aero/Space Sci. 26, 321-328, June 1959.
3. Lees, L., "Similarity Parameters for Surface Melting of a Blunt Nosed Body in a High Velocity Gas Stream," ARS Journal vol. 29, no. 5, May 1959, pp. 345-354.
4. Adams, M. C., Powers, W. E. and Georgiev, S., "An Experimental and Theoretical Study of Quartz Ablation at the Stagnation Point," Avco-Everett Research Lab. Rept. 57, June 1959.
5. Georgiev, S., "Unsteady Ablation," Avco-Everett Research Lab. Rept. 94, September 1959.
6. Hidalgo, H., "Ablation of Glassy Materials Around Blunt Bodies of Revolution," ARS J. 30, 806-814, September 1960.
7. Scala, S. M. and Sutton, G. W., "The Two-Phase Hypersonic Laminar Boundary Layer--A Study of Surface Melting," Proc. 1958 Heat Transfer and Fluid Mechanics Institute, Stanford U. Press.
8. Roberts, L., "Mass Transfer Cooling Near the Stagnation Point," NASA TR-R-8, 1959.
9. Roberts, L., "A Theoretical Study of Stagnation Point Ablation," NASA TR-R-9, 1959.
10. Roberts, L., "Stagnation--Point Shielding by Melting and Vaporization," NASA TR-R-10, 1959.
11. Scala, S. M. and Vidale, G. L., "Vaporization Processes in the Hypersonic Laminar Boundary Layer," Journal of Heat and Mass Transfer, vol. 1, no. 1, 1960.
12. Scala, S. M., "Vaporization of a Refractory Oxide During Hypersonic Flight," 1959 Heat Transfer and Fluid Mechanics Institute, UCLA, Stanford University Press.
13. Fledderman, R. and Hurwicz, H., "Transient Ablation and Heat Conduction at a Vaporizing Surface," Avco RAD-TR-9(7)-60-9, (1960).

14. Zlotnick, N. and Nordquist, B., "Calculations of Transient Ablation," Avco RAD-9-TM-60-83.
15. Koh, C. Y. and Hartnett, J. P., "The Multiphase Hypersonic Laminar Boundary Layer on a Flat Plate," HTL Tech. Rept. 28 Heat Transfer Laboratory, University of Minnesota, Nov. 1960.
16. Hartnett, J. P., and Koh, C. Y., "The Multiphase Hypersonic Laminar Boundary Layer on a Flat Plate," HTL Tech. Rept. 29 Heat Transfer Laboratory, University of Minnesota, Nov. 1960.
17. Adams, E., "Theoretical Investigation of the Ablation of a Glass Type Heat Protection Shield of Varied Material Properties at the Stagnation Point of a Re-entering IRBM," NASA TND-564, January 1961.
18. Harmon, D. B. and McFarland, B. L., "Heat Transfer Through a Melting Layer with External Gas Flow," 1961 Heat Transfer and Fluid Mechanics Institute, Stanford University Press.
19. Adams, E. W., "Analysis of Quartz and Teflon Shields for a Particular Re-entry Mission," 1961 Heat Transfer and Fluid Mechanics Institute, Stanford University Press.
20. Steg, L. and Lew, H., "Hypersonic Ablation," General Electric Rept. R62SD55, May 1962.
21. Chen, S. and Allen, S. J., "Similarity Analysis for Transient Melting and Vaporizing Ablation on Blunt Nosed Bodies," American Rocket Society, Preprint 2098-61, October 1961.
22. Chen, S., "Body Force Effects on Transient Melting and Vaporizing Ablation," AIAA Journal, vol. 1, no. 9.
23. Hidalgo, H. and Kadanoff, L. P., "Comparison Between Theory and Flight Ablation Data," AIAA Journal, vol. 1, no. 1, January 1963.
24. Schick, H. L., "An Analysis of Some of the Physical and Chemical Properties of Silica ( $\text{SiO}_2$ ) of Importance in Ablation Behavior," Avco RAD-TR-2-58-6, 1958.<sup>2</sup>
25. Pierson, H., "Behavior of Fused Silica in Plasma Environment," Presented at Fall Meeting of the Ceramic Metal Systems Division of The American Ceramic Society, French Lick, Indiana, September 1965.
26. Walton, J. D., and Poulos, N. E., "Slip-Cast Fused Silica," Special Rept. No. 43, Georgia Institute of Technology (1964).

27. Walton, J. D., et al., "Design and Development of an E-M Window for Air Lift Reentry Vehicles," Interim Engineering Reports Numbers 1, 2, and 3, Georgia Institute of Technology, 1963-1964.
28. Ibid.
29. Ibid.
30. Walton, J. D., "Fused Silica Manual," Georgia Institute of Technology, 1964.
31. "An Experimental and Analytical Study of Ablation in a High Shear Environment," Cornell Aeronautical Laboratory, Inc., Report No. BM-1526-G-8, 1964.
32. "Properties of Selected Commercial Glasses," Corning Glass Works Bulletin B-83, Revised, 1960.
33. Lees, L., "Convective Heat Transfer with Mass Addition and Chemical Reactions," Third AGARD Combustion and Propulsion Colloquium, Pergamon Press, New York, 1958.
34. Bowen, M. D., and Smyly, E. D., "A Study of Laminar Boundary Layers on Tungsten, Graphite and Pyrolytic Boron Nitride," Combustion Institute III Conference on High Temperature Systems, 1965, Gordon and Breach Publishers, To be published.
35. Polezhaev, Yu. V., "Effect of Nonequilibrium Evaporation and Dissociation of Vapors on the Mass Transport Parameters of Heatproof Glassy Materials," High Temperature, Vol. 2, No. 1, pp. 25-30, 1964.
36. Adams, E. W., "Calculation of the Transient Molten Film in the Vicinity of the Forward Stagnation Point on the Surface of a Vehicle Descending Through the Atmosphere," ABMA DA-TM-81-59, 30 June 1959.
37. Bethe, H. A., and Adams, M. C., "On the Accuracy of an Approximate Theory for the Ablation of Glassy Materials--a Reply," J.A.S., Vol. 26, No. 11, pp. 768, Nov. 1959.
38. Bowen, M. D., and Gorton, C. W., "The Combustion of Pyrolytic-Boron Nitride," *Heterogeneous Combustion--Progress in Aeronautics and Astronautics*, Volume XV, AIAA, 1964.
39. Dorrance, W. H., *Viscous Hypersonic Flow*, McGraw-Hill Book Co., Inc., 1962.
40. Tombs, N. C., and Welch, A. J., "Thermodynamic Properties of Silicon Monoxide," J. Iron Steel Institute, 172, 69, 1952.

41. Lees, L., "Laminar Heat Transfer Over Blunt-Nozed Bodies at Hypersonic Flight Speeds," *Jet Propulsion*, Vol. 26, No. 4, pp. 259-269, 1956.
42. Mickley, H. S., Ross, R. C., Squyers, A. L., and Stewart, W. E., NACA TN 3208, 1954.
43. Baron, R. B., "The Binary-Mixture Boundary Layer Associated with Mass Transfer Cooling at High Speeds," MIT Naval Supersonic Laboratory, TR 160, 1956.
44. Fay, J. A., and Riddell, F. R., "Theory of Stagnation Point Heat Transfer in Dissociated Air," *J.A.S.*, Vol. 27, No. 2, pp. 73-85, February 1958.
45. Weinstein, I., "Heat Transfer and Pressure Distributions on a Hemisphere-Cylinder and a Bluff-Afterbody Model in Methane-Air Combustion Products and in Air," NASA TN D-1503.
46. "Investigation of High Temperature Resistant Materials," Summary Report No. 3, By Georgia Institute of Technology, for the Department of the Navy, Bureau of Ordnance, Contract No. NOrd-15701, 1958-1959.
47. Schneider, P. J., *Conduction Heat Transfer*, Addison-Wesley Publishing Company, Inc., 1955.
48. Carslaw, H. S., and Jaeger, J. C., *Conduction of Heat in Solids*, Oxford at the Clarendon Press, 1959.
49. Hartsel, J. E., and Nerem, R. M., "Predicted Re-entry Performance of a Trailblazer II Vehicle," The Ohio State University Research Foundation, Report 1573-7 for Air Force Avionics Laboratory, September 1964.
50. Cohen, N. B., "Correlation Formulas and Tables of Density and Some Transport Properties of Equilibrium Dissociating Air for Use in Solutions of the Boundary-Layer Equations," NASA TN D-194, 1960.
51. Tanzilli, R. A., "Evaluation of Graphite Composites in Re-Entry Environments," General Electric Company, AFML-TR-65-328, 1965.
52. Hansen, C. F., "Approximations for the Thermodynamic and Transport Properties of High-Temperature Air," NACA TN 4150, 1958.
53. Svehla, R., "Thermodynamic and Transport Properties for the Hydrogen-Oxygen System," NASA SP 3011, 1964.

54. "Investigation of High Temperature Resistant Materials," Quarterly Report No. 12, Project No. A-212, By Georgia Institute of Technology for the Department of the Navy, Bureau of Ordnance, Contract No. NOrd-15701, 1958.
55. "Thermodynamic Properties to 6000°K for 210 Substances Involving the First 18 Elements," NASA SP-3001, 1963.
56. Libby, P. A., "Theoretical Analysis of Turbulent Mixing of Reactive Gases with Application to Supersonic Combustion of Hydrogen," ARS Journal, March 1962.
57. Hottel, H. C., and Hawthorne, W. R., "Diffusion in Laminar Flame Jets," Third Symposium on Combustion, Flame and Explosive Phenomena, 1948.
58. Grube, G. and Speidel, "The Silicon Monoxides. I. Precipitated Forms of Silicon Monoxide from the Vapor Phase," Z. Elektrochem. Vol. 53, pp. 339, 1949.
59. Sosman, R. B., *Phases of Silica*, Rutgers University Press, pp. 187-191, 1965.
60. Gatland, K. W., *Space Flight Technology*, Proceedings of the First Commonwealth Space Flight Symposium, pp. 173-203, 1959.
61. *U. S. Standard Atmosphere*, Sponsors, NASA, USAF, and USWB, U. S. Government Printing Office, Washington 25, D. C., 1962.
62. *JANAF Interim Thermochemical Tables*, Vol. 1 and 2, The Advanced Research Projects Agency Program, Contract AF 33(616)-6149.
63. Wilke, C. R., "A Viscosity Equation for Gas Mixtures," J. Chem. Phys., Vol. 18, pp. 517, 1950.
64. Ibid.
65. Svehla, R., "Estimated Viscosities and Thermal Conductivities of Gases at High Temperatures," NASA TR R-132, 1961.
66. Bird, R., Stewart, W., and Lightfoot, E., *Transport Phenomena*, John Wiley and Sons, Inc., 1962.
67. Mason, E. A., and Saxena, S. C., "Approximate Formula for the Thermal Conductivity of Gas Mixtures," The Physics of Fluids, Vol. 1, No. 5, 1958.
68. Hirschfelder, J. O., "Heat Conductivity in Polyatomic of Electrically Excited Gases. II," J. Chem. Phys., Vol. 26, pp. 282-285, 1957.

69. Sweigert, R. L., and Beardsley, M. W., "Empirical Specific Heat Equations Based upon Spectroscopic Data," Georgia School of Technology Bull. Vol. 1, No. 3, June, 1938.
70. Kaplan, W., *Ordinary Differential Equations*, Addison-Wesley Publishing Co., pp. 130, 1960.

## VITA

Charles Everage Willbanks was born in Royston, Georgia on August 8, 1940. He graduated from Lavonia High School, Lavonia, Georgia in May, 1958. He entered the Georgia Institute of Technology in the fall of that same year and graduated with honor in 1962 with the degree of Bachelor of Mechanical Engineering. After being employed as a research assistant in the Department of Mechanical Engineering for the summer of 1962, he resumed his studies at Georgia Tech in the fall and received a Master of Science in Mechanical Engineering in June of 1965.

He is a member of Tau Beta Pi, Phi Kappa Phi, and the Society of Sigma Xi.

Mr. Willbanks was married in 1962 to the former Annette Dunn. They have no children.